EXISTENCE AND IMPORTANCE OF MAGNETIC FIELDS IN TIGHT PAIRS AND GROUPS OF GALAXIES

BŁAŻEJ NIKIEL-WROCZYŃSKI

A PhD thesis written under the supervision of Professor Marek Urbanik
and co-supervision of Doctor Marek Jamrozy

Astronomical Observatory
Faculty of Physics, Astronomy and Applied Computer Science
Jagiellonian University

June 2015

SUPERVISORS:
Prof. dr hab. Marek Urbanik
Dr Marek Jamrozy

ALMA MATER:
Jagiellonian University, Faculty of Physics, Astronomy and Applied Computer Science

Dedication

This work is dedicated to **R**ugia for being (probably unknowingly)
an Earth-based analogue of the MHD dynamo, that amplified my
determination to collect all the presented articles into one thesis,
transferring the kinetic energy of my turbulent movements into
a genuinely regular (not just anisotropic), scientific dissertation.

ABSTRACT

This dissertation is an attempt to investigate the existence and role of the intergalactic magnetic fields in compact groups and tight pairs of galaxies. Radio emission from several, well known objects of these types is analysed and properties of the discovered intergalactic magnetised structures are discussed. Together, these results are used to show that wherever found, intergalactic magnetic fields play important role in the galactic dynamics and evolution. Non-thermal, intergalactic radio emission, which signifies existence of the magnetic fields, can be used as a very sensitive tracer of interactions and gas flows. Unusual magnetised objects and structures can be found in the intergalactic space, and their studies open a possibility to discover more about the cosmic magnetism itself.

PUBLICATIONS

This dissertation has been written as a summary of the scientific activities previously reported in these articles:

- **Nikiel-Wroczyński, B.**, Jamrozy, M., Soida, M., Urbanik, M., *Multiwavelength study of the radio emission from a tight galaxy pair Arp 143*, 2014, MNRAS, 444, 1729
- **Nikiel-Wroczyński, B.**, Soida, M., Bomans, D. J., Urbanik, M., *Discovery of a Tidal Dwarf Galaxy in the Leo Triplet*, 2014, ApJ, 786, 144
- **Nikiel-Wroczyński, B.**, Soida, M., Urbanik, M., Beck, R., Bomans, D. J., *Intergalactic magnetic fields in Stephan's Quintet*, 2013, MNRAS, 435, 149
- **Nikiel-Wroczyński, B.**, Soida, M., Urbanik, M., Weżgowiec, M., Beck, R., Bomans, D. J., Adebahr, B., *Radio continuum observations of the Leo Triplet at 2.64 GHz*, 2013, A&A, 553, 4

A single article just submitted to the *MNRAS* was also referred to:

- **Nikiel-Wroczyński, B.**, Jamrozy, M., Soida, M., Urbanik, M., Knapik, J., *Probing the magnetic field of the nearby galaxy pair Arp 269*, submitted to MNRAS at 10.06.2015

After sleeping through a hundred million centuries
we have finally opened our eyes on a sumptuous planet,
sparkling with colour, bountiful with life.
Within decades we must close our eyes again.
Isn't it a noble, an enlightened way
of spending our brief time in the Sun,
to work at understanding the Universe
and how we have come to wake up in it?

— *Richard Dawkins,* Unweaving the Rainbow

ACKNOWLEDGEMENTS

First and foremost, I would like to thank my Advisor, Professor Marek Urbanik of the Jagiellonian University in Krakow, for inevitable help, guidance, and ideas for new research projects. Without his help, it would not be possible to write this dissertation.

I am very thankful to my Co-Advisor, Dr Marek Jamrozy, who has shown me how useful the metrewave radioastronomy can be, and spent enormous amount of time with me to reduce and analyse data in all the projects done with the help of the GMRT.

Great thanks should be given to Dr hab. Marian Soida, who was keen for long discussions of physics that lies beyond the detected structures, taught me how to analyse both interferometric and single-dish data, and was always willing to help me with any usual, or unusual problems I ran into while analysing the observations.

Dr hab. Krzysztof Chyży and the whole personnel of the Department of Radio Astronomy and Space Physics of the Astronomical Observatory of the Jagiellonian Univeristy should also be mentioned here. Thank you for being my work colleagues for more than four years I spent as a PhD student, giving me a possibility to learn a lot about the cosmic magnetism – not only in Kraków, but also in various institutions throughout the world, to where I was made able to travel.

I wish to thank Dr Rainer Beck and Dr Andreas Horneffer from the Max-Planck Instut für Radioastronomie in Bonn, Professor Ralf-Jürgen Dettmar and Privat-Dozent Dr. Dominik Bomans of the Astronomisches Institut der Ruhr-Universität Bochum, and Dr George Heald and Dr Roberto Pizzo from ASTRON, the Netherlands Institute for the Radio Astronomy, as well as the whole crews of the aforementioned Institutes. Gates of these Institutions were always open for

me, and it would be impossible to complete this thesis without the helping hand lent by them.

I would also like to thank the personnel of the Effelsberg Telescope of the Max-Planck Instut für Radioastronomie, the Karl G. Jansky Very Large Array in Socorro, NM, and the Giant Metrewave Radio Telescope near Pune, India for performing the observations that made my studies possible.

Finally, I acknowledge funding from the scientific grant from the National Science Centre (NCN), dec. No. 2011/03/B/ST9/01859, which was used for most of my scientific activities that were connected to this dissertation.

Contents

ACRONYMS

AGN Active Galactic Nuclei

DSS Digitized Sky Survey

HCG Hickson Compact Group

IGM Intergalactic medium

ISM Interstellar medium

JVLA Karl G. Jansky Very Large Array, the name for the modernised VLA

FGC Flat Galaxies Catalogue by Karachentsev et al. 1993, a catalogue of 4455 flat, edge-on galaxies

GMRT Giant Metrewave Radio Telescope near Pune, India

MHD Magneto-Hydrodynamics

NGC New General Catalogue – Dreyer's catalogue of 7840 *nebulae*, from 1881

NVSS The NRAO VLA Sky Survey, a 1.4 GHz continuum survey of the entire radio sky north of -40 deg declination, published by Condon et al. in 1998

POSS Palomar Observatory Sky Survey

RGB Red, Green, and Blue colour model

RVB Red, Visible, and Blue bands of the Johnson's UBVRI system

SDSS Sloan Digital Sky Survey

TDG Tidal Dwarf Galaxy

UGC Uppsala General Catalogue of 12921 galaxies, first published by Nilson in 1973

VATT Vatican Advanced Technology Telescope

VLA the Very Large Array radio interferometer near Socorro, USA

The term *inter-* refers to the matter and structures *outside* of an object, whereas the term *intra-* refers to matter and structures *inside* it. In the case of the ring galaxies, *inter-ring* refers to the area between the ring structure and the galaxy center, while *intra-ring* refers to the interior of ring structure.

Part I

CURRENT STATE OF THE KNOWLEDGE

In the first part of this dissertation, poor systems of multiple galaxies are introduced. Their basic properties and state of the knowledge are described. Then, magnetic fields in galaxies and beyond them are briefly characterised.

1 INTRODUCTION

1.1. GALAXY SYSTEMS

Even before they were properly identified, galaxies were known to exhibit tendency of pairing, grouping, and clustering. The earliest accounts of a discovery of such multiple systems can be traced down to 1781, when Pierre Mechain directed the tube of his telescope towards one of the *nebulae* he has been studying together with his colleague Charles Messier, namely, M51. What Mechain discovered is referred to as the first account of a multiple galaxy system: the simplest one, a galaxy pair (Messier, 1781).

For M51 being a tight, nearby pair it was easy for the connection between its members to be revealed. With more numerous systems, the galaxy groups, it was not that simple. Those nearby ones, available for the contemporary observers to be detected – like the Leo Triplet – are comprised of angularly distant objects, and so their identification as related objects was beyond the reach of 18^{th} century astronomers. Therefore, only with the advent of more sophisticated instruments it became possible to discover the first galaxy group. This finding is attributed to Èdouard Jean-Marie Stephan, who in 1877 reported discoveries of numerous *nebulae*, among them four very faint ones in the Pegasus constellation (Stephan, 1877). Later, a fifth one – also discovered by Stephan, but not resolved from one of those four – was co-opted to the original ones and henceforth is this group known as the Stephan's Quintet.

However, these early records did explore neither the reasons that lie beyond the mutual proximity of group members nor the physical processes that are spawned by it. In fact, the astronomers were simply unable to do so, as it was even impossible to judge whether a given galaxy is indeed connected to its neighbours, or is it merely a projection effect. There were no reliable methods of estimating the cosmic distance to the *nebulae* known at that time. Most of all, it is doubtful if such a question would be even posed, as galaxies – still referred to as *nebulae* – where believed to be entities residing *inside* the Milky Way, not its distant analogoues. The concept of the *island Universe*, proposed more than a century earlier by Immanuel Kant (1755), was not very popular in those times. As a result, there was no straightforward reason to investigate multiple galaxies.

A spark to initiate studies of the galaxy interactions was set by the well known Great Debate between Harlow Shapley and Heber Curtis. In this debate, the concept of the *island Universe* was defended, and soon after it, observational results proving this theory were presented by Edwin Hubble (1926). Knowing that the galaxies – the term *nebulae* become quickly restricted to gaseous objects – are systems like our own, and like our own galaxy, they are not solid bodies, astronomers turned their attention into the galaxy interactions. Swedish astronomer Erik Holmberg was the pioneer of this type of the studies. Holmberg, who dedicated his scientific career to the study of galaxy systems, was the first one to present a scientific article describing them, in 1937 (Holmberg, 1937). He has also addressed the nuances of studying multiple galaxies, like the need to distinguish objects angularly grouped from those physically connected. This milestone work was soon ensued by catalogues of interacting and multiple systems, out of them most known being those by Boris A. Vorontsov-Velyaminov (first published in 1959) and by Halton Arp (1972). Plenitude of endless forms most beautiful that interacting galaxies can evolve into began widely known, and it then become noticeable, that many – if not most – of the galaxies seem to bear evidence for interactions they experienced during their evolution.

1.2. THE REASONS BEYOND THIS THESIS

One of the best known articles concerning tight systems of multiple galaxies is the study presented by Paul Hickson in 1982. Hickson surveyed red optical plates of the Palomar Observatory Sky Survey (POSS) to identify dense, low-number groupings of galaxies. He published a list of 100 objects, later referred to as the Hickson Compact Groups (HCG). Despite some of the galaxies being erroneously connected with objects lying either in foreground or background, most of the HCG's constitute systems of objects indeed gravitationally bound to each other. High density and enormous amounts of matter and energy involved in tidal interactions in such objects causes plenitude of activities with strength and occurrence frequency not seen in isolated, field galaxies, or more loose system. As Hickson recollected in his 1997 paper, [...] *Most compact groups contain a high fraction of galaxies having morphological or kinematical peculiarities, nuclear radio and infrared emission, and starburst or active galactic nuclei (AGN) activity. They contain large quantities of diffuse gas and are dynamically dominated by dark matter. They most likely form as subsystems within looser associations and evolve by gravitational processes. Strong galaxy interactions result and merging is expected to lead to the ultimate demise of the group. Compact groups are surprisingly numerous, and may play a significant role in galaxy*

evolution [...] (Hickson, 1997). This is basically what drives subsequent generations of astronomers into the study of tight systems: the abundance of different phenomena.

One thing that is missing in Hickson's words is the role and importance of the magnetic field. So it is with the observational evidence, case or survey studies: only a handful of detailed papers on this topic have been published. This is mostly due to the technical problems that intergalactic magnetic fields cause to the willing observers. Primordial magnetic fields need to be amplified to break through the detection threshold; this is, in spiral (and, as discovered recently, also in irregular) galaxies, done by the MHD dynamo process. But this mechanism is not eager to start in the intergalactic medium, where neither strong rotation, nor shear is present. Furthermore, even if there is magnetic field frozen into the gas that was torn from the host galaxy, if it is to be detected, there needs to be a source of synchrotron radiation. Synchrotron radiation from the cosmic magnetic fields manifests as radio emission. A supply of charged, relativistic particles that can be accelerated in this magnetic field is needed, and as such particles are mostly a result of the powerful supernovae explosions, there should be massive stars present – which rather do not travel out of the cosy galactic disks.

But is there really a need to study of these intergalactic magnetic fields? Is there a point in devouring resources and manpower in a virtually hopeless projects, that could be used in different, more promising ones? Are there any arguments in favour of such difficult study? My answer is simple – yes, because it turns out that the situation is not as dreary as it could look. First of all, the magnetic field is an excellent tracer of the gas flows, its direction indicators (the so-called *polarisation B-vectors*) precisely following the escaping gas. But there is a much more pronounced reason for studying the magnetic field out of galaxies: it is its role in the dynamics of the gas. It is widely known that the energy of the magnetic field is large enough for it to play an important, non-negligible role in the dynamics *inside* the galaxies. Considering then gas that has been freed from the gravitational bond of the galactic disk, it is easy to see that intergalactic structures depend on the magnetic field much more than the intra-galactic. Therefore, overall understanding of the configurations, morphologies and phenomena that are found in interacting systems is possible only should the magnetic field influence be included. Last but not least, investigating structures where the magnetic field acts so profoundly yields an unique possibility to learn more about itself. That can not be done while restraining oneself to the intra-galactic studies only. In general, the intergalactic magnetic field can be considered as an excellent laboratory of cosmic plasma physics, with the physical con-

ditions and spatial scales of extent not accessible on Earth.

With this thesis I would like to summarise the case studies of some of the iconic tight pairs and groups of galaxies that I have undertaken during my PhD studies. Together they conclude as follows: *Wherever are the intergalactic magnetic fields found, they tend to play a significant role in the evolution of the system. And these are the tidal tails that give a very striking hint in the search for the ISM phase to which may be the magnetic field bound*.

2

MAGNETIC FIELDS IN GALAXIES AND BEYOND

2.1. PHYSICS OF COSMIC MAGNETIC FIELDS

2.1.1. *Origin and amplification of cosmic magnetic fields*

Little is known why are the cosmic magnetic fields present. What is generally accepted is that the fields observed today are a result of an amplification of the primordial ones. A source or mechanism that produced these primordial structures is still debated. Among possible explanations, thermal plasma oscillations (Schlickeiser, 2012), Biermann battery (Biermann, 1950), or Weibel instabilities (Lazar et al., 2009) were proposed. No matter the mechanism chosen, it would result in producing a magnetic field of a pikogauss strength. Such a magnetic field could be then amplified by the dynamo processes that operate on these seed fields. This mechanism not only amplifies, but also orders the previously random magnetic field. Small-scale dynamo mechanisms are able to amplify the magnetic field to microgauss strengths (Subramanian, 2008).

The most common, large-scale field amplification mechanism is the α–ω dynamo. It transfers the mechanical energy of turbulent gas motions and differential rotation into the magnetic one with the help of magnetic diffusivity (Parker, 1979). Unlike the small-scale ones, this mechanism is efficient in producing large-scale, regular magnetic fields that are found in spiral galaxies in a cosmologically acceptable amount of time. The galactic-size extent of coherence achieved is the main difference between these two mechanisms. They can co-exist together, with the small-scale one playing the role of a preamplifier, and the large-scale one being a method of ordering.

Originally the dynamo action has been believed to operate only in spiral galaxies, as they provide crucial conditions for this mechanism to work effectively. This was not expected for the irregular ones. However, from the observational works of Chyży and Klein (eg. Klein 1993, Chyży et al. 2000) it was clear that there are examples of large-scale, regular fields in dwarf galaxies. These magnetic fields can be a result of the so-called fast dynamo action (Siejkowski et al., 2010, 2014, and references therein). This mechanism, driven by the cosmic rays (from random supernovae explosions), is able to produce a large-scale magnetic field even in the presence of low shearing rate and slow rotation

of the medium.

Depending on the initial conditions and outcome of the amplification, different modes of the magnetic field can result from dynamo action. This implies also, that disks and halos of galaxies can exhibit different magnetic morphologies, as different modes were the dominant ones in each of these structures. Nevertheless, usually the global symmetry is present and reflects the mode that has been dominating throughout the whole system. Also, magnetic field tends to retain signs of its origin even if transported from one area into another through outflows.

2.1.2. *Methods of observing and studying galactic magnetic field*

There are two historically common methods used to observe the galactic magnetic fields. The first one of them is polarisation of optical and infrared emission. If there is magnetic field perpendicular to the line of sight to a distant star, and the dust grains also are oriented perpendicular to the field lines, the light becomes polarised due to the spatial differences in extinction level (Davis & Greenstein, 1951). This method was used for the first detection of magnetic field in a nearby galaxy (for M31, Hiltner 1958). However, its applicability is restricted only to regions constantly illuminated by stars, so it has no use for the star-devoid intergalactic areas.

The second method is the most used one. It relies on the fact that charged particles that undergo gyration in magnetic field manifest as radio emission with a specific spectrum (Elder et al., 1947). If a galactic – or intergalactic – structure is magnetised, electrons supplied eg. by the supernova emission will interact with the magnetic field perpendicular to the line of sight and cause emission of a radio wave. Both the frequency of emission maximum and lifetime of the emitting electrons depend on the strength of the magnetic field involved and on their energy. From the initial energy spectrum of these electrons one can derive the spectral index (and vice-versa), a parameter that describes the slope of the power-law distribution that reflects the dependence of the emission intensity with emitting frequency (Pacholczyk, 1973).

Derivation of the strength of the magnetic field from the radio emission is possible. This is usually done under the assumptions of equipartition of the magnetic field and cosmic ray energy density, or from the minimum energy formula (Beck & Krause, 2005). The equipartition is widely accepted and observationally tested to with-

stand for spatially extended, evolved population of electrons. The lower end constraints for its applicability are usually taken as several hundreds of parsecs and several millions of years (diffusion length and acceleration timescales for the cosmic ray electrons – see Beck & Wielebinski 2013). The minimum energy formula generally gives lower estimates than the equipartition assumption (Beck & Krause, 2005).

2.1.3. *Polarisation of the synchrotron emission*

From the theory of synchrotron emission, one can expect the radio emission to be highly linearly polarised (Elder et al., 1947). However, the intrinsic level of polarisation is observed as a much reduced one, as spatially extended telescope beam averages all fluctuations and changes within itself – both along the line of sight and in the sky plane. Furthermore, the degree of polarisation can be reduced also by Faraday effects, or by the existence of thermal emission (but the latter effect is not *physical* in its origin – it's just that as there is additional, thermal flux in the studied area, the ratio of the polarised to total intensity is lower). The large-scale distribution of polarised magnetic field allows to distinguish if it is isotropic, or not. Turbulent fields are unpolarised and isotropic, while regular ones are polarised and anisotropic – and signify the dynamo process. However, there is an intermediate form, the ordered one – a turbulent field that has been stretched, or squeezed, developing one dominant direction of the magnetic field. The difference between ordered and regular magnetic fields can not be told on the basis of their orientations due to the 180° ambiguity. Faraday effects can be used do disentangle these two. Coherency of a magnetised matter results in non-zero values of the Rotation Measure, whilst stretched turbulent one has locally different values of the Rotation Measure and as a result, its average, large-scale value is equal to zero, as it happens for the totally unordered fields.
Unfortunately, the Faraday effects that are useful in determination whether the field is or not genuinely regular are also problematic for polarisation studies. Polarisation would be best observed at lower frequencies, where losses of relativistic electrons due to ageing are not as significant as at the higher ones. However, Faraday depolarisation becomes much stronger in this regime and thus usage of classical techniques of observations is limited. A promising solution is given by the Rotation Measure Synthesis Method (Brentjens & de Bruyn, 2005), but for it is a novel one, there are no accounts of its successful use in the intergalactic medium of a galaxy pair or group.

The first studies of the galactic magnetic field where that of optical polarisation. M31 was the first one to have been studied in this manner (Hiltner, 1958). Since that study, a comprehensive image of diverse galaxies hosting magnetic fields has been created. The mean value for the total equipartition magnetic field that is found in spiral galaxies is equal to $9 \pm 1.3\,\mu$G (Niklas, 1995). A newer study of bright objects by Fletcher (2010) gives app. $17 \pm 3\,\mu$G. This refers to the total field, averaged over all the directions and areas of radio emission in a given galaxy. In particular structures magnetic field strength might be even higher. In the arm regions of spiral galaxies, values of 20-25μG are not unusual (Fletcher et al., 2011). The absolute records of the magnetic field strength in normal galaxies are held by the rapidly star-forming centers of spiral galaxies, where several tens of μG can be expected (Beck et al., 2005). The highest value measured is $98\,\mu$G achieved in the central region of starburst galaxy M82 (Adebahr et al., 2013). In other galaxies, however, magnetic fields are by order of magnitude weaker: objects of moderate star formation, like M33 galaxy, host magnetic field of a few μG (Tabatabaei, 2008). For the regular component, the maximal local values are equal to $8\,\mu$G (in the so-called magnetic arms of NGC 6946, Beck 2007), and typical values are of 1–5 μG.

How important is the magnetic field in galaxies? Beck & Wielebinski (2013) compile a long list why magnetic fields are crucial for the galaxy evolution. Among the different roles magnetic fields play one would find influence on the dynamics of ISM and gas in galactic arms, as they affect the properties of shocks in spiral density waves. They are a major stabiliser, both in galaxy disks (where they balance the disk pressure) and in gas clouds. In the latter ones, they act as moderators of the star formation (at the same moment being their initiators). The dynamo mechanism, known for its role in magnetic field amplification, can serve as a heat and turbulence source in galaxies that lack both of them. There is also a hint for their role in driving galactic outflows. To shortly summarise, Beck & Wielebinski (2013) write: *Understanding the interaction between the gas and the magnetic field is a key to understand the physics of galaxy disks and halos and the evolution of galaxies*. This is a very clear indication how significant the magnetic fields are.

One last important remark concerning magnetic fields in galaxies is that due to the presence of star formation regions, significant fraction of radio flux at certain areas may be of thermal origin. This com-

ponent has to be ruled out before any estimations of magnetic field properties can be made. Two possible methods have been developed to solve this problem. One of them uses star formation indicators like dust, or Hα emission to estimate and subtract the thermal contribution (eg. Deeg et al. 1997, Calzetti et al. 2007), the second one uses data from many radio frequencies to estimate the thermal fraction basing on the radio spectrum alone (Niklas, 1995). Both of these methods rely on the quality of the data and include, to some extent, an element of speculations.

2.3. What was previously known about the magnetised intergalactic medium?

As already said in Chapter 1, intergalactic magnetic fields rather did not attract much attention. The first paper to report extended emission from interacting galaxy systems is that of Stocke et al. (1978), who report seven pairs of galaxies (out of 603 surveyed) that show radio emission larger in extent than the optical size of these systems. A rare and very neat survey was done by Drzazga et al. (2011), who did a study of the evolution of magnetic field in merging galaxies, showing that the strength of the magnetic field in an interacting system increases as it evolves through the Toomre Sequence (Toomre & Toomre, 1972) towards its ultimate demise and rebirth as a supergalaxy. One very important conclusion of Drzazga's article is that the magnetic field (and radio emission, through which it manifests) is a much more sensitive tracer of the ongoing interactions than the optical data that were originally used to define the Toomre's sequence. Another conclusion is that amplified magnetic field can be expected for objects that are undergoing interactions; during the process, it grows to app. 15 μG as it passes the weak interaction state, reaching more than 25 μG during the nuclear coalescence, and afterwards diminishing to only a few μG as a post-merger object. Unfortunately, due to the scarcity of radio data for galaxy groups, none of them could have been included in this study. Also, only the objects for which polarised emission was detected were analysed, as study of the evolution of regular component of the magnetic field (which follows a similar path throughout the interaction) was intended.

Several case studies of interacting systems of galaxies have been also published. A good summary of the efforts undertaken on multiple systems is given by Beck & Wielebinski (2013). Beck & Wielebinski (2013) first mention the case of the Antennae Galaxies. This evolved pair of galaxies is undergoing final steps before it merges into one object. Chyży et al. (2004) has shown that heavily distorted, strong magnetic fields can be found, mostly in one of the tidal tails, which

is a remnant of a spiral arm of one of the colliding objects. Another example are the "Taffy" pairs of galaxies. They are pairs of spiral galaxies connected by a bridge of polarised radio emission, a rather rare occurrence. Condon et al. (1993) has presented results from 1.49 and 4.86 GHz VLA observations of a galaxy pair UGC 12914/15. The genuine morphology of the radio emission gave rise to the nickname of this pair, the "Taffy". Several years later, discovery of a second similar system was announced Condon et al. (2002). This one was notable for a different orientation of the magnetic field, detected by Drzazga et al. (2011), and later investigated by Vollmer et al. (2012).

Apart from pairs, several richer systems are mentioned by Beck & Wielebinski (2013). A handful of examples from the Virgo Cluster are presented, showing effects of interaction between them themselves and the intra-cluster medium. Little is, however, known about the galaxy groups: interaction effects in Leo Triplet's spiral galaxy NGC 3627 were studied by Soida et al. (2001). The last example is the Stephan's Quintet. For the study of this object is a part of this thesis, I will now restrain myself from describing this system, leaving it to a more detailed account in Chapter 3. Nevertheless, such a situation clearly shows how strong is the need for studies of the magnetic fields in galaxy groups.

Another study relevant for the topic of intergalactic magnetic field was made using the GMRT, by Giacintucci et al. (2012). These authors have investigated GMRT data for a handful of galaxy systems that are known for hosting AGNs. Extended radio emission was detected in a number of interacting systems, eg. for HCG 15, one of the not numerous HCG's that show extended continuum emission in the NVSS (Kuśper, 2006). The survey study by Kuśper (2006) provides a very valuable insight to the galaxy groups, with a potential to be used as list of compact galaxy groups that demand radio observations. Unfortunately, it is just a catalogue of radio emission without any inferences drawn on its parameters (except for a general determination of flux values) and has not been made publicly available in a scientific journal – it is only accessible through the master's thesis archive. What should be mentioned here is that the paper by Giacintucci et al. (2012) is one of the signs of a rising interest in combined radio–X-ray studies of galaxy groups in the last years, visualised also by articles like Gastaldello et al. (2011), or Vrtilek et al. (2013). However, here the radio emission is rather a tracer, than an equally-righted part-taker of the studied processes. Therefore, properties of the magnetic field are not investigated in these works. Generally, by the time my PhD studies have started, there were no detailed attempts to study magnetic

fields inside a galaxy group, whereas the studies of tight pairs were rather scarce and usually focused on the properties of the member objects, not on the intergalactic component.

For the consistency I note the fact that more abundant systems of galaxies, the galaxy clusters, are objects of frequent radio studies. Here investigating the magnetic field properties is one of the basic scientific activities. However, much different energies and masses are present in the galaxy clusters, interactions are violently stronger, and therefore the conditions in the IGM are dramatically different than in smaller systems. This difference places the study of clusters beyond the scope of this dissertation.

Part II

ON THE EXISTENCE AND IMPORTANCE OF MAGNETIC FIELDS IN TIGHT PAIRS AND GROUPS OF GALAXIES

Second part of this thesis is a summary of my scientific efforts undertaken to explore the intergalactic magnetic fields. Relevant publications are being recalled and recapitulated, and on their basis are the final conclusions drawn.

3

SUMMARY OF THE PUBLISHED ARTICLES

3.1. PROBING THE INTERGALACTIC MEDIUM OF AN ICONIC GAS STREAMER: LEO TRIPLET AT 2.64 GHZ

Based on Nikiel-Wroczyński, B., Soida, M., Urbanik, M., Wezgowiec, M., Beck, R., Bomans, D. J., Adebahr, B., 2013, A&A, 553, 4

In my first study, I decided to search for hints for the intergalactic magnetic fields in a nearby galaxy group, the Leo Triplet. Together with the M81/82 group these objects constitute the nearest galaxy groups to the Milky Way. Leo Triplet is best recognised for a giant, 140-kpc long tidal tail that extents eastwards from the main galaxy of the system, NGC 3628. This tail has been first detected in the optical regime (Zwicky, 1956), but the real interest in its study was because of the neutral gas counterpart, reported by Haynes et al. (1979). Since its discovery, analogous structures have been found in other systems (eg. in Arp 143, Appleton et al. 1987, or FGC 1287, Scott et al. 2012. Such objects show that the galactic gas can be transported far away from the host galaxy whilst it is exposed to the tidal interactions. Search for a magnetised counterpart for such a tail might be promising – especially, as the Leo Triplet galaxy NGC 3627 shows outstanding magnetic field morphology peculiarities.

The Leo Triplet was observed at 2.64 GHz using the Effelsberg telescope. Unfortunately, despite the excellent sensitivity to extended radio structures provided by this instrument, no significant intergalactic, magnetised structures have been found. The extent of the galactic disks of individual galaxies was not larger than at higher frequencies, at which they have been previously studied (Soida et al., 2001; Dumke & Krause, 1997). Polarised emission was also not detected, despite higher sensitivity in polarised intensity. Upper constraints for the magnetic field between galaxies – 2.8 μG – leave not much space for yet undetected magnetic field. Especially, the maximal undetected magnetic field energy was estimated as two orders of magnitude lower than in the Taffy Galaxies (Condon et al., 1993, 2002), or Stephan's Quintet (see Section 3.2.). This has clearly shown that for the Leo Triplet, detectable intergalactic magnetic field is not present, and therefore, no matter how trivial does such a conclusion sound, it can not play any role in the dynamics and evolution of the gaseous tails.

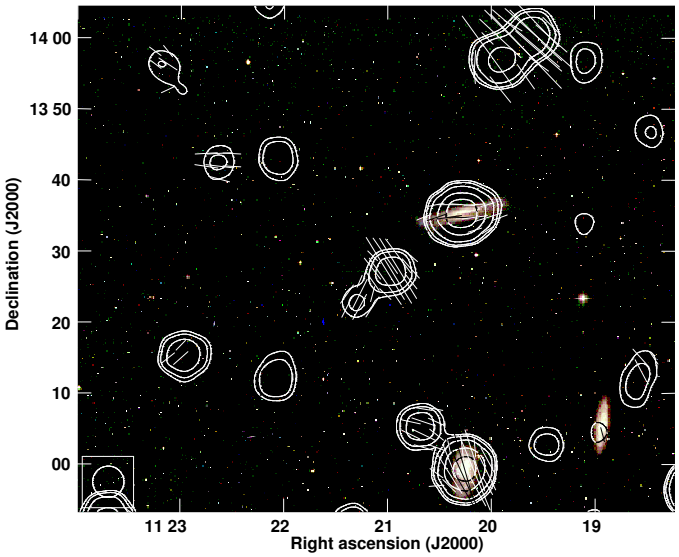

Figure 1: Leo Triplet: Contours of the 2.64 GHz radio emission (with magnetic field directions indicated) overlaid on a RGB mosaic made from the DSS RVB bands.

Despite the failure to detect extended, intergalactic magnetised structures, one remark has been made: there was a hint for a magnetic field in one of the HI clumps, located at the tip of the tail. The estimated magnetic field was not very strong (3.5 μG), but still similar to what is found in dwarf galaxies (Beck & Wielebinski, 2013). However, this proposed detection did not stand the trial of the time, and in a subsequent side study it has been confirmed that the magnetic field of this object is in fact connected to a background source, and its assignment to the dwarf was only because of the large beamsize of the Effelsberg observations. Nevertheless, this remark is worth noticing as it gave an impulse to what became a discovery of the most proximate TDG, as the discussed paper was the first one to propose a possible object of this type in the Leo Triplet.

3.2. WHERE FIVE WORLDS COLLIDE: THE MAGNETISED INTRAGROUP MEDIUM OF THE STEPHAN'S QUINTET

Based on Nikiel-Wroczyński, B., Soida, M., Urbanik, M., Beck, R., Bomans, D. J., 2013, MNRAS, 435, 149

Already aforementioned in Chapter 3, the Stephan's Quintet is the best known galaxy group. History of its study reflects well the evolution of the understanding of galaxies and their properties. While discovered in 1877, it was known just as *four excessively faint, excessively small nebulae* (Stephan, 1877). The fifth member of the Quintet

was also discovered, however, it's membership was not attributed for a long time – it was first suggested by Arp & Kormendy (1972). Originally a triplet of galaxies (NGC 7317, NGC 7318A, and NGC 7319) that underwent a close passage with NGC 7320C (Moles et al., 1997, 1998), this galaxy group is currently experiencing another collision. Galaxy NGC 7318B is infalling into the group, causing compression of the group halo and giving birth to one of the most extended shockwaves in the known Universe. The brightest galaxy in the area of the Quintet – NGC 7320 – is a foreground interloper, which, by chance, looks as its size is similar to other group members. In fact, it is a dwarf spiral galaxy, located not much further than the Leo Triplet (Moles et al., 1998).

What drew particular attention to this object is the discovery by Xu et al. (2003). These authors presented a VLA study of the radio emission from this galaxy group at 1.49 and 4.86 GHz. What they have found is a large ridge of intergalactic emission between the galaxies that form the Quintet, most likely representing an intergalactic shock caused by the infall of NGC 7318B. However, sparse configuration of the interferometer – necessary for a high-resolution study – yielded no detection of polarised emission, as well as the extended halo. Aptly, there was still solace, as the NVSS data (Condon et al., 1998) yields hints for polarised emission right in the position of the ridge reported by Xu et al. (2003).

My Stephan's Quintet datasets consisted of both VLA and Effelsberg observations. Maps of the radio emission – both of total power and polarised intensity – were acquired at 1.49, 4.86 and 8.35 GHz. Out of these spectral windows, the middle one – at 4.86 GHz – offered both very high sensitivity and good angular resolution. With these data it was easily possible to reveal the plenitude of different, magnetised structures inside the galaxy group. The target of the study – a ridge of intergalactic radio emission – is easily visible between the galaxies. Worth noticing is the energy density of its magnetic field of $0.5 \pm 0.15 \times 10^{-11}\,\mathrm{erg\,cm^{-3}}$. If the energy equipartition between magnetic field and cosmic rays is assumed, it turns out that the total energy density that can be attributed to the magnetic field is comparable to that of the thermal gas (estimated from X-ray data, O'Sullivan et al. 2009). This, in turn, implies that the dynamics of intergalactic gas is significantly dependent on the magnetic field, and understanding of the past history as well as prediction of the future evolution is possible only if taking magnetic forces into account. The total magnetic field strength in this regions is equal to $11 \pm 2.2\,\mu\mathrm{G}$ – a value higher than the average one for spiral galaxies (which is $9 \pm 1.3\,\mu\mathrm{G}$, as given by Niklas 1995). The intergalactic ridge of emission is no-

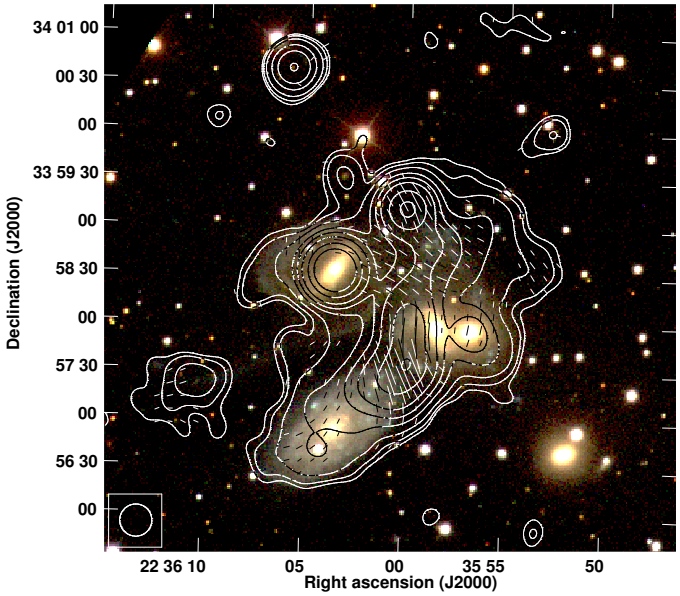

Figure 2: The Stephan's Quintet: Contours of the 4.86 GHz radio emission (with magnetic field direction, corrected for the foreground Faraday effects, indicated) overlaid on a RGB mosaic made from the SDSS i',r',g' bands.

ticeable also because the emission is polarised; the strength of the ordered magnetic field is equal to $2.6 \pm 0.8\,\mu$G. From the study of depolarisation hints can be acquired, that it is not only ordered, but genuinely regular. This result suggests that the magnetic field in the IGM was stripped from the galaxies, and then re-regularised in the intergalactic space. Also, the magnetic forces still govern the gas flow, even in the presence of a powerful shock front.

Apart from the intergalactic shock, a handful of other phenomena connected to the magnetic field can be seen. Among them, the magnetised idal dwarf galaxy is definitely the most interesting one. The magnetic field it possesses is weaker than that found between the galaxies ($\approx 6.5\,\mu$G), but still, such a value is higher than it would be expected for a dwarf galaxy. It also shows a noticeable ordered component, due to the high polarisation degree. What brings the attention is that, so far, there are no other TDGs with magnetic field detected, yielding this object the only one of its kind. Additionally, as there are no signs of magnetic field in the tidal tail that gave rise to this small galaxy, it becomes clear that there must be some mechanism of amplification going on inside this object. And as such an object has a rather low mass, it might constitute the smallest galaxy that is able to host the MHD dynamo – possibly altering the understanding of this process.

Careful analysis of the radio data reveals two other extended, intergalactic structures. First of them becomes visible only after the directions of the magnetic field are corrected for the foreground Faraday rotation – it is a bridge of polarised emission between two galaxy members that formed the original triplet millions of years ago, namely NGC 7319 and NGC 7318A. This bridge resembles the one from the Taffy pairs quite well. Probably its role and importance is the same – it is a result of an ongoing interaction accompanied by transport of the magnetised material from one galaxy into another. The second intergalactic structure is an extension of the radio emission envelope at the southern end of the group, where the interloper galaxy NGC 7320 is located. The scheme of the polarisation B-vectors here suggests that the magnetic field can be transported through this entity into the intergalactic area *outside* the member galaxies. These all findings clearly render Stephan's Quintet the most outstanding example of intergalactic magnetic fields in a galaxy group. From the study of this galaxy group only one can see the importance of the magnetic field in the overall picture, its role as an interaction tracer, and the significance of intergalactic magnetic field studies for the understanding of the cosmic magnetic fields physics.

3.3. Collisional ring of radio emission: galaxy pair Arp 143

Based on Nikiel-Wroczyński, B., Jamrozy, M., Soida, M., Urbanik, M., 2014, MNRAS, 444, 1729

Collisional ring galaxies are rather scarce objects. They are a product of a collision of two galaxies, in which one of them – usually, a compact one – passes through another one, disrupting its original structure. As a result of such collision, a shockwave is produced that propagates outwards in the disk, similarly to a ripple on water. This causes amplification of the stellar formation in a toroidal area – causing the galaxies to manifest in the visible regime of the electromagnetic spectrum as luminous rings. After a certain amount of time – measured in tens of Myrs – the spiral structure begins to restore, but the toroidal wave can still remain visible (Zwicky, 1941). Arp 143 is one of the most interesting collisional rings, as it is accompanied by a giant neutral gas tail – a result of the close passages and collision with the compact member of the pair, NGC 2444. This collision took place around 85 Myrs ago (Beirão et al., 2009) and the pre-collisional structure of NGC 2445 has not yet been restored.

Similarly to the case of Leo Triplet, the main goal was to investigate possible magnetisation of the gaseous tail. In order to do so, GMRT observations were performed – especially that at 240 MHz, where the primary beam is large enough to capture the giant neutral gas tail. Un-

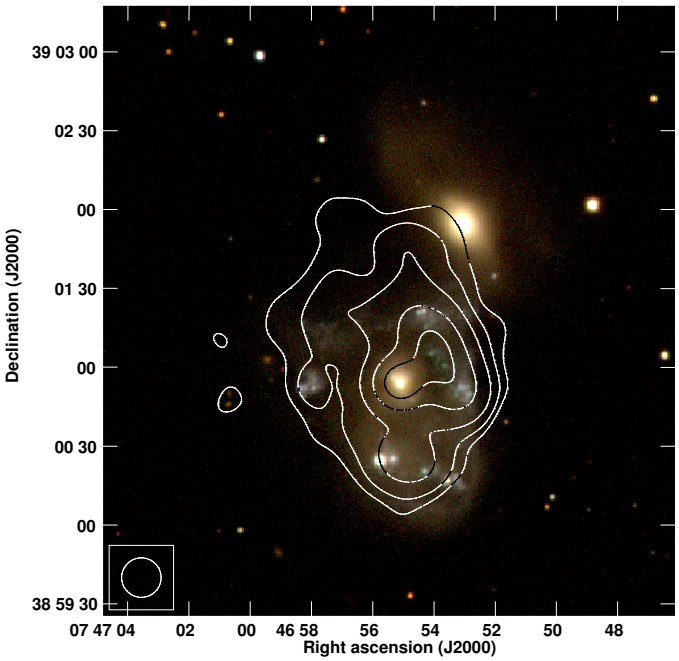

Figure 3: Arp 143: Contours of the 612 MHz radio emission overlaid on a RGB mosaic made from the SDSS i',r',g' bands.

fortunately, similarly to case of Leo-Triplet, a direct detection was not made. Upper constraints for the undetected magnetic field vary depending on the pathlength of the supposed-to-be-emitting medium, but if one assumes cylindrical symmetry of the tail, the undetected magnetic field is then not stronger than 5 μG. No matter the fact that it is higher than upper limit for the Leo Triplet, complete lack of any radio structures that might coincide with the gaseous tail is rather clear.

Searching for magnetised component in the tidal tail was not the only one reason to study this object. The second one was that nothing was previously known about the configuration of the magnetic field in such galaxy. A review article on collisional rings (Appleton & Struck-Marcell, 1996) mentions an unpublished study on several collisional rings, but details are not provided. In my study, usage of the GMRT data together with the good quality VLA observations allowed to construct a multifrequency image of the radio emission from the collisional ring galaxy. It turned out that radio emission concentrates in the luminous center – probably undergoing starburst activity – and in the collisional ring. The interring medium is radio-quiet at higher frequencies, suggesting older electron population, that has aged significantly enough to become undetectable. In the intra-ring area, the emitting entities are of low – several Myrs – spectral age, clearly indi-

cating connection to the propagating shockwave. The magnetic field is strong, reaching strengths of 10–12 μG, suggesting amplification in the areas of recent star formation. The second member of the pair is radio silent.

Worth mentioning is that Arp 143 shows in general an asymmetry between its NW and SE sides. The SE one is much weaker and less pronounced both in the radio and optical regime, while the NW one is prominent, and the radio distribution ends with an intergalactic bridge – a unique structure not detected at any other frequency, that shows that the interaction between the pair' members is ongoing. Unfortunately, due to the sparse interferometric configurations – mandatory to obtain the 10-arsec resolution necessary to study this angularly small object – detection of polarised emission was impossible.

3.4. THE SIDE STUDY OF LEO TRIPLET: DETECTION OF THE MOST PROXIMATE TIDAL DWARF GALAXY

Based on Nikiel-Wroczyński, B., Soida, M., Bomans, D. J., Urbanik, M., 2014, ApJ, 786, 144

Leo Triplet was the target of my first study, and the conclusion was that apart from the TDG candidate, no intergalactic sources of radio emission can be found. The fourth paper constituting my dissertation explores the neutral gas distribution to find the evidence that this candidate is indeed authorised to bear the designation of galaxy. Whereas TDGs are no doubt interesting objects, and are inseparably connected to tidal interactions in multiple galaxy systems, detailed analysis of its physical properties is not a study of the intergalactic magnetic field sources. And as it was found using the higher resolution VLA neutral hydrogen data, the coincidence between the radio emission and gas distribution was just an effect of the large beamsize of both Effelsberg and Arecibo observations. However, there is one important conclusion for the intergalactic magnetic field studies that can be drawn basing on this article: should this TDG host magnetic field, it would be the second where it has been found. It wouldn't be very surprising to see a dynamo action here, as it is a massive one, with higher neutral hydrogen mass than the Triplet's member NGC 3623. But lack of detection retains the TDG in Stephan's Quintet the single one tidal dwarf that hosts and amplifies the magnetic field, opening a possibility, that there are two different classes of tidal dwarf galaxies magnetised, and unmagnetised. Nevertheless, even though the one in the Leo Triplet is unmagnetised, it is a very unusual member of its class, being very dim and HI abundant. Large velocity gradient (around 35 km/s), and visible detachment from the rotation of the tidal tail make this object one of the most certain detections of a TDG.

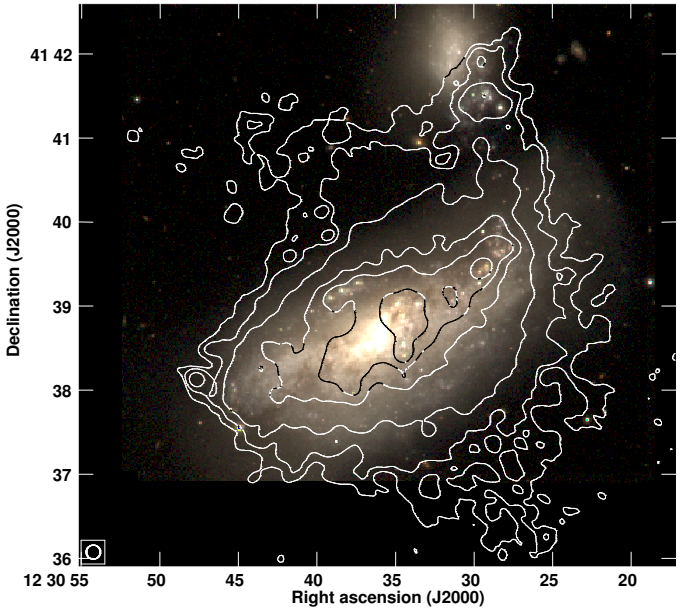

Figure 4: Arp269: Contours of the 4.86 GHz radio emission overlaid on a RGB mosaic made from the VATT RVB bands.

3.5. A MAGNETISED TAIL THAT DOES NOT FOLLOW THE NEUTRAL ONE: THE CASE OF ARP 269

Based on Nikiel-Wroczyński, B., Jamrozy, M., Soida, M., Urbanik, M., Knapik, J.,submitted to MNRAS on 10.06.2015

The last article included in my thesis focuses on one of the nearby galaxy pairs, Arp 269, also known as the Cocoon Galaxy – a nickname gained due to the ongoing collision between its members: small barred spiral NGC 4490 and dwarfish NGC 4485. The Cocoon Galaxy is best known for a symmetric, 60-kpc long neutral gas tail that extends northwest and southeast from the galaxy disk (Dean & Davies, 1975; Viallefond et al., 1980; Clemens et al., 1998). The origin of this tail as well as the multifrequency characteristics of this galaxy pair was investigated in a series by papers by Marcel Clemens and his colleagues (Clemens et al., 1998, 1999, 2000; Clemens & Alexander, 2002). My work was intended to search for any extension of the emission in the direction of the gaseous tail, and to study the age of the structures hosting magnetic field, like it was done for Arp 143 (Sect. 3.3.). To achieve this goals, I have performed sensitive GMRT observations at 612 MHZ and, what turned out to be a very fruitful, merged the interferometric data of Clemens et al. with the Effelsberg single dish data.

The most important result was achieved at 4.86 GHz. Whereas in the original data no extensions beyond the galactic disk are visible, the merged ones show a symmetrical distribution of radio emission outside of it. What is most striking is that the angle between the disk and the radio emitting extensions is different from that between the disk and the H I tail – providing a very clear suggestion that there are two outflows present in this galaxy pair. One of them consists of the neutral gas. It extends far into the intergalactic medium, but no continuum radio has been detected inside. The second one is much less pronounced, magnetised, and is not accompanied with an enhanced neutral gas density. This, in turn, supports the claim that magnetic field is *not* bound to the neutral gas – and any coincidence with an HI distribution would just mean that at least two gas phases – neutral one and the other, still unknown one, to which the magnetic field is bound to – are present in the same area.

The discoincidence between continuum and HI emission was an unexpected and most sound conclusion of this study, but apart from it some other interesting facts about NGC 4490/85 system were found, thanks to the plenitude and quality of the data.

4

CONCLUSIONS: WHAT CAN BE SAID ABOUT THE MAGNETIC FIELDS IN GALAXY PAIRS AND GROUPS?

The goal of this thesis was to show that intergalactic magnetic fields, where are present, may play significant role in the dynamics of the system, can be used as a useful tracer of past interactions, and yield information about the physics of the magnetism non-obtainable while restraining oneself to the study of intra-galactic magnetic fields. Below I summarise the results that confirm each of these statements.

4.1. CAN THE MAGNETIC FIELD PLAY A SIGNIFICANT ROLE IN AN INTERGALACTIC STRUCTURE?

This question is best answered by the study of the Stephan's Quintet. The intergalactic shock area, a product of a galaxy infall, is an entity for which estimation of magnetic, cosmic ray and thermal energy components is possible. It turns out that energy contained in the magnetic field is comparable to that of the thermal gas. This means that the *life of the system* – dynamics, evolution, morphology – can be understood, analysed and predicted only if the magnetic field is included into the consideration. The result acquired is important also because the magnetic field energy density estimated for the intergalactic medium of the Quintet is very similar to that calculated for eg. Taffy galaxies, Arp 143, or for the intergalactic bridge in Arp 269. In case of these galaxy pairs, thermal energy is undoubtedly lower, as there is no evidence for a large-scale shockwave (the wave that gives rise to the ring structure in Arp 143 is much less energetic and temperatures of 0.6 keV found for Stephan's Quintet are not expected there). This means that the thermal component would be much lower, and the magnetic field energy turns out to be even more important in these galaxy pairs.

4.2. HOW USEFUL IS THE MAGNETIC FIELD AS AN INTERACTION TRACER?

A non-negligible aspectof the magnetic field studies is that it is a good tracer of interactions. My works have revealed several structures, which can be best – or only – traced with the use of magnetic field. The intergalactic bridge between NGC 2444 and 2445 is a structure that was not detected in any other regime. Yet it is important, as it confirms an ongoing interaction between the pair members. So it is

with the magnetised tails of NGC 4490: hints for this outflows can be found only in the study of the continuum radio emission.

In case of Stephan's Quintet, the data allowed study of the ordered magnetic fields. Possibility of determining the magnetic field orientation resulted in detection of the intergalactic bridge between NGC 7319 and 7318A. Without this knowledge, it would not be possible to detect this structure, as the morphology of the intra-group matter of the Quintet is very complicated and bears signs of many previous interaction events. It should be emphasised here, that this bridge could be distinguished only when using the polarised intensity map – there are no obvious signs that could allow to distinguish this structure from the surrounding, total power radio emission. The claim that the magnetic field in the southern part is being pulled out from the intra-group area also bases on the alignment of magnetic field vectors, that seem to resemble an arc-like structure. Should the polarised intensity data be unavailable, the radio emission in the southern part could unhesitantly be attributed to the foreground galaxy.

4.3. What can we learn about the magnetic field itself while detecting it in the intergalactic medium?

4.3.1. *A prospect for the further study: unexpected areas of magnetic field amplification and regularisation*

Magnetic fields in galaxies are constantly being amplified, evolving thanks to the MHD dynamo process. Assuming fast dynamo action, this is an efficient mechanism and allows to explain the observed morphologies and strengths. However, it is rather believed that necessary conditions for this process to occur are met only in more massive galaxies – preferably spiral ones, or more dwarfish, but still not small and lighweight irregulars. Study of the Stephan's Quintet gives evidence that this belief might need to be altered. The magnetic field was detected in the TDG found in the tidal tail of NGC 7319. This lightweight object – the only known of its type visible in the radio domain – hosts magnetic field expressing hints of regularity. It might possibly be the most extreme case of a galactic object that maintains and amplifies the magnetic field. Even if this is the only object of its kind, this small galaxy might play an important role in defining the constraints for environmental conditions for the dynamo-like processes to take place. Worth mentioning is also the anisotropy of the magnetic field in the intergalactic ridge of radio emission. It can be just a mere effect of compression – a natural explanation for a shock area – but there are non-negligible hints for genuine regularity. Should it be the case, it would mean that the observed, magnetised

intergalactic structures might have been re-regularised during the interaction process.

4.3.2. *To which phase of the ISM is the magnetic field bound to?*

While surveying the neutral gas tails for the magnetic field, one can conclude that they might not be magnetised at all. Such a claim seems supported by my findings, and also by known works concerning other galaxy systems. For instance, many efforts have been undertaken to detect intergalactic magnetic fields in the intra-group medium of the nearby system M81/M82, but nothing was detected so far (Adebahr et al. 2013, also Adebahr et al. and Drzazga et al., priv. comm.). Careful study of the NVSS data (Kuśper, 2006) does not provide any signs of continuum counterpart of the neutral gas tail recently detected in HCG44 (Serra et al., 2012). However, as Martin Rees once said, *absence of evidence is no evidence of absence*. A proper scientific hypothesis is a falsifiable one, and to show that neutral gas tails are unmagnetised entities, a counterexample is needed. It is important to indicate here, that such a finding would be more than just revealing some new information about the tidal tails and intergalactic medium. It would be a very strong hint to which gas phase is the magnetic field connected to – or rather, to which it is *not related*.

In my studies of the Leo Triplet, Arp 143, and Arp 269 magnetic field has not been detected in the neutral gas tails. But Arp 269 might provide us with a very plausible counterexample mentioned above: an intergalactic extension that is magnetised and does not coincide with the neutral one. This suggests that the magnetic field might not be bound to the cold, neutral and dense component of the ISM, or at least there are more favourable environments for it. It should be emphasised here, that arriving at this conclusion was only possible whilst studying gas outflows, present in intergalactic systems.

4.4. THE FINAL WORD ON THE INTERGALACTIC MAGNETIC FIELDS

Four different objects have been studied, with an initial assumption to search for the magnetic field in the intergalactic areas. What was supposed to be the most favourable region to search for such phenomena turned out to be the unmagnetised one. Intergalactic magnetic field have been found between the infalling galaxies as well as betwixt original members of the Stephan's Quintet, where they compete with the thermal processes to lead the dynamics and evolution of the intragroup medium. They are tracing the ongoing interaction between NGC 2444 and 2445 and signify the passage of the toroidal shockwave that reminisces past collision. They escape from the galactic disk of NGC 4490, choosing strikingly different route than the neu-

tral gas. In the light of the analysed evidence, it can be clearly stated that wherever found, intergalactic magnetic fields leave the observers in awe, how important they can be to the whole systems and how bold conclusions can this frequently omitted in analysis of the evolution and scarcely studied phenomena yield. And, paraphrasing the famous words of Charles Darwin, *whilst galaxies have gone cycling on according to the fixed law of gravity, from so simple a beginning endless forms most beautiful and most wonderful of intergalactic magnetism have been, and are being, evolved*.

Part III

APPENDIX

The Appendix contains all five journal articles that have been used as a basis of this dissertation. All of them have been included in the default journal format.

A&A 553, A4 (2013)
DOI: 10.1051/0004-6361/201321089

Astronomy & Astrophysics

Radio continuum observations of the Leo Triplet at 2.64 GHz⋆

B. Nikiel-Wroczyński[1], M. Soida[1], M. Urbanik[1], M. Weżgowiec[2], R. Beck[3], D. J. Bomans[2,4], and B. Adebahr[2]

[1] Obserwatorium Astronomiczne Uniwersytetu Jagiellońskiego, ul. Orla 171, 30-244 Kraków, Poland
e-mail: iwan@oa.uj.edu.pl
[2] Astronomisches Institut, Ruhr-Universität Bochum, Universitätsstrasse 150, 44780 Bochum, Germany
[3] Max-Planck-Institut für Radioastronomie, Auf dem Hügel 69, 53121 Bonn, Germany
[4] Research Department "Plasmas with Complex Interactions", Ruhr-Universität Bochum, Universitätsstrasse 150, 44780 Bochum, Germany

Received 11 January 2013 / Accepted 14 March 2013

ABSTRACT

Context. The Leo Triplet group of galaxies is best known for the impressive bridges of neutral gas that connect its members. One of the bridges forms a large tidal tail extending eastwards from NGC 3628 that hosts several H I plumes and carries the material from this galaxy to the intergalactic space.
Aims. The magnetic fields of the member galaxies NGC 3628 and NGC 3627 show morphological peculiarities, suggesting that interactions within the group may be caused by stripping of the magnetic field. This process could supply the intergalactic space with magnetised material, a scenario considered as a possible source of intergalactic magnetic fields (as seen eg. in the "Taffy" pairs of galaxies). Additionally, the plumes are likely to be the tidal dwarf galaxy candidates.
Methods. We performed radio continuum mapping observations at 2.64 GHz using the 100-m Effelsberg radio telescope. We obtained total power and polarised intensity maps of the Triplet. These maps were analysed together with the archive data, and the magnetic field strength (as well as the magnetic energy density) was estimated.
Results. Extended emission was not detected either in the total power or the polarised intensity maps. We obtained upper limits of the magnetic field strength and the energy density of the magnetic field in the Triplet. We detected emission from the easternmost clump and determined the strength of its magnetic field. In addition, we measured integrated fluxes of the member galaxies at 2.64 GHz and estimated their total magnetic field strengths.
Conclusions. We found that the tidal tail hosts a tidal dwarf galaxy candidate that possesses a detectable magnetic field with a non-zero ordered component. Extended radio continuum emission, if present, is weaker than the reached confusion limit. The total magnetic field strength does not exceed 2.8 μG and the ordered component is lower than 1.6 μG.

Key words. galaxies: groups: individual: Leo Triplet – galaxies: interactions – intergalactic medium – galaxies: magnetic fields – radio continuum: galaxies – polarization

1. Introduction

Galaxy groups are known to contain large reservoirs of intergalactic gas (Trinchieri et al. 2005). The intergalactic matter is a subject to violent tidal interactions (Hickson 1982) caused by gravitational forces of the member galaxies. Studies of H I morphologies revealed that there is a variety of objects that contain outflows visible in the neutral hydrogen line (e.g. Williams et al. 1991; Yun et al. 1994; Stierwalt et al. 2009). There are two different types of intergalactic H I emission: "wells" and "streamers". Which of these is present depends on the compactness of the system. In compact groups, the gravitational forces prevent the gas from escaping from the intergalactic space between the galaxies, and the emitting medium is usually contained in a potential well between them (e.g. HCG 44, Williams et al. 1991, or the "Taffy" pairs of galaxies, Condon et al. 1993, 2002b; Drzazga et al. 2011). Conversely, loose groups are sometimes called "streamers", because the emitting gas – now weakly bound to the group members – forms bridges and tails that extend far into the intergalactic space, like in the M81/M82 group (Yun et al. 1994).

The magnetic fields can play a significant role in the evolution and dynamics of galaxy systems, because the energy densities of the thermal and magnetic components may be comparable. Not much is known about the magnetic fields in galaxy groups, however. Several studies were carried out in compact groups, especially in Stephan's Quintet. Xu et al. (2003) detected intergalactic nonthermal emission (thus an intra-group magnetic field) in that group. Our own studies (Nikiel-Wroczyński et al. in prep.) revealed intergalactic polarised emission between its member galaxies. The magnetic field energy density was determined to be approximately 5×10^{-12} erg/cm^3 – comparable to the thermal energy density estimated from X-ray observations (Trinchieri et al. 2003). Additionally, we found that the strength of the magnetic field of a tidal dwarf galaxy candidate SQ-B is comparable to that of normal spiral galaxies.

The origin of the intergalactic magnetic fields is lively debated and a variety of physical processes was proposed (e.g. reviews by Rees 2002; and Stone 2002). Usually, two scenarios are suggested: Kronberg et al. (1999) proposed dwarf irregular galaxies with strong winds that expell magnetic fields into intergalactic space (which was subsequently supported by numerical simulations by Siejkowski et al. 2010). Because these dwarfs are not always present in galaxy groups, the scenario of the production of the magnetic field in spiral galaxies and interaction-driven supply to the intergalactic space (as in the Antennae galaxies, Chyży & Beck 2004) is another possibility.

⋆ Based on observations with the 100-m telescope of the MPIfR (Max-Planck-Institut für Radioastronomie) at Effelsberg.

Table 1. Properties of the emission from the Leo Triplet sources at 2.64 GHz.

NGC	TP [mJy]	PI [mJy]	Pol. fract. [%]	Mean pol. ang. [°]	α^1	Tot. magn. field [μG]
3623	19 ± 2^2	1.3	7	10	n/a	3.5 ± 1
3627	299 ± 14	15	5	25	0.69 ± 0.14	11 ± 1
3628	364 ± 17	18	5	98	0.59 ± 0.15	9 ± 1.5
TDGc	5.6 ± 1.0	1.0	20	35	0.7 ± 0.3	3.3 ± 0.5

Notes. [(1)] Calculated between our 2.64 GHz observations and 1.4 GHz data from Condon et al. (2002a). [(2)] Background sources not subtracted (see Sect. 4.1 for details).

However, insufficient observational data make it impossible to distinguish whether one of these mechanisms is dominating or another explanation is needed. Likewise, little is known if magnetic fields in tidal dwarf galaxy (TDG) candidates are a common phenomenon. The properties and strength of these fields are scarcely explored. Thus, deep studies of various galaxy groups, of both streamer and compact types, are needed.

The Leo Triplet, also known as Arp 317 (Arp 1966), is an example of a nearby streamer group. With its distance of 15.7 Mpc it is among the nearest objects of this type. The group consists of three tidally interacting spiral galaxies, NGC 3623, NGC 3627, and NGC 3628. The galaxies are connected by bridges of neutral gas (Stierwalt et al. 2009; Haynes et al. 1979). The most prominent one is the tidal tail that extends eastwards from NGC 3628, which is visible also in the infrared at 60 and 100 microns (Hughes et al. 1991).

Since NGC 3627 possesses a perturbed magnetic field (see Soida et al. 1999, 2001 for details), the question arises if the field is being stripped from galaxies into the intergalactic medium. As a possible explanation of the unusual morphology of NGC 3627, including its magnetic field, a collision with a dwarf galaxy was recently suggested by Weżgowiec et al. (2012). The tidal tail of the Leo Triplet is known to host several H I clumps, spatially coincident with optical traces of star formation reported by Chromey et al. (1998), indicating that they might be TDG candidates. This could lead to the conclusion that both the intergalactic and interstellar matter of spiral galaxies in the Leo Triplet galaxy group can be influenced by dwarf objects via ram-pressure/collision heating and magnetic field enhancement. Therefore, studying TDG candidates becomes an important part of the studies of galaxy groups.

The proximity of the Triplet and its angular size of nearly 1° mean that it is best observed with a single-dish telescope. Such observations are characterised by high sensitivity to extended structures. This allows searching for traces of magnetic field in H I clumps – which constitute TDG candidates because they exhibit traces of stellar formation. Therefore we performed a deep mapping of the Triplet using the 100-m Effelsberg radio telescope at 2.64 GHz. Our results are presented and discussed below.

2. Observations

We mapped the Triplet in June 2012 with the 100-m Effelsberg radio telescope. Observations were performed around the frequency of 2.64 GHz, using a single-beam receiver installed in the secondary focus of the telescope. The receiver has eight channels and total bandwidth of 80 MHz. The first channel (central frequency 2604 MHz) was dropped due to the radio frequency interference (RFI). We performed 12 coverages with a size of $80' \times 80'$ each, scanned alternatively along RA and Dec. We used a scanning velocity of $120'$/min and a grid size of $2'$. The data reduction was performed using the NOD2 data analysis system. The maps were averaged and combined to reduce the scanning effects using the basket-weaving method (Emerson & Gräve 1988), yielding final Stokes I, Q and U maps. During the observations we used the radio source 3C286 to establish the flux density scale. The flux of the calibrator was taken from Mantovani et al. (2009). The polarisation was calibrated using 3C286 as well. We assumed no circular polarisation (Stokes V signal = 0). The polarised fraction from our observations is equal to $11.2 \pm 0.1\%$ and the polarisation position angle is $33° \pm 4°$ – consistent with the values given in the aforementioned article. The instrumental polarisation does not exceed 1%. The Astronomical Image Processing System (AIPS) was used to produce the distribution of the polarised intensity and the polarisation angle. The resolution of the final maps is $4'.5$ (half-power beam width).

The uncertainties of the integrated flux densities include a 5% uncertainty of the flux scale determination. The term "apparent polarisation B-vectors" used in this paper is defined as the observed polarisation E-vectors direction rotated by 90°, uncorrected for the Faraday rotation. Because the foreground Faraday rotation is relatively low (20°−30° based on the data presented by Taylor et al. 2009), these vectors constitute a reasonable approximation of the sky-projected magnetic field.

3. Results

Table 1 presents the properties of the detected sources that belong to the Leo Triplet. Details on the total and polarised emission can be found in Sects. 3.1 and 3.2.

3.1. Total power emission

Figure 1 shows the distribution of the total power (TP) emission superimposed with apparent B-vectors of polarised intensity, obtained at the center frequency of 2644 MHz with the 100-m Effelsberg radiotelescope. The rms noise level of the total power map is 1.0 mJy/beam. The field of view is dominated by strong background sources. However, the highest signal comes from NGC 3628. The total intensity of that galaxy is equal to 364 ± 17 mJy. Owing to the high signal level, emission in the vicinity of NGC 3628 is affected by the sidelobes of the telescope beam. Interferometric observations (Dumke & Krause 1998) showed that the angular size of the galactic halo at 4.86 GHz is around $3'$. A similar scaleheight has been reported at 1.49 GHz (Reuter et al. 1991). Therefore the 2.64 GHz emission should not exceed the main lobe of the beam and is not affected by its first negative sidelobe.

The second-most luminous object is the barred spiral NGC 3627, with an integrated flux of 299 ± 14 mJy. The third member of the Triplet, NGC 3623, is also visible, but

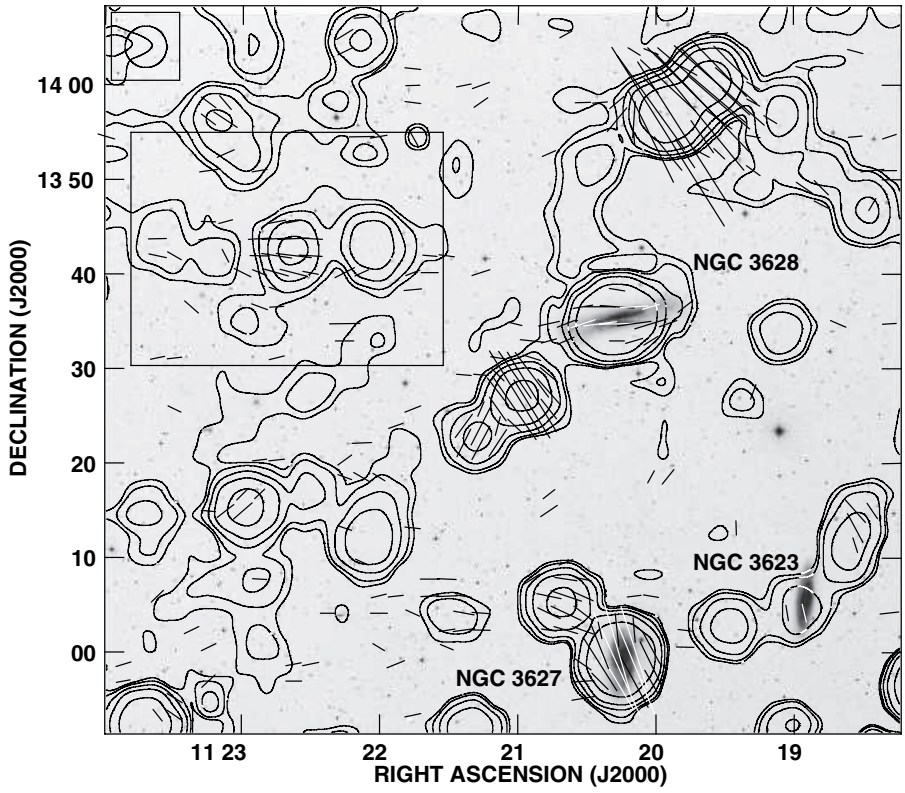

Fig. 1. Contour map of the total power emission of the Leo Triplet at 2.64 GHz. Superimposed are the apparent B-vectors of polarised intensity overlaid upon the blue image from DSS. The contour levels are 3, 5, 10, 20, 50, and 100 × 1.0 mJy/beam. A polarisation vector of 1′ corresponds to a polarised intensity of 1 mJy/beam. The beam size is 4.′5. The rectangular frame represents the area covered by Fig. 3.

is significantly weaker with an integrated flux of 19 ± 2 mJy. It should be noted here that the large beam of our observations causes flux contamination by the background sources at RA_{2000} = $11^h19^m01^s$, Dec_{2000} = +13°01′47″ and RA_{2000} = $11^h18^m57^s$, Dec_{2000} = +13°04′08″. An attempt to estimate the real value at 2.46 GHz is described in Sect. 4.1.

Most of the emission comes from (background) sources that are not associated with the Leo Triplet. There are nearly no signs of radio continuum emission from H I tails, apart from a weak source coincident with an H I clump located at RA_{2000} = $11^h23^m11^s$, Dec_{2000} = +13°42′30″ (flux of 5.6 ± 1.0 mJy; it is marked with an arrow in Figs. 2 and 3). This source could be a tidal dwarf galaxy (TDG) candidate; details can be found in Sect. 4.3.

There is a tail-like structure north of NGC 3628 (at RA_{2000} = $11^h20^m20^s$, Dec_{2000} = +13°45′00″), but a comparison with the NRAO VLA Sky Survey (NVSS; Condon et al. 1998) shows that this probably results from smoothing of two point sources with the large beam of the telescope. Two luminous sources visible eastwards from NGC 3628 (at RA_{2000} = $11^h22^m00^s$, Dec_{2000} = +13°42′30″ and RA_{2000} = $11^h22^m40^s$, Dec_{2000} = +13°42′20″) are not connected to the H I tail either.

3.2. Polarised intensity

Figure 2 presents the distribution of the polarised intensity (PI) with apparent B-vectors of the polarisation degree. As mentioned in Sect. 2, the expected amount of the Faraday rotation is approximately 20−30°. The rms noise level is equal to 0.35 mJy/beam. Similarly to the total power emission map, the polarised intensity distribution shows mostly background (point) sources that are not related to the object of study. All three main galaxies were detected, with mean polarisation fraction for NGC 3623, NGC 3627, and NGC 3628 equal to 7%, 5%, and 5%. The only extended structure is the disk of NGC 3628. The PI vectors at 2.64 GHz are oriented along the galactic plane, resembling the structure previously reported at 4.86 GHz by Soida (2005).

There is also a marginal detection for the TDG candidate at the 2.5σ level. Its polarisation degree reaches about 20%. However, because the detection is very close to the noise level, the real polarisation degree can be significantly different from the value we derived (it is presumably lower).

4. Discussion

4.1. Integrated flux densities of the member galaxies

The radio spectrum of the member galaxies has already been investigated in several articles, allowing us to compare the flux values from our study with previous works. Table 2 presents a comparison of our data with results from de Jong (1967), Kazes et al. (1970), and Pfleiderer et al. (1980), who all studied radio-luminous galaxies at 2.64 GHz. For NGC 3627 and NGC 3628 we obtained similar values; the better quality of the data resulted in lower measurement uncertainties. For NGC 3623 the data were much more scarce than for the other galaxies. Our value of 19 ± 2 mJy is consistent with the one given by de Jong (1967); however, because of the background source contamination mentioned in Sect. 3.1, the real value is very likely lower. To estimate the real flux value, we calculated the 2.64 GHz flux of the confusing sources using 1.4 GHz data from the NVSS (Condon et al. 1998) and assumed spectral index of 0.7. The integrated flux corrected for the background sources is equal to 6 ± 3 mJy.

To derive the spectral indices for the galaxies, we used data from Condon et al. (2002a). Our results can be found in Table 1. The value of 0.69 ± 0.14 derived for NGC 3627 agrees well with the mean spectral index given by Soida et al. 1999 (0.64 ± 0.04). For NGC 3628, our measurement (0.59 ± 0.15) and the mean

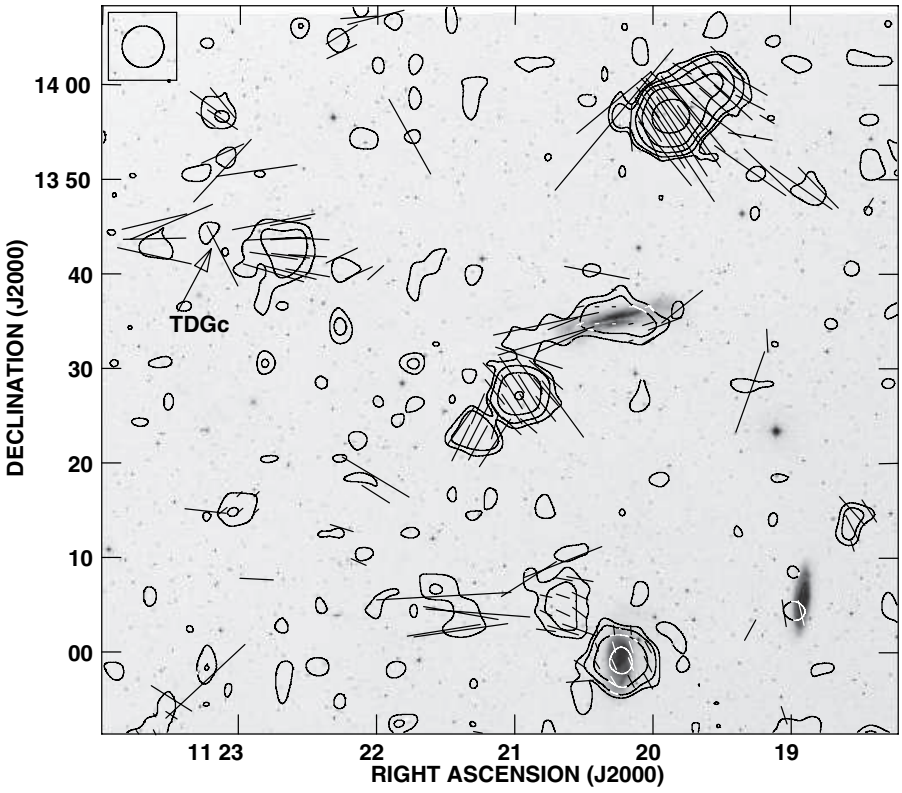

Fig. 2. Contour map of the polarised intensity of the Leo Triplet at 2.64 GHz. Superimposed are the apparent B-vectors of the polarisation degree overlaid upon the blue image from DSS. The contour levels are 3, 5, 10, 20 and 50 × 0.35 mJy/beam. A polarisation vector of 1′ corresponds to a polarisation degree of 2%. The TDG candidate is marked with an arrow. The beam size is 4.′5.

Table 2. Integrated fluxes (in mJy) for the member galaxies at 2.64 GHz.

NGC	this study	de Jong	Kazes	Pfleiderer
3623	6 ± 3[1]	≤40	no data	no data
3627	299 ± 14	359 ± 28	206 ± 41	310 ± 50
3628	364 ± 17	280 ± 22	240 ± 48	410 ± 70

Notes. References to the original publications can be found in the text. [(1)] Background sources subtracted (see Sect. 4.1 for details).

spectral index from Dumke et al. 1995 (0.67 ± 0.02) also agree well. For NGC 3623, the contamination prevents us from giving reliable estimate of its spectral index; however, using the flux value after subtracting the background sources, we obtained α = 0.75 ± 0.2 – which is within uncertainties consistent with the other two galaxies.

4.2. Constraints on the magnetic field strength of the Leo Triplet

To calculate the magnetic field strength, we assumed energy equipartition between the cosmic ray (CR) and the magnetic field energies and followed the procedure outlined by Beck & Krause (2005). Because large-scale magnetised outflows were not detected, only upper constraints for the magnetic field strength can be estimated. For the H I tail, we adopted cylindrical symmetry and a diameter of at least 25 kpc based on images presented by Stierwalt et al. (2009) and physical dimensions calculated from the NASA Extragalactic Database (NED). The extragalactic emission is typically characterised by a rather steep spectrum, with $\alpha > 1.0$ (e.g. Pacholczyk 1973; Chyży & Beck 2004). However, this refers to the CR electrons, not to the protons, which have higher energies than the electrons and lose their energy more slowly (Beck & Krause 2005). Moreover, higher losses of the CR electrons result in an increase of the proton-to-electron ratio K_0. On the other hand, in dense star-forming regions, interactions between CR protons and the nuclei of the IGM gas may result in the generation of the secondary electrons (e.g. Dennison 1980; Ensslin et al. 2011), for which it is yet unknown if the equipartition formula is applicable. Recent investigations by Lacki & Beck (2013) show that it is still valid for starburst galaxies, but nothing is known for the intergalactic fields. However, because the generation of secondary electrons would be a rather extreme scenario, we assumed that the K_0 value is equal to 100. The magnetic field strength is rather weakly bound to the proton-to-electron ratio; their dependence is given by a power-law function, and for the Leo Triplet, a change of the K_0 value by an order of magnitude results in adjusting the magnetic field strength by not more than a factor of two. The nonthermal spectral index was estimated to be 1.1.

To obtain the constraints, we used the rms values for the TP and PI emission as the upper limits for the nonthermal intensity. Using the parameters mentioned above, we obtained a total magnetic field strength of $\lesssim$2.8 μG, an ordered field component of $\lesssim$1.6 μG and a magnetic field energy density of $\lesssim 3.4 \times 10^{-13}$ erg/cm^3. Comparing these values with those obtained for Stephan's Quintet (Nikiel-Wroczyński et al., in prep.) and the "Taffy" galaxy pairs (Condon et al. 2002b; Drzazga et al. 2011), the large-scale magnetic field – if present – has an energy density lower by approximately two orders of magnitude than in the Quintet and the first Taffy pair, and about an order of magnitude lower than in the second Taffy pair. It is possible, however, that the magnetic field energy in the Leo Triplet is not in equipartition with the CR energy.

To make the picture more complete, we calculated the magnetic field strength also for the member galaxies. For NGC 3627 and NGC 3628 we used the spectral index values derived in

Sect. 4.1 and a pathlength of 2–4 kpc and 8–12 kpc, respectively. For NGC 3623 we decided to use our estimate of 0.75 ± 0.2 (calculated after subtracting the background sources); the pathlength was adopted as 6–8 kpc. The magnetic fields of the first two galaxies (see Table 1) are relatively strong, although similar to the median value for the galaxies in the field, 9 ± 1.3 μG (Niklas 1995). A slightly higher result obtained for NGC 3627 might be due the aforementioned collision with a dwarf galaxy (Wężgowiec et al. 2012). The magnetic field of NGC 3623 is weaker; however, this galaxy is smaller than the other two, which may explain the difference. It should be noted here that the values presented in this paragraph should be used only to visualize the magnitude of the magnetic field, not the exact value, due to the uncertainties in the parameter estimation. Especially for NGC 3623, the magnetic field strength estimate is influenced by the flux (and spectral index) estimate error due to the background sources.

4.3. Possible tidal dwarf galaxy?

As mentioned in Sect. 3.1, only one of the radio continuum sources visible in the TP map belongs to the H I tail. This source is spatially coincident with the H I clump reported by Stierwalt et al. (2009) that is also associated with faint emission in the optical domain (Chromey et al. 1998) and with the local maximum in the IRAS infrared data (Hughes et al. 1991). The coincidence of the recent (optical) and past (infrared) stellar formation and neutral gas indicates that this object is a TDG candidate. Such objects were first proposed by Zwicky (1956). Since the detection of a TDG candidate in the Antennae galaxies (Mirabel et al. 1992), such sources have frequently been reported in interacting systems (see e.g. Kaviraj et al. 2012).

We investigated available VLA Faint Images of the Radio Sky at Twenty-Centimeters (FIRST; Becker et al. 1995) and NVSS (Condon et al. 1998) data and found that the source was not detected by the FIRST survey, but there is a detection in the NVSS (which is more sensitive to extended emission than FIRST). The total flux at 1.4 GHz is equal to 8.4 ± 0.5 mJy. Figure 3 presents contours from the NVSS overlaid on the 2.64 GHz data, clearly showing the 1.4 GHz counterpart for our detection (marked with an arrow). The faint source near $RA_{2000} = 11^h23^m40^s$, $Dec_{2000} = +13°43'30''$ is a background source.

We calculated the spectral index using our 2.64 GHz and NVSS data and obtained a value of 0.7 ± 0.3. This could indicate that the radio continuum emission is coming from a recent star-formation period, supporting our claim for a TDG candidate. The size of the TDG candidate was assumed to be 4–6 kpc, because Chromey et al. (1998) gave 5.1 kpc as the size of the stellar clump. Using the same method as in Sect. 4.2, we obtained a total magnetic field strength ≈3.3 ± 0.5 μG and a magnetic field energy density ≈4.5 ± 1.5 × 10^{-13} erg/cm^3. These values are somewhat lower than for the TDG candidate found in Stephan's Quintet (Nikiel-Wroczyński et al., in prep.), but still reasonable for a large-scale magnetic field: Niklas (1995) derived B_{TOT} = 9 ± 1.3 μG as mean for the normal-sized spiral galaxies – a value about three times higher. The clump was marginally detected in the PI map. If we attribute this detection to the TDG candidate, it gives a polarisation degree of about 20% (see Sect. 3.2) and yields a strength of the ordered magnetic field of ≈1.5 ± 0.3 μG.

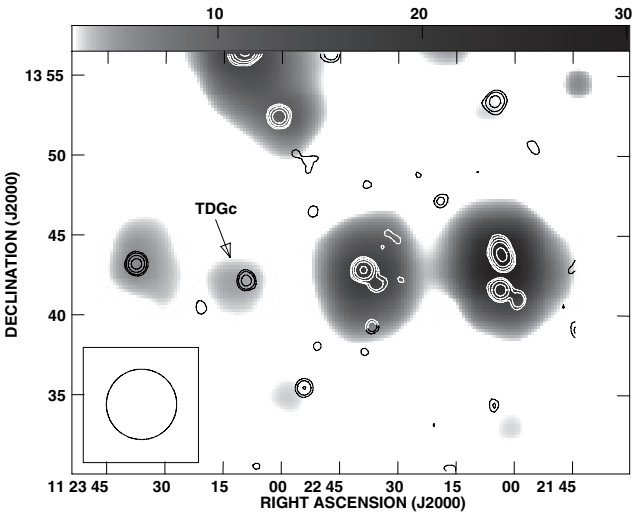

Fig. 3. Contours of the total power emission taken from the NVSS overlaid on a greyscale Effelsberg map of the TDG candidate at 2.64 GHz. The contour levels are 3, 5, 10, 20, and 50 × 0.45 mJy/beam. The TDG candidate is marked with an arrow. The beam size of the contour map is 45″. The faintest structures in the greyscale are at the 3σ level. The beam ellipse in the picture represents the 4.′5 Effelsberg beam.

5. Summary and conclusions

We observed the Leo Triplet of galaxies using the 100-m Effelsberg radio telescope at a frequency of 2.64 GHz. We obtained maps of total power (TP) emission and polarised intensity (PI). These maps were analysed together with the available archive data, yielding the following results:

- Although the high sensitivity of our observations did not allow a direct detection of the H I bridges in the radio continuum at 2.64 GHz (neither in the TP nor in the PI map), we were able to calculate upper limits for the magnetic field in the intergalactic space of the Leo Triplet. Assuming equipartition between the magnetic field and the CRs, the total field is not stronger than 2.8 μG, with an ordered component at most of 1.6 μG.
- NGC 3623, NGC 3627, and NGC 3628 are visible both in the TP and the PI map. The easternmost H I clump – visible also in the optical and infrared domains – was also detected.
- The H I clump detected in radio continuum could be an example of a tidal dwarf galaxy because there are traces of recent star formation and infrared emission in its position. The strength of its magnetic field is about 3.3 ± 0.5 μG and the magnetic field energy density reaches 4.5 ± 1.5 × 10^{-13} erg/cm^3. These values – although lower than estimated for another known TDG candidate, the SQ-B source of Stephan's Quintet – are high enough to indicate a large-scale magnetic field. The ordered component is about 1.5 ± 0.3 μG.
- The total fluxes for the main galaxies are equal to 19 ± 2 mJy for NGC 3623 (6 ± 3 mJy after subtraction of background sources), 299 ± 14 mJy for NGC 3627, and 364 ± 17 mJy for NGC 3628. The mean polarisation degree is 7, 5, and 5%, respectively.

The planned analysis of existing X-ray data for the Leo Triplet spiral galaxies will allow a comparison of the estimated intergalactic magnetic fields with the thermal properties of both galaxies and the group gaseous medium. This will provide important constraints on evolutionary models of galaxy groups.

Acknowledgements. We would like to thank an anonymous referee for helpful comments and suggestions. B.N.W. and M.S. are indebted to the whole staff of the radio telescope Effelsberg for all the help and guidance during the observations. We thank Marita Krause from the MPIfR Bonn for valuable comments. We acknowledge the usage of the HyperLeda database (http://leda.univ-lyon1.fr) and the NASA/IPAC Extragalactic Database (NED), which is operated by the Jet Propulsion Laboratory, California Institute of Technology, under contract with the National Aeronautics and Space Administration. This research has made use of NASA's Astrophysics Data System. This research has been supported by the scientific grant from the National Science Centre (NCN), decision no. DEC-2011/03/B/ST9/01859 and by the Dean of the Faculty of Physics, Astronomy and Applied Computer Sciences of the Jagiellonian University, decision no. DSC/0708/2012. R.B. and D.J.B. acknowledge support by the DFG SFB 591 "Universal Behaviour of non-equilibrium plasmas" and DFG FOR 1254, "Magnetisation of Interstellar and Intergalactic Media".

References

Arp, H. 1966, ApJS, 14, 1
Beck, R., & Krause, M. 2005, AN, 326, 414
Becker, R. H., White, R. L., & Helfand, D. J. 1995, ApJ, 450, 559
Chromey, F. R., Elmegreen, D. M., Mandell, A., et al. 1998, ApJ, 115, 2331
Chyży, K. T., & Beck, R. 2004, A&A, 417, 541
Condon, J. J., Helou, G., Sanders, D. B., et al. 1993, ApJ, 105, 1730
Condon, J. J., Cotton, W. D., Greisen, E. W., et al. 1998, ApJ, 115, 1693
Condon, J. J., Cotton, W. D., & Broderick, J. J. 2002a, ApJ, 124, 675
Condon, J. J., Helou, G., & Jarrett, T. H. 2002b, AJ, 123, 1881
de Jong, M. L. 1967, ApJ, 150, 1
Dennison, B. 1980, ApJ, 239, 93
Drzazga, R. T., Chyży, K. T., Jurusik, W., et al. 2011, A&A, 533, 22
Dumke, M., & Krause, M. 1998 in The Local Bubble and Beyond, Lyman-Spitzer Colloquium, Proc. IAU Colloq. 166, eds. D. Breitschwerdt, M. J. Freyberg, & J. Truemper (Berlin Heidelberg New York: Springer-Verlag), Lect. Notes Phys., 506, 555
Dumke, M., Krause, M., Wielebinski, R., et al. 1995, A&A, 302, 691
Emerson, D. T., & Gräve, R. 1988, A&A, 190, 353
Ensslin, T., Pfrommer, C., Miniato, F., et al. 2011, A&A, 527, A99
Haynes, M. P., Giovanelli, R., & Roberts, M. S. 1979, ApJ, 229, 83
Hickson, P. 1982, ApJ, 255, 382
Hughes, D. H., Appleton, P. N., & Schombert, J. M. 1991, ApJ, 370, 176
Kaviraj, S., Darg, D., Lintott, C., et al. 2012, MNRAS, 419, 70
Kazes, I., Le Squeren, A. M., & Nguyen-Quang-Rieu 1970, ApJ, 6, 193
Kronberg, P. P., Lesch, H., & Hopp, U. 1999, ApJ, 511, 56
Lacki, B., Beck, R. 2013, MNRAS, 430, 3171
Mantovani, F., Mack, K.-H., Montenegro-Montes, F. M., et al. 2009, A&A, 502, 61
Mirabel, I. F., Dottori, H., & Lutz, D. 1992, A&A, 256, 19
Niklas S. 1995, Ph.D. Thesis, University of Bonn
Pacholczyk, A. G. 1970, Radio Astrophysics (Freeman, San Francisco, Mir, Moscow, 1973)
Pfleiderer, J., Durst, C., & Gebler, K.-H. 1980, MNRAS, 192, 635
Rees, M. 2002, in: Highlights of Astronomy, XXIVth GA IAU, eds H. Rickman (San Francisco: ASP), 12, 727
Reuter, H.-P., Krause, M., Wielebinski, R., et al. 1991, A&A, 248, 12
Siejkowski, H., Soida, M., Otmianowska-Mazur, K., et al. 2010, A&A, 510, A97
Soida, M. 2005, in Proc. Magnetized Plasma in Galaxy Evolution Conf., 185
Soida, M., Urbanik, M., Beck, R., et al. 1999, A&A, 345, 461
Soida, M., Urbanik, M., Beck, R., et al. 2001, A&A, 378, 40
Stierwalt, S., Haynes, M. P., Giovanelli, R., et al. 2009, ApJ, 138, 338
Stone, J. M. 2002, in Highlights of Astronomy, XXIVth GA IAU, eds H. Rickman (San Francisco: ASP), 12, 709
Taylor, A. R., Stil, J. M., & Sunstrum, C. 2009, ApJ, 702, 1230
Trinchieri, G., Sulentic, J., Breitschwerdt, D., et al. 2003, A&A, 401, 73
Trinchieri, G., Sulentic, J., Pietsch, W., et al. 2005, A&A, 444, 697
Weżgowiec, M., Soida, M., & Bomans, D. J. 2012, A&A, 544, A113
Williams, B. A., McMahon, P. M., & van Gorkom, J. H. 1991, ApJ, 101, 1957
Xu, C. K., Lu, N., Condon, J. J., et al. 2003, ApJ, 595, 665
Yun, M. S., Ho, P. T. P., & Lo, K. Y. 1994, Nature 372, 530
Zwicky, F. 1956, Ergebnisse der Exakten Naturwissenschaften 29, 344

Monthly Notices
of the
ROYAL ASTRONOMICAL SOCIETY

MNRAS **435,** 149–157 (2013)
Advance Access publication 2013 August 20

doi:10.1093/mnras/stt1263

Intergalactic magnetic fields in Stephan's Quintet

B. Nikiel-Wroczyński,[1]★ M. Soida,[1] M. Urbanik,[1] R. Beck[2] and D. J. Bomans[3,4]

[1]*Astronomical Observatory, Jagiellonian University, ul. Orla 171, Kraków PL 30-244, Poland*
[2]*Max-Planck-Institut für Radioastronomie, Auf dem Hügel 69, D-53121 Bonn, Germany*
[3]*Astronomisches Institut, Ruhr-Universität Bochum, Universitätsstrasse 150, D-44801 Bochum, Germany*
[4]*Research Department 'Plasmas with Complex Interactions', Ruhr-Universität Bochum, Universitätsstrasse 150, D-44801 Bochum, Germany*

Accepted 2013 July 4. Received 2013 July 2; in original form 2013 March 13

ABSTRACT

We present the results from the Very Large Array radio continuum total power and polarized intensity observations of Stephan's Quintet at 1.43 and 4.86 GHz, along with complementary 4.85- and 8.35-GHz Effelsberg observations. Our study shows a large envelope of radio emission encompassing all the member galaxies and hence a large volume of intergalactic matter. Infall of the galaxy NGC 7318B produces a ridge of intergalactic, polarized emission, for which the magnetic field strength has been estimated as 11.0 ± 2.2 μG, with an ordered component of 2.6 ± 0.8 μG. The energy density of the field within the ridge area is of the same order as estimates of the thermal component, implying that the magnetic field has a significant role in the dynamics of the intergalactic matter. We also report that the tidal dwarf galaxy candidate SQ-B possesses a strong and highly anisotropic magnetic field, with a total strength equal to 6.5 ± 1.9 μG and an ordered component reaching 3.5 ± 1.2 μG, which is comparable to that found in normal-sized galaxies.

Key words: polarization – galaxies: groups: individual: HGC 92 (Stephan's Quintet) – galaxies: interactions – intergalactic medium – galaxies: magnetic fields – radio continuum: galaxies.

1 INTRODUCTION

Intergalactic magnetic fields are among the least studied phenomena related to galaxy groups. So far, only a limited sample of such objects has been studied at radio wavelengths. All these studies (e.g. Xu et al. 2003; Giacintucci et al. 2012) have focused on the total power (TP) emission, not taking into account the polarized intensity (PI).

The detection of intergalactic polarized emission is an important issue. Polarization is caused by magnetic fields that show some degree of ordering. This could mean either genuinely unidirectional fields (called 'regular' fields, with no reversals of lines) or squeezed/stretched random fields (called 'anisotropic' fields), which have a preferred direction of fluctuations but frequent reversals. The existence of a unidirectional field suggests that it originated in galaxies hosting large-scale dynamos. Such a magnetic field is recognized by non-zero Faraday rotation measures (RMs), while a lack of measurable RMs indicates the generation of a twisted magnetic field, possibly compressed by intergalactic shocks (Chyży et al. 2000). The discrimination is possible by determining the RMs via multifrequency polarization observations or by using the RM synthesis method (Brentjens & de Bruyn 2005). Moreover, the polarized emission provides an extremely sensitive tool to reveal possible gas compression and shearing flows, which cause the magnetic field to be aligned along the compression front and/or perpendicular to the velocity gradients (Urbanik 2005; Weżgowiec et al. 2012).

Stephan's Quintet (located approximately 85 Mpc from the Milky Way; Hickson et al. 1992) is one of several galaxy groups that possibly host intergalactic magnetic fields, and is known for magnificent dust tails emerging from NGC 7319. Additionally, it contains a radio ridge produced by the interactions with infalling NGC 7318B galaxy (Xu et al. 2003), as well as a large-scale H I tail overlapping the interloper galaxy NGC 7320 (Williams, Yun & Verdes-Montenegro 2002).

Since its discovery in 1877, Stephan's Quintet, named after its discoverer Èdouard Jean-Marie Stephan, has been subject to extensive, multiwavelength studies, much more detailed than for any other compact group. Denoted HCG 92 (Hickson 1982), the group is known to exhibit numerous interaction-related phenomena, such as changes in the morphology of the galaxies, starburst activity (Xu et al. 2003), gas outflows visible in various regimes (Williams et al. 2002; Xu et al. 2003; Guillard et al. 2012; Natale et al. 2012) and possible shock compression (Appleton et al. 2006; O'Sullivan et al. 2009). The group is also clearly visible in radio continuum (Williams et al. 2002), and a careful study of the data from the New Very Large Array (VLA) Sky Survey (NVSS) shows some evidence for polarized emission at 1.4 GHz (Condon et al. 1998).

★ E-mail: iwan@oa.uj.edu.pl

Table 1. Noise levels (σ) obtained in the final TP and PI maps.

Frequency (GHz)	σ (TP) (μJy beam^{-1})	σ (Stokes Q and U) (μJy beam^{-1})		σ (PI) (μJy beam^{-1})	Beam size (arcsec)	Telescope/ Configuration
8.35	100	48	54	71	85	Effelsberg
4.86	6	6	6	6	20	D-array
1.43	110	22	24	32	42	CD- and D-array

Several radio continuum studies of Stephan's Quintet and its member galaxies have been performed since 1972 (Allen & Hartsuiker 1972; Arp 1972). The most recent are the high-resolution study of the active galactic nuclei in NGC 7319 (Aoki et al. 1999) and that of the extended emission at 1.43 and 4.86 GHz by Xu et al. (2003), who have presented images of the TP emission, made using the VLA interferometer in its B and C configurations. These images show a large-scale radio emitting ridge between NGC 7318B and 7319 at both wavelengths, coincident with an ultraviolet (UV) emitting region and X-ray features (as presented by Trinchieri et al. 2003, 2005; O'Sullivan et al. 2009). Their high-resolution configurations of the VLA caused a substantial flux loss, and most of the extended emission was not detected. Moreover, the weak polarized emission (marginally visible in the NVSS map) remained undetected.

Recently, Geng et al. (2012) have simulated the distribution of the magnetic field (together with the X-ray morphology) of Stephan's Quintet. Both models (from Renaud, Appleton & Xu 2010 and from Hwang et al. 2012) adapted by Geng et al. (2012) suggest a collisional origin for the shock region and a significant magnetic field between NGC 7319 and 7318B.

In this paper, we present observations of Stephan's Quintet made using the VLA D-array, sensitive to the extended emission, with special attention paid to polarization. The observations were performed at two different frequencies: 1.43 and 4.86 GHz. Additionally, we made single-dish observations using the 100-m Effelsberg radio telescope at 4.85 and 8.35 GHz.

2 OBSERVATIONS AND DATA REDUCTION

2.1 Interferometric observations

The 4.86-GHz data were obtained in 2008 August using the VLA of the National Radio Astronomy Observatory (NRAO)[1] in the D-array configuration. The total on-source time (TOS) was 21.5 h. The 1.43-GHz data were also acquired using the D-array, with a TOS of 4 h. Moreover, we were granted 3.5 h in dynamic time allocation mode (CD- and D-arrays), obtained between 2007 February and April. In both cases, the bandwidth was 2 × 50 MHz, centred at 4835 and 4885 MHz in the C-band, and 1385 and 1465 in the L-band.

The data were reduced using the Astronomical Image Processing System (AIPS) and calibrated using 3C 48 at 1.43 GHz and 3C 286 at 4.86 GHz as the flux and polarization position angle calibrators. The nearby point source 2236+284 was used as a phase and instrumental polarization calibrator. For the 4.86-GHz data, we made a set of Stokes I, Q and U maps using Briggs weighting (robust parameter = 3), yielding a beam size of 13.65 × 12.28 arcsec. These maps were later convolved to a circular beam of 20 arcsec. We have also produced a uniformly weighted map of the Stokes I channel, with a beam of 6.8 arcsec. The lower-resolution set was used to produce distributions of diffuse TP and PI emission, while the uniformly weighted map shows details of the TP emission. At 1.43 GHz, maps in all Stokes parameters were convolved to a common beam of 42 arcsec. Finally, the U and Q maps at both frequencies were combined to yield the distributions of PI and polarization angle.

2.2 Single-dish observations

Single-dish mapping of Stephan's Quintet was performed using the 100-m radio telescope at Effelsberg.[2] Observations were performed at 8.35 GHz, using a single-beam receiver installed in the secondary focus of the telescope. The bandwidth was 1.1 GHz and the final resolution (after some convolution) is 85 arcsec. In order to produce the final map, 27 coverages were obtained, each of size 16 × 16 arcmin^2, scanned alternatively along RA and Dec. The scanning velocity was 30 arcsec s^{-1} and the grid spacing was 30 arcsec. All coverages were combined in the Fourier domain to reduce the scanning effects (Emerson & Gräve 1988), for the Stokes parameters I, Q and U separately. Again, we obtained maps of the PI and polarization angle from our combined U and Q data. The flux density scale was established using the source 3C 286, according to the flux values given by Baars et al. (1977). Additional 4.85-GHz mapping has also been performed in order to provide the zero-spacing information that is missing in the interferometric data. These complementary single-dish observations yielded no larger integrated total flux, indicating that there were no flux losses in the interferometric data. Thus, no merging was performed.

Because the uncertainties of the flux values based on the rms noise levels have turned out to be small compared to the uncertainties of the calibration, we assume a 5 per cent error for each integrated flux value for the radio maps. The noise levels obtained for all radio maps are presented in Table 1.

2.3 X-ray map

To further characterize the magnetic field in the ridge (which is considered to be formed by shock compression; O'Sullivan et al. 2009), a map of emission in the X-ray regime has been created using archival data from *Chandra* (Programme no. 7924; PI: Vrtilek 2006). The data were taken from the Project Archive and then reprocessed using CIAO software, version 4.3. The data were collected in the VFAINT mode, applicable for tracing the weak extended emission. The set was cleaned for bad events; the total exposure time is 93.2 ks. We have created an image in the soft X-ray regime (0.4–3 keV), later smoothed using the CSMOOTH tool.

[1] NRAO is a facility of the National Science Foundation, operated under cooperative agreement by the Associated Universities, Inc.

[2] Based on observations with the 100-m telescope of the Max-Planck-Institut für Radioastronomie (MPIfR) at Effelsberg.

3 RESULTS

In this paper, we use the term 'apparent polarization B-vectors', defined as the observed polarization E-vector direction rotated by 90°, uncorrected for the Faraday rotation, except for the maps in Section 4.

3.1 Total power emission at 4.86 GHz

The TP maps of HCG 92 at 4.86 GHz are shown in Figs 1 and 2. The high-resolution map, with a half-power beam width (HPBW) of 6.8 arcsec, shows two bright point sources and some extended emission.

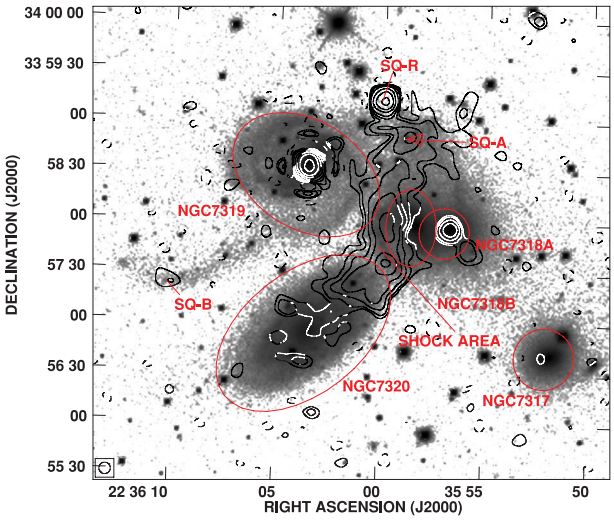

Figure 1. Uniformly weighted VLA D-array map of the TP emission of Stephan's Quintet (SQ) at 4.86 GHz overlaid upon an SDSS-R image. The contour levels are −3 (dashed), 3, 5, 10, 20, 50, 100, 200 and 500 × 10 μJy beam^{-1} (rms noise level). The angular resolution is 6.8 arcsec. The ellipses mark the positions, sizes and orientations of discussed radio sources (taken from the HyperLeda data base).

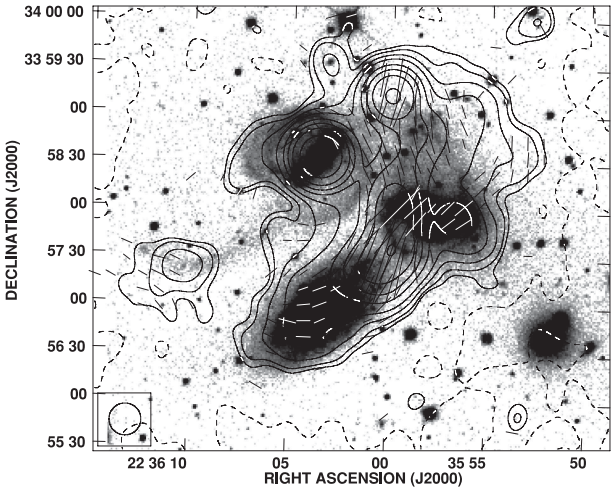

Figure 2. Briggs weighted VLA D-array map of the TP emission of Stephan's Quintet at 4.86 GHz with apparent B-vectors of the PI overlaid upon an SDSS-R image. The contour levels are −3 (dashed), 3, 5, 10, 20, 50, 100, 200 and 500 × 6 μJy beam^{-1} (rms noise level). A B-vector of 1-arcsec length corresponds to a PI of 2 μJy beam^{-1}. The clip limit for the vectors is 15 μJy (2.5 × PI noise level). The angular resolution of the map is 20 arcsec.

The most important structure in this study is the intergalactic emission ridge located between the galaxies that form the group, near RA$_{2000}$ = 22^{h}36^{m}00^{s} and Dec.$_{2000}$ = +33°57′30″. In the observations by Xu et al. (2003), the structure of the ridge is similar to the one presented in Fig. 1. By integrating the flux within the same boundaries, we have obtained 10.6 ± 0.6 mJy, which is very similar to their value of 10.9 ± 1.1 mJy.

The brightest source in the map (located at RA$_{2000}$ = 22^{h}36^{m}04^{s}, Dec.$_{2000}$ = +33°58′33″) is the core of the Seyfert type 2 galaxy NGC 7319. The core is barely resolved and its flux of 9.38 ± 0.49 mJy agrees with the value given by Aoki et al. (1999).

The 0.61 ± 0.03 mJy peak at RA$_{2000}$ = 22^{h}35^{m}57^{s}, Dec.$_{2000}$ = +33°57′55″ is the core of NGC 7318A. The flux is higher than that presented by Xu et al. (0.44 ± 0.03 mJy), which might indicate the presence of an extended structure or variability.

In the northern part of the group, a strong point source can be seen near RA$_{2000}$ = 22^{h}36^{m}00^{s}, Dec.$_{2000}$ = +33°59′12″. The peak represents an unresolved double radio source, denoted SQ-R by Xu et al. (2003), most probably unrelated to the group. Our 4.86-GHz total flux of 4.0 ± 0.2 mJy remains in very good agreement with the value of 3.7 ± 0.4 mJy obtained by Xu et al. (2003).

South of SQ-R, a weak peak near RA$_{2000}$ = 22^{h}35^{m}56^{s} and Dec.$_{2000}$ = +33°59′20″ represents the SQ-A starburst region. Its flux of 0.32 ± 0.02 mJy is in excellent agreement with 0.3 ± 0.1 mJy obtained by Xu et al. (2003).

More extended emission can be seen in the lower-resolution map (Fig. 2). The second starburst region, SQ-B (which is likely to be a part of the tidal arm – a remnant of the past interactions with NGC 7320C), located at RA$_{2000}$ = 22^{h}36^{m}10^{s}, Dec.$_{2000}$ = 33°57′22″, has an integrated flux of 0.16 ± 0.01 mJy, which is similar to the value given by Xu et al. (0.2 ± 0.1 mJy). A comparison with our uniformly weighted map (Fig. 1) shows the presence of the extended, diffuse emission in that region.

In the southern part of the group, the diffuse emission terminates near the outskirts of the interloper galaxy NGC 7320. The H I emission studies by Williams et al. (2002) show that the southern part of the group is connected to an H I tail, extending eastwards from the group and containing the SQ-B starburst region. Unfortunately, our map does not allow a reliable discrimination of whether or how the radio emission is connected to the interloper galaxy (this issue is discussed in Section 4.1.4).

The envelope of diffuse emission has an extension towards the western edge, which has no counterpart in the optical regime. The extension is located near RA$_{2000}$ = 22^{h}35^{m}53^{s}, Dec.$_{2000}$ = 33°58′30″. The lower-resolution map shows another extension – towards the eastern part of the group, overlapping the spiral arm of NGC 7319.

3.2 Distribution of the polarized intensity at 4.86 GHz

Fig. 3 shows the contours of the PI distribution overlaid on a grey-scale optical image, with the apparent B-vectors proportional to the polarization degree. The most prominent structure is the emission ridge with a mean polarization degree of around 4–5 per cent. The ridge is a part of an extended structure, also filling a large volume between NGC 7318A and 7319 as well as containing the SQ-R source. The polarization degree of the latter is approximately 3 per cent.

Whereas the core of NGC 7319 and the galaxy itself seem to be unpolarized, the core of NGC 7318A is present in the PI

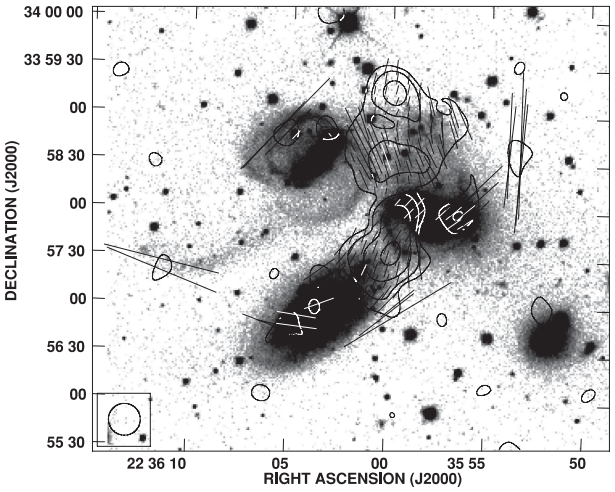

Figure 3. Briggs weighted contour map of the PI distribution of Stephan's Quintet at 4.86 GHz with apparent B-vectors of the PI overlaid upon an SDSS-R image. The contour levels are −3 (dashed), 3, 5, 10 and 20 × 6 μJy beam^{-1} (rms noise level). A polarization vector of 1 arcsec corresponds to a polarization degree of 0.5 per cent. The angular resolution of the map is 20 arcsec.

distribution map, with a polarization degree of approximately 6 per cent (averaged over the central area). The 4.86-GHz PI distribution also shows a large pool of polarized emission north from the ridge. The western extension of the TP envelope is also visible in our PI map.

East of the group, a spot of polarized emission spatially coincident with SQ-B can be seen. The polarization fraction of this source reaches 33 per cent.

3.3 Total power and polarized emission at 1.43 GHz

Fig. 4 shows the TP map of HCG 92 at 1.43 GHz with superimposed apparent polarization B-vectors. The resolution is considerably lower and this enables us to trace the emission further out. Two point sources can easily be distinguished from the surrounding emission: the core of NGC 7319 and SQ-R. The flux of the first, estimated by a Gaussian fit centred on the galactic core, is 32 ± 2 mJy, which is therefore slightly higher than 28.5 mJy as given by Aoki et al. (1999) and Xu et al. (2003).

Polarized emission from the ridge has not been detected at this frequency. Instead, weak emission is present in the tidal tail of NGC 7319. However, because of large depolarization (Section 4.2), we were unable to produce sufficiently reliable maps of the PI.

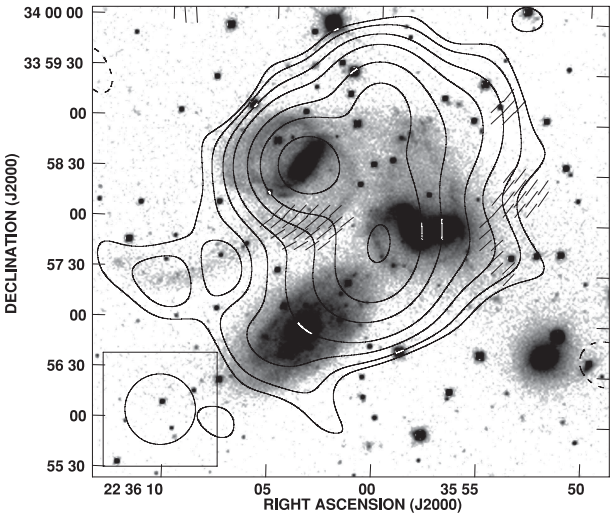

Figure 4. Contour map of the TP emission of Stephan's Quintet at 1.43 GHz with apparent B-vectors of the PI overlaid upon an SDSS-R image. The contour levels are −3 (dashed), 3, 5, 10, 20, 50, 100 and 200 × 110 μJy beam^{-1} (rms noise level). A polarization vector of 1 arcsec corresponds to a PI of 10 μJy beam^{-1}. The clip limit for the vectors is 80 μJy (2.5 × PI noise level). The angular resolution of the map is 42 arcsec.

3.4 Total power and polarized emission at 8.35 GHz

Fig. 5 shows the TP emission distribution at 8.35 GHz. Despite the lower resolution (compared to the VLA), we can easily see that the total emission contours correspond fairly well to those seen at 1.43 and 4.86 GHz. The polarized emission exceeds the 3σ rms level only at distinct regions in the group area, such as between NGC 7319 and 7318A.

The strong and polarized background source J223552+335425, located south of Stephan's Quintet, was used to determine the foreground RM. The best λ^2 fit to the polarization angles of this source at all three frequencies (1.43, 4.86 and 8.35 GHz) yields a RM of 182 rad m^{-2}, which agrees well with the values measured in the vicinity of the group (Taylor, Stil & Sunstrum 2009). With a value of 182 rad m^{-2}, the polarization angle is rotated more than 360° at 1.43 GHz, 40° at 4.86 GHz and no more than 14° at 8.35 GHz.

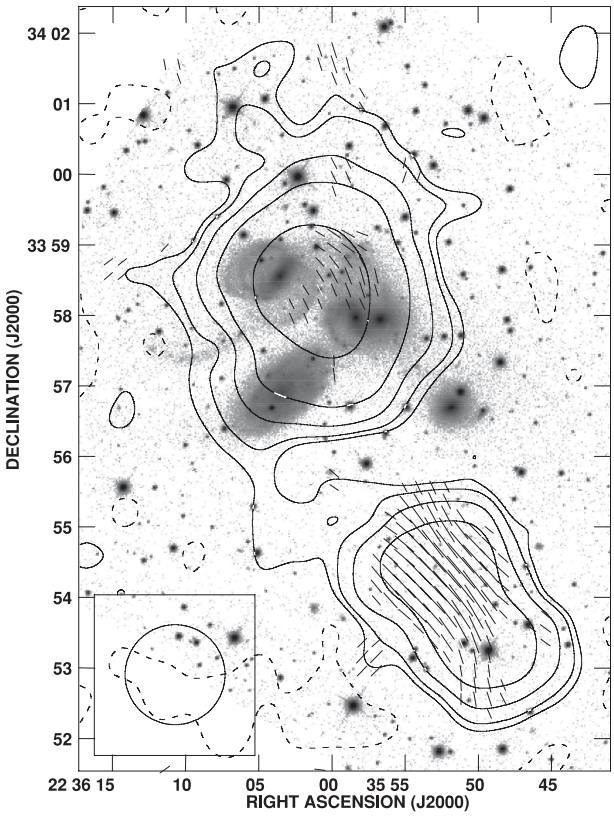

Figure 5. Contour map of the TP emission of Stephan's Quintet at 8.35 GHz with apparent B-vectors of the PI overlaid upon an SDSS-R image. The contour levels are −3 (dashed), 3, 5, 10, 20 and 50 × 100 μJy beam^{-1} (rms noise level). A polarization vector of 1 arcsec corresponds to a PI of 20 μJy beam^{-1}. The clip limit for the vectors is 180 μJy (2.5 × PI noise level). The angular resolution of the map is 85 arcsec.

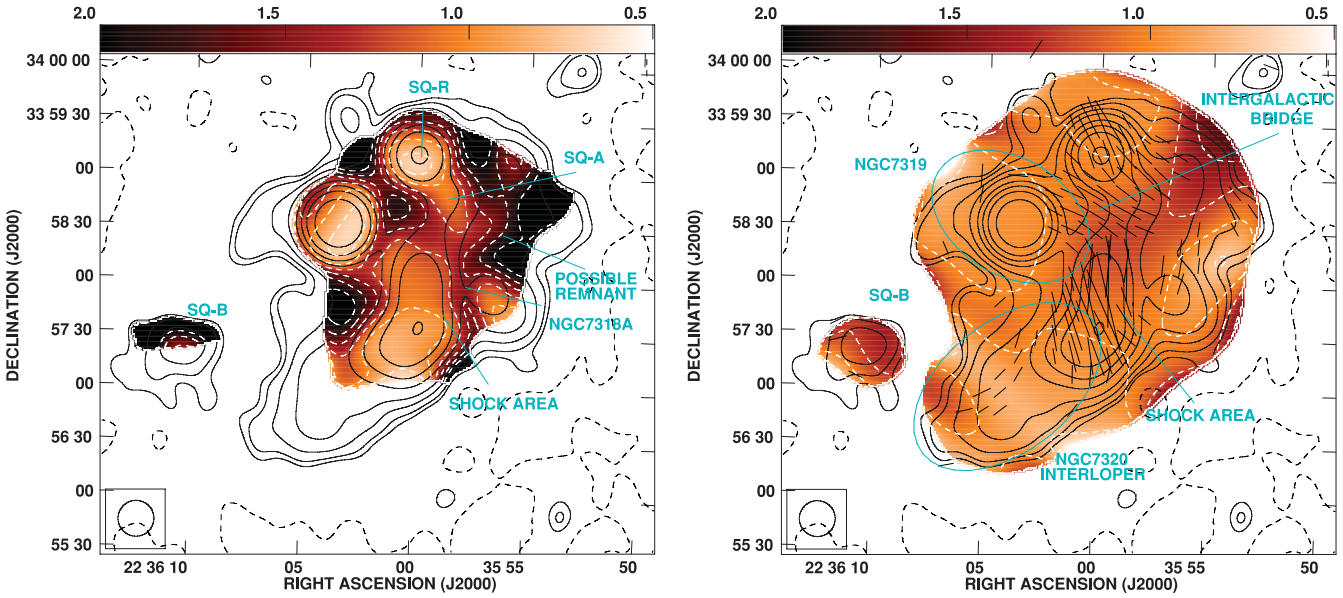

Figure 6. Distribution of the spectral index in Stephan's Quintet, calculated from 4.86- and 1.43-GHz data, superimposed with black contours for the TP emission at 4.86 GHz and with (dashed) white contours for the spectral indices. Left panel: high-resolution (20-arcsec) map. Right panel: low-resolution (42-arcsec) map with B-vectors of the magnetic field at 4.86 GHz corrected for the foreground Faraday rotation. In both panels, the radio emission contour levels are -3, 3, 5, 10, 20, 50, 100, 200 and 500 $\times$ 6 μJy beam^{-1} (rms noise level). The spectral index contour levels are 2.0, 1.75, 1.5, 1.25, 1.0 and 0.5. A polarization vector (in the right panel) of 1 arcsec corresponds to a PI of 2 μJy beam^{-1}. The clip limit for the vectors is 15 μJy (2.5 $\times$ PI noise level).

4 DISCUSSION

4.1 Spectral index

In order to calculate the spectral index distribution, we have added to our 1.43-GHz observations, the data sets obtained by Xu et al. (2003) in the VLA B-configuration at the same frequency, taken from the NRAO archive. By combining all available data at 1.43 GHz, we obtain maps with similar resolution as at 4.86 GHz. Maps at both frequencies were convolved with a Gaussian function to obtain a final circular beam with a HPBW of 20 arcsec (small enough to distinguish point-source emission from the extended emission). An additional map, with a beam of 42 arcsec, has been made in order to provide information about the regions of weak, diffuse emission, not visible in the high-resolution map. The spectral index distribution is shown in Fig. 6. Throughout the paper, we use the $S_\nu \propto \nu^{-\alpha}$ definition of the spectral index α.

4.1.1 Point sources

The spectral index of the core of NGC 7319 (approximately 0.83 $\pm$ 0.07) is, within errors, consistent with the value given by Xu et al. (2003). The lower-resolution map also allows us to compute the spectral index in the area of the spiral arm, where $\alpha = 0.95 \pm 0.04$, which is a reasonable value for galactic synchrotron emission.

The resolution of 20 arcsec is high enough to measure the spectral index for the background source SQ-R. The value of 0.81 $\pm$ 0.09 agrees very well with the value of 0.85 $\pm$ 0.12 given by Xu et al. (2003).

The core of NGC 7318A is surrounded by steep-spectrum emission. The spectral index derived for the region close to the peak of the emission is 1.1 $\pm$ 0.1, which is substantially higher than the value given by Xu et al. (0.62 $\pm$ 0.07), possibly indicating the presence of a diffuse, steep-spectrum component in our 1.43-GHz map.

4.1.2 Star formation regions

The SQ-B region is marginally visible in the high-resolution map, but it can be clearly seen in the lower-resolution image. The spectral index of this region is approximately 1.2 $\pm$ 0.2, a value that is higher than the value of 0.7 $\pm$ 0.4 measured by Xu et al. (2003), but still within the measurement uncertainties. Our low-resolution TP map shows more extended diffuse emission. Because the beam is about three times larger than in the study cited, the integrated flux value now not only represents the point source, but also has a contribution from the diffuse structure around. A diffuse, steep-spectrum emission ($\alpha = 1.4$) contribution of about 50 per cent in our larger beam map would explain the difference.

The area of the flatter spectrum within the intergalactic emission, which is spatially correlated with the SQ-A region, can be distinguished from the surrounding emission only in the high-resolution map. The value obtained for the region (1.1 $\pm$ 0.1) is higher than that given by Xu et al. (0.8 $\pm$ 0.3), but, as in the case of SQ–B, within the given uncertainties. Again, this might be a result of a contamination of the extended, steep-spectrum emission, as in the case of SQ-B.

4.1.3 Intra-group emission

The emission ridge is clearly visible in both the high- and low-resolution maps. The spectrum steepens from approximately 0.85 near the southern boundaries to 1.1–1.3 in the central part. The mean spectral index of this region is equal to 1.1 $\pm$ 0.15 and is consistent, within errors, to the value obtained by Xu et al. (0.93 $\pm$ 0.13).

The 20-arcsec resolution is sufficient to separate the point sources from the diffuse emission, allowing us to determine the spectral index. The values vary from 1.3 in the central part to 1.8 in the outskirts, and are typical for an ageing population of synchrotron electrons.

Table 2. Spectral indices calculated for Stephan's Quintet.

Emission	$\alpha_{1.43\text{-}4.86\,\mathrm{GHz}}$	$\alpha_{4.86\text{-}8.35\,\mathrm{GHz}}$
Total	1.1 ± 0.2	1.1 ± 0.2
Point	0.8 ± 0.2	0.6 ± 0.2
Diffuse	1.2 ± 0.2	1.7 ± 0.2

The western extension coincides with a region that shows a significantly steeper spectrum with a mean index of 2.0 ± 0.2. Such a steep spectrum indicates that this region could be a remnant of a past interaction within the group, because it shows the effects of spectral ageing. The PI distribution map (Fig. 3) shows a high degree of polarization of that region, approximately 40 per cent.

The mean spectral index of the whole diffuse emission of the group has been determined by calculating the total flux of the radio envelope in each of the three frequencies (taking into account only those regions that are visible over the 3σ rms level) and then subtracting the flux of all point sources (taken from Aoki et al. 1999 and Xu et al. 2003). The obtained values are given in Table 2, which shows a steepening of the diffuse emission spectrum with increasing frequency. This is a phenomenon typical for ageing particles in the intergalactic medium (IGM; as mentioned above, the steepening occurs because of electron energy losses; see, for example, Pacholczyk 1973). Any significant thermal component would manifest a substantial flattening of the spectrum between higher frequencies, which is not the case here.

4.1.4 H I tail or an interloper galaxy?

The low-resolution map (Fig. 6, right panel) was made to visualize the spectral index of the diffuse emission regions, which have a surface brightness that is too low to be visible in the high-resolution map. One of these is the southern extension, where the HI tail overlaps the galaxy NGC 7320 (Williams et al. 2002). The measured α of approximately 0.9 ± 0.1 is a relatively flat spectrum (similar to NGC 7318A and 7319), which suggests that the emission is related to the star-forming interloper galaxy rather than to an intergalactic structure. The polarized fraction of this region reaches 13 per cent, as mentioned in Section 3.2. Fig. 7 demonstrates the alignment of the vectors in the southern tail of the group. The vectors form an arc bending in the eastern direction, matching the H I tail. The arc itself is connected to the vectors overlapping the shock area. However, because the inclination of NGC 7320 is approximately 60°, this might only be a projection of the magnetic field lines of the foreground galaxy.

NGC 7320 is an example of a late-type, slowly rotating, low-mass system (see HyperLeda, Paturel et al. 2003), similar to the galaxies described by Chyży et al. (2007). Such galaxies are characterized by a relatively flat spectral index ($\alpha \simeq 0.5$). If such radiation is overlapping the emission from the H I tail, a combination of the two components (assuming that 30 per cent of the flux comes from interloper galaxy) would explain the observed value of the spectral index.

4.2 Faraday depolarization

Because the PI distribution map at 1.43 GHz shows very weak polarized emission (see Section 3.3), we decided to estimate the depolarization level between 1.43 and 4.86 GHz. We use the term 'depolarization' defined as $DP = 1 - p_{1.43}/p_{4.86}$, where p refers to the polarization degree at a given frequency. Because both maps were made with the same beam size, such a definition makes this parameter independent of beam depolarization. The mean depolarization of the radio-emitting envelope between 1.43 and 4.86 GHz is equal to 0.84. In contrast, the background source J223552+335425 shows depolarization of only 40 per cent. The exact values can be affected by differences in the bandwidth depolarization at both frequencies, but this effect cannot affect the variation of DP with the position in the map. These values indicate that the depolarization caused by the foreground Faraday dispersion is not likely to explain the high degradation of the polarized emission estimated for Stephan's Quintet. The alternative explanation is that the depolarization in the group is caused either by Faraday rotation inside Stephan's Quintet or by internal Faraday dispersion. The first possibility is that the intergalactic space in Stephan's Quintet hosts a substantial unidirectional, dynamo-type magnetic field. However, the present data do not allow us to disregard the scenario of depolarization via Faraday dispersion. Moreover, there is a possibility that the depolarization estimate for the background source is influenced by its internal depolarization. Furthermore, the foreground depolarization distribution might be patchy. The RM synthesis method (as described by Brentjens & de Bruyn 2005) will probably be able to distinguish between these two mechanisms, but it needs much better frequency coverage and higher resolution than those offered by the existing data.

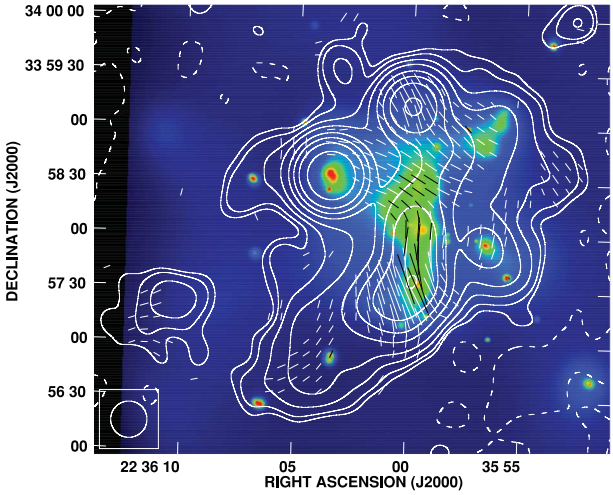

Figure 7. Map of B-vectors of the PI at 4.86 GHz after the correction for the foreground Faraday rotation overlaid upon the soft X-ray image from *Chandra*. The contour levels are −3 (dashed), 3, 5, 10, 20, 50, 100, 200 and 500 × 6 μJy beam^{-1} (rms noise level). A polarization vector of 1 arcsec corresponds to a PI of 4.5 μJy beam^{-1}. The clip limit for the vectors is 15 μJy (2.5 × PI noise level). The angular resolution of the radio data is 20 arcsec.

4.3 Magnetic field strengths in Stephan's Quintet

The strength of the magnetic field and its energy density were calculated from the 4.86-GHz data, assuming energy equipartition between the cosmic rays and the magnetic field, following the formulae presented by Beck & Krause (2005). Table 3 presents the chosen values of the parameters (the total path-length D, the proton-to-electron energy density ratio K_0, the spectral index α, the 4.86-GHz flux $S_{4.86}$ and the polarization degree p) for each of the regions. This table also contains the calculated total and ordered field strength, as well as the magnetic field energy density in each case.

Table 3. Parameters used to estimate the magnetic field properties and resulting values.

Region	D (kpc)	K_0	α	$S_{4.86}$ (mJy)	p (per cent)	$B_{\rm TOT}$ (μG)	$B_{\rm ORD}$ (μG)	E_B (erg cm^{-3})
Ridge	12.5 ± 2.5	100 ± 50	1.1 ± 0.15	10.6 ± 0.6	5	11.0 ± 2.2	2.6 ± 0.8	$0.5 \pm 0.15 \times 10^{-11}$
SQ-A	6 ± 3	100	1.1 ± 0.1	0.32 ± 0.02	–	8.8 ± 2.3	–	$3.0 \pm 1.6 \times 10^{-12}$
SQ-B	6 ± 3	100	1.2 ± 0.2	0.16 ± 0.01	33	6.5 ± 1.9	3.5 ± 1.2	$1.8 \pm 0.9 \times 10^{-12}$
Group	32 ± 6	100	1.2 ± 0.2	4.6 ± 0.6	2	6.4 ± 1.1	1.1 ± 0.3	$1.8 \pm 0.5 \times 10^{-12}$

4.3.1 Magnetic field in the ridge

The path-length D through the ridge was estimated to be 10–15 kpc (based on the size of the shock region from the high-resolution radio map and assuming cylindrical symmetry). The flux and spectral index were taken from our VLA data. Because the spectrum is relatively steep, the thermal fraction contribution is negligible. The problem arises with the value of the K_0 coefficient. Its value depends on the strength of a shock, and for strong shocks (compression ratio $r \geq 3.4$) K_0 reaches 40–100. Assuming $K_0 = 100 \pm 50$, the total magnetic field strength in the ridge is 11.0 μG $\times$ $(K_0/100)^{0.244} \pm$ 2.2 μG with an ordered component of 2.6 ± 0.8 μG. However, it is not certain whether the shock in Stephan's Quintet is a strong or a weak shock, because weak shocks would also be able to produce the observed X-ray properties of the group (see O'Sullivan et al. 2009, section 5.3, for a detailed discussion). In that case, the K_0 value would be much higher (even by several orders of magnitude). For relatively weak shocks ($r \leq 2.2$), the magnetic field strength would increase more than three times.

The total magnetic energy density of the shock area is estimated as $E_B = 0.5 \pm 0.15 \times 10^{-11}$ erg cm^{-3}. The thermal energy of the shock area is estimated from the X-ray data using the temperature of 0.6 keV and gas density of 1.167×10^{-2} cm^{-3} taken from O'Sullivan et al. (2009), yielding a value of $\approx 1.1 \times 10^{-11}$ erg cm^{-3}. This means that the magnetic field plays an important role in the dynamics of the IGM, contrary to the statement by Xu et al. (2003). Its contribution to the total energy, comparable to the thermal component, proves that it is necessary to take the magnetic field into account while performing simulations of the intra-group medium.

4.3.2 Magnetic field in the tidal dwarf galaxy

Stephan's Quintet is known to be a host group for at least 13 tidal dwarf galaxy (TDG) candidates, located in the tidal tail connected to NGC 7319 (Hunsberger, Charlton & Zaritsky 1996). One of these is the star formation region SQ-B. For SQ-B, we have calculated the properties of the magnetic field under the assumption that the K_0 ratio is equal to 100, because we do not expect the field to be produced by secondary electrons or shocks (see Beck & Krause 2005 for details). The total path-length through the emitting volume was chosen to be equal to 6 ± 3 kpc. The flux and spectral index were taken from our VLA data. Because the spectrum is relatively steep (1.2 ± 0.2), the thermal fraction contribution is negligible.

The magnetic field of the TDG candidate is relatively strong ($\approx$6.5 μG), similar to those found in normal-sized spiral galaxies, for which the median value is 9 ± 1.3 μG (Niklas 1995). The ordered component (reaching 3.5 ± 1.2 μG) is also significant, because the polarization degree is substantial (33 per cent).

The strength of the magnetic field and its anisotropy suggest an *in situ* amplification of the field in the TDG candidate. The presence of the star formation and the shearing flow of infalling plasma debris left by the passage of NGC 7320C can efficiently amplify the magnetic field, even if we assume a low mass and slow rotation of a dwarf galaxy (Siejkowski et al. 2010). Given that the plasma debris is likely to have already been magnetized, the amplification process could result in values as high as those in normal galaxies.

The second starburst region, SQ-A, lies inside an extended polarized region. Hence, it cannot be distinguished from the surrounding emission. The total magnetic field strength of this region is estimated to be 8.8 ± 2.3 μG. This translates into a magnetic field energy density of $3.0 \pm 1.6 \times 10^{-12}$ erg cm^{-3}.

4.3.3 Mean magnetic field in the group area

In order to estimate the mean magnetic field in the group area, we have subtracted the point sources (from Aoki et al. 1999) and the ridge area, and then clipped the resulting map at the level of approximately 8σ to obtain the integrated flux of the group. The path-length was adopted as equal to the separation between the galaxies originally forming Stephan's Quintet (NGC 7317, 7318A and 7319), and K_0 was adopted as 100. The spectral index was taken from our VLA data. Because the spectrum is relatively steep, we decided to neglect the thermal flux contribution. We estimated the strength of total magnetic field to be 6.4 ± 1.1 μG with an ordered component of 1.1 ± 0.3 μG, indicating an energy density of $1.8 \pm 0.5 \times 10^{-12}$ erg cm^{-3}. The magnetic field in the intergalactic space is of similar strength as in the star-forming regions SQ-A and SQ-B.

4.3.4 Shock compression as a possible origin of the magnetic field in the ridge

The emission ridge has been studied extensively in different regimes of the electromagnetic spectrum (see references in Section 1). Three mechanisms explaining the observed properties of the ridge have been described and then tested for Stephan's Quintet, the proposed mechanisms being the accretion of the primordial gas (Osmond & Ponman 2004; O'Sullivan et al. 2009), the heating of the medium by high-mass X-ray binaries and supernovae (O'Sullivan et al. 2009) and shock heating (Appleton et al. 2006; O'Sullivan et al. 2009). The latter was suggested as the most probable, providing the most accurate explanation of the observed energy and temperature distributions of the X-ray emitting medium, as well as explaining phenomena seen in other regimes of the electromagnetic spectrum. The study of the magnetic field can provide arguments for or against the shock scenario, because propagation of the shock waves through the magnetized plasma should result in a change in the orientation of the magnetic field; in particular, the magnetic field can thus be squeezed, resulting in a higher polarization degree (Urbanik 2005). Because the emission ridge is expected to be formed by means of shocking the IGM as a result of the high-speed infall of NGC 7318B to the group, there should be a polarized structure between the galaxies mentioned above. In Fig. 7, the TP emission contours and B-vectors of the PI, corrected for the foreground Faraday rotation, from our 4.86-GHz observations have been overlaid upon the *Chandra* image presenting the X-ray emission. The area of the shock agrees well with the polarized radio ridge, with the maximum located near

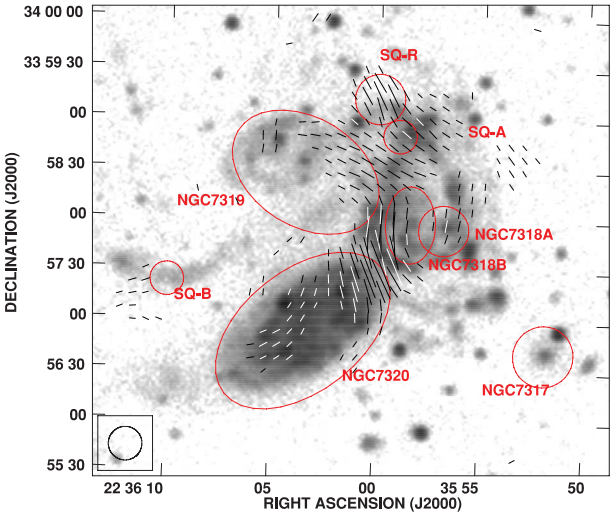

Figure 8. Map of B-vectors of the PI at 4.86 GHz after the correction for the foreground Faraday rotation overlaid upon the near-UV image from *GALEX*. A polarization vector of 1 arcsec corresponds to a PI of 4.5 μJy beam^{-1}. The clip limit for the vectors is 15 μJy (2.5 × PI noise level). The angular resolution of the radio data is 20 arcsec. The ellipses mark the positions, sizes and orientations of discussed radio sources (taken from the HyperLeda data base). NGC 7320C lies approximately 1° away from the eastern boundary of this image.

the southern end of the X-ray ridge, which indicates an increased polarization degree of the IGM in that region. Because the shock is clearly visible in the UV data, we have superimposed the *Galaxy Evolution Explorer* (*GALEX*) near-UV image of Stephan's Quintet with the polarization B-vectors (corrected for the foreground RM) at 4.86 GHz (Fig. 8). The orientation of the vectors (parallel to the shock) strongly supports the idea of an enhancement of the anisotropy because of shock-driven compression.

4.3.5 Magnetic field as a tracer of the previous interactions

Fig. 3 shows an extended area of enhanced polarization degree between the radio ridge and NGC 7319 (near $RA_{2000} = 22^h36^m00^s$, $Dec._{2000} = +33°58'20''$). The polarized fraction is significant, ranging from approximately 6 per cent near the ridge up to 13 per cent in the outskirts of the western spiral arm of NGC 7319. The magnetic field, represented by the B-vectors (corrected for the foreground Faraday rotation of 182 rad m^{-2}, as seen in Fig. 8) seems to connect NGC 7319 with the pair NGC 7318A/B. The low-resolution map of the spectral index (Fig. 6, right panel) shows that α varies from approximately 1.2 to 1.8, with a mean value of 1.45 ± 0.15.

NGC 7319 is known to be perturbed by the previous interactions. It is usually suggested that they were the result of a hypothetical passage of NGC 7320C (Shostak, Allen & Sullivan 1984; Moles, Sulentic & Marquéz 1997; Moles, Marquéz & Sulentic 1998) that caused stripping of the material through the tidal tail containing SQ-B. However, NGC 7318A (as well as NGC 7317) is considered to be a non-interacting member of the group.

The diffuse emission with a steep spectrum and a high degree of polarization is likely to originate in the material stripped from NGC 7319, because this galaxy shows hardly any signs of the emission in H I (Shostak et al. 1984; Williams et al. 2002), Hα (Arp 1972; Moles et al. 1997) and CO (Yun et al. 1997). An active role of NGC 7318A in the previous interactions was first proposed by Shostak et al. (1984) and later supported by Xu et al. (2005), who proposed that the 'UV loop' structure connected to NGC 7319 might be a 'counter-tidal' tail formed during an encounter.

5 CONCLUSIONS

We have observed the Stephan's Quintet group of galaxies using both the VLA at 1.43 and 4.86 GHz and the Effelsberg 100-m radio telescope at 4.85 and 8.35 GHz. We have obtained maps of TP emission and PI. These maps have been analysed together with the archive X-ray and UV data in order to explore the properties of the magnetic field in the group. We come to the following conclusions.

(i) The group has a large radio envelope, visible at 1.43, 4.86 and 8.35 GHz. The envelope encompasses all the member galaxies.

(ii) There is a narrow, S-shaped region of radio emission between the member galaxies. It extends from the background source at $RA_{2000} = 22^h36^m00^s$, $Dec._{2000} = +33°59'11''$ towards the shock region, and diminishes near the north-western edge of the foreground galaxy NGC 7320.

(iii) The mean polarization degree of the shock region is 5 per cent. The magnetic field strength obtained within this region is equal to 11.0 μG × $(K_0/100)^{0.244}$ ± 2.2 μG, with an ordered component of 2.6 ± 0.8 μG. The energy density of $0.5 \pm 0.15 \times 10^{-11}$ erg cm^{-3} is comparable to that of the thermal component, indicating the dynamical importance of the magnetic field in the physics of the intra-group medium.

(iv) The radio emission from the aforementioned envelope is polarized, with a mean polarization degree of 2 per cent. The strength of the mean magnetic field within its boundaries is equal to 6.4 ± 1.1 μG, with an ordered component of 1.1 ± 0.3 μG. The average magnetic field energy density is $1.8 \pm 0.5 \times 10^{-12}$ erg cm^{-3}.

(v) The depolarization of the emission from Stephan's Quintet calculated from the 1.43- and 4.86-GHz data exceeds 80 per cent. This is more than two times higher than the depolarization of the neighbouring background source. Such a difference suggests depolarization of the emission from the group either by intrinsic (within the emitting region) Faraday rotation or internal Faraday dispersion. In the first case, it would indicate the presence of a regular magnetic field.

(vi) The intergalactic emission has a rather steep spectrum, with a mean spectral index of 1.2 ± 0.2 between 1.43 and 4.86 GHz, and 1.7 ± 0.2 between 4.86 and 8.35 GHz. The steepness of the spectrum indicates that the intergalactic emission might be dominated by an ageing population of electrons and that the thermal component does not play a significant role.

(vii) There is a region of steep-spectrum (2.0 ± 0.2), highly (40 per cent) polarized emission on the north-western edge of the radio envelope. This region might be a remnant of the past interactions among the group members.

(viii) In the southern part of the group, the emission forms an extension overlapping the H I tail (detected by Williams et al. 2002). Although the orientation of the B-vectors seems to follow the H I tail, the spectral index of the emission (0.9 ± 0.1) indicates that it emerges not only from within the group, but also from the interloper galaxy NGC 7320. Moreover, the high inclination of NGC 7320 might result in projecting its magnetic field so that the B-vectors form an arc-like structure.

(ix) The radio emission from the starburst region SQ-B is substantially polarized (33 per cent), indicating the presence of a magnetic field with a total strength of 6.5 ± 1.9 μG and an ordered component reaching 3.5 ± 1.2 μG. Because this structure is supposed to be an example of a TDG, the detected field is likely to

be intrinsic to the dwarf, amplified by the flow of infalling magnetized plasma, stripped from the neighbour galaxy NGC 7319 during the passage of NGC 7320C.

ACKNOWLEDGEMENTS

We thank Kerstin Weis (Ruhr-Universität Bochum) and Marita Krause (MPIfR, Bonn) for valuable comments. This research has been supported by the scientific grant from the National Science Centre (NCN), DEC. no. 2011/03/B/ST9/01859. DJB and RB acknowledge support by the DFG SFB 591 'Universal Behaviour of Non-Equilibrium Plasmas' and DFG FOR 1254, 'Magnetization of Interstellar and Intergalactic Media'. This research has made use of the NASA/IPAC Extragalactic Database (NED), which is operated by the Jet Propulsion Laboratory, California Institute of Technology, under contract with the National Aeronautics and Space Administration (NASA). This research has made use of NASA's Astrophysics Data System. Funding for the SDSS and SDSS-II has been provided by the Alfred P. Sloan Foundation, the Participating Institutions, the National Science Foundation, the US Department of Energy, NASA, the Japanese Monbukagakusho, the Max Planck Society and the Higher Education Funding Council for England. The SDSS website is http://www.sdss.org/. This research has made use of data obtained from the *Chandra* Data Archive and of software provided by the *Chandra* X-ray Center (CXC) in the application packages CIAO, CHIPS and SHERPA. We acknowledge the use of *GALEX*.

REFERENCES

Allen R. J., Hartsuiker J. W., 1972, Nat, 239, 5371, 324
Aoki K., Kosugi G., Wilson A. S., Yoshida M., 1999, ApJ, 521, 565
Appleton P. N. et al., 2006, ApJ, 639, L51
Arp H., 1972, ApJ, 174, L111
Baars J. W. M., Genzel R., Pauliny-Toth I. I. K., Witzel A., 1977, A&A, 61, 99
Beck R., Krause M., 2005, AN, 326, 414
Brentjens M. A., de Bruyn A. G., 2005, A&A, 441, 1217
Chyży K. T., Beck R., Kohle S., Klein U., Urbanik M., 2000, A&A, 355, 128
Chyży K. T., Bomans D. J, Krause M., Beck R., Soida M., Urbanik M., 2007, A&A, 462, 933
Condon J. J., Cotton W. D., Greisen E. W., Yin Q. F., Perley R. A., Taylor G. B., Broderick J. J, 1998, ApJ, 115, 1693
Emerson D. T., Gräve R., 1988, A&A, 190, 353
Geng A., Beck A. M., Dolag K., Bürzle F., Beck M. C., Kotarba H., Nielaba P., 2012, MNRAS, 426, 3160
Giacintucci S. et al., 2011, ApJ, 732, 95
Guillard P. et al., 2012, ApJ, 749, 158
Hickson P., 1982, ApJ, 255, 382
Hickson P., Mendes de Oliveira C., Huchra J. P., Palumbo G. G., 1992, ApJ, 299, 353
Hunsberger S. D., Charlton J. C., Zaritsky D., 1996, ApJ, 462, 50
Hwang J-S., Struck C., Renaud F., Appleton P. N., 2012, MNRAS, 419, 1780
Moles M., Sulentic J. W., Marquéz I., 1997, ApJ, 485, L69
Moles M., Marquéz I., Sulentic J. W., 1998, A&A, 334, 473
Natale G. et al., 2012, ApJ, 725, 955
Niklas S., 1995, PhD thesis, University of Bonn
Osmond J. P. F., Ponman T. J, 2004, MNRAS, 350, 1511
O'Sullivan E., Giacintucci S., Vrtilek J. M., Raychaudhury S., David L. P., 2009, ApJ, 701, 1560
Pacholczyk A. G., 1973, Radio Astrophysics. Freeman, San Francisco (1970, Mir, Moscow)
Paturel G., Petit C., Prugniel P., Theureau G., Rousseau J., Brouty M., Dubois P., Cambrésy L., 2003, A&A, 412, 45
Renaud F., Appleton P. N., Xu C. K., 2010, ApJ, 724, 80
Shostak G. S., Allen R. J., Sullivan W. T. III, 1984, A&A, 139, 15
Siejkowski H., Soida M., Otmianowska-Mazur K., Hanasz M., Bomans D. J., 2010, A&A, 510, 97
Taylor A. R., Stil J. M., Sunstrum C., 2009, ApJ, 702, 1230
Trinchieri G., Sulentic J., Pietsch W., Breitschwerdt D., 2003, A&A, 401, 73
Trinchieri G., Sulentic J., Pietsch W., Breitschwerdt D., 2005, A&A, 444, 697
Urbanik M., 2005, in Chyży K., Otmianowska-Mazur K., Soida M., Dettmar R.-J., eds, The Magnetized Plasma in Galaxy Evolution Conference. Jagiellonian University, Krakow, p. 201
Vrtilek J., 2006, Chandra Proposal ID 08800951
Weżgowiec M., Urbanik M., Beck R., Chyży K. T., Soida M, 2012, A&A, 545, A69
Williams B. A., Yun M. S., Verdes-Montenegro L., 2002, AJ, 123, 2417
Xu C. K., Lu N., Condon J. J., Dopita M., Tuffs R. J., 2003, ApJ, 595, 665
Xu C. K. et al., 2005, ApJ, 619, L95
Yun M. S., Verdes-Montenegro L., del Olmo A., Perea J., 1997, ApJ, 475, L21

This paper has been typeset from a TEX/LATEX file prepared by the author.

The Astrophysical Journal, 786:144 (5pp), 2014 May 10 doi:10.1088/0004-637X/786/2/144

DISCOVERY OF A TIDAL DWARF GALAXY IN THE LEO TRIPLET

B. Nikiel-Wroczyński[1], M. Soida[1], D. J. Bomans[2], and M. Urbanik[1]
[1] Obserwatorium Astronomiczne Uniwersytetu Jagiellońskiego ul. Orla 171, 30-244 Kraków, Poland;
iwan@oa.uj.edu.pl, soida@oa.uj.edu.pl, urb@oa.uj.edu.pl
[2] Astronomisches Institut, Ruhr-Universität Bochum Universitätsstrasse 150, D-44780 Bochum, Germany; bomans@astro.rub.de
Received 2013 November 12; accepted 2014 March 27; published 2014 April 25

ABSTRACT

We report the discovery of a dwarf galaxy in the Leo Triplet. Analysis of the neutral hydrogen distribution shows that it rotates independently of the tidal tail of NGC 3628, with a radial velocity gradient of 35–40 km s^{-1} over approximately 13 kpc. The galaxy has an extremely high neutral gas content, accounting for a large amount of its total dynamic mass and suggesting a low amount of dark matter. It is located at the tip of the gaseous tail, which strongly suggests a tidal origin. If this is the case, it would be one of the most confident and nearest (to the Milky Way) detections of a tidal dwarf galaxy and, at the same time, the object most detached from its parent galaxy (≈140 kpc) of this type.

Key words: galaxies: groups: individual (Arp 317, Leo Triplet) – galaxies: interactions – intergalactic medium

Online-only material: color figures

1. INTRODUCTION

The idea of dwarf objects forming from the tidal debris left by galaxy mergers was first proposed by Zwicky (1956), who suggested that interactions in systems of multiple galaxies can lead to an ejection of the tidal material and formation of an intergalactic structure, possibly even a dwarf galaxy. However, the "recycled" galaxies did not achieve much attention, apart from a symposium talk by Schweizer (1978). The first object of this type was discovered by Mirabel et al. (1992), who presented a photometric study of the Antennae galaxies, showing a tidal dwarf galaxy (TDG) formed from the collisional debris. Since then, many similar objects have been detected—see, e.g., Brinks et al. (2004) or Duc et al. (2007). Recently, Kaviraj et al. (2012) presented a study of a sample of 405 nearby TDG candidates, conducting a statistical analysis of their properties. Tidal dwarf galaxy candidates have also been found in the Local Volume (within 11 Mpc; Hunter et al. 2000). The M81 group hosts some of the nearest examples of TDGs. The small distance allowed the authors to use *HST*-based color–magnitude diagrams (Makarova et al. 2002) to analyze the star formation history of the TDG candidates and search for additional signs of the tidal origin.

What makes the TDGs especially interesting is their mass composition. Whereas "normal" galaxies consist mostly of dark matter (DM), TDGs do not; the velocity of the DM particles in the galactic halo is much higher than the escape velocity of a TDG (Bournaud 2010), so they are not kinematically bound to it. Hence, such systems usually consist of only baryonic matter. Additionally, as they are formed in the outer parts of the galactic disks, their metallicity is higher than in non-tidal dwarfs.

Only a few TDGs were estimated to be heavy enough to contain a significant nonbaryonic fraction, but most estimates suggest that the DM content is similar to the baryonic mass—far below the typical order of magnitude of difference in non-tidal dwarf systems (Bournaud 2010). Lack of DM content and a specific environment cause the evolution of TDGs to be different from that of typical field galaxies, which still needs to be studied and described. With a low dark matter content, TDGs should also be more susceptible to the formation of galactic outflows driven by strong star formation. Alternately, a different mass distribution may lead to a lower overall star formation rate and therefore to low surface brightness of evolved TDGs.

TDGs are interesting, not only because of their mass composition, but also because of their influence on the intergalactic environment. Tidal debris can interact with other group members, like in the case of the Leo Triplet galaxy NGC 3627, known for its unusual magnetic field morphology (Soida et al. 2001). Recently, Weżgowiec et al. (2012) suggested these peculiarities could be the result of a past collision with a dwarf galaxy. Thus, TDGs might play an important role in the further evolution of their progenitors.

Galaxy systems with massive tidal tails and/or rings constitute favorable objects to use when searching for TDG candidates. One of the best examples of such objects is the Leo Triplet, a nearby group of galaxies known for a large tidal plume extending eastward from NGC 3628. Originally described by Zwicky (1956), the plume was later confirmed by photographic observations by Kormendy & Bahcall (1974). Neutral hydrogen studies by Rots (1978) and Haynes et al. (1979) revealed a thick H I structure, longer and wider than its optical counterpart. A detailed analysis of the H I distribution (Stierwalt et al. 2009) suggested numerous candidates for nontidal dwarf satellites.

Recently, Nikiel–Wroczyński et al. (2013) presented a study of the magnetic field in the Triplet. The authors suggested that the H I clump at the tip of the tidal tail could be a TDG. Additionally, Karachentsev et al. (2008) have reported that it exhibits an unusually high $M_{\rm H\,I}/L_{\rm B}$ ratio. However, as pointed out in most of the TDG studies (see, e.g., Kaviraj et al. 2012), determining whether a candidate is self-gravitating (galaxy) or a larger part of the tidal debris (that will never become a self-bound, independent object) is crucial.

In this paper we use the archive neutral hydrogen and optical data to show that the velocity field of the TDG candidate detected in the Leo Triplet exhibits a velocity gradient and has a faint optical counterpart. These findings strongly support the idea of its independent rotation, thus confirming its identification as a galaxy.

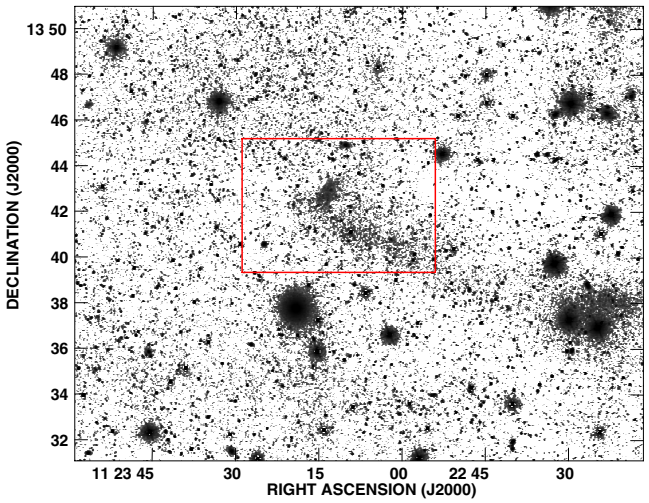

Figure 1. Processed stack of the SDSS g', r', and i' bands. The faint concentration contained in the central frame is the Leo TDG.

(A color version of this figure is available in the online journal.)

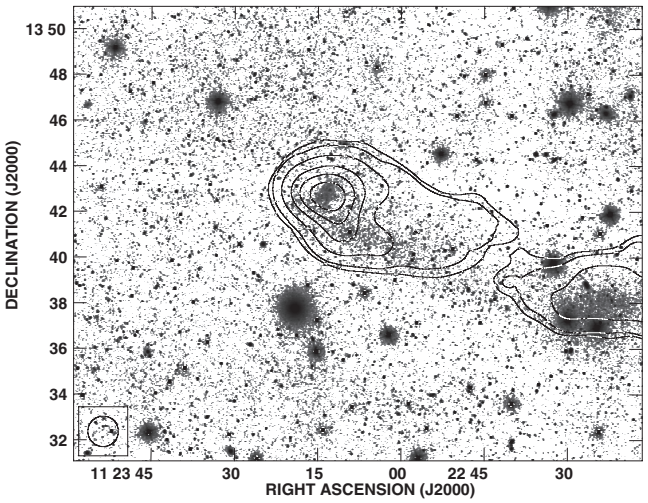

Figure 2. Contours of the zeroth moment of the H I distribution from the VLA overlaid on a multi-band (g', r', and i') image stack from the SDSS. The contour levels are 5, 10, 25, 50, 75 × 30 Jy/beam × m/s. The angular resolution of the radio data is 80 arcsec.

2. OBSERVATIONS AND DATA REDUCTION

2.1. Neutral Hydrogen Observations

The 1.41 GHz spectral data, made with the Very Large Array (VLA) of the National Radio Astronomy Observatory (NRAO)[3] in the D-array configuration, were taken from the NRAO Data Archive (Project AB1074, PI: A. Bolatto). Two intermediate frequencies were set, the first at 1.41527 GHz, the second at 1.41761 GHz, each with a bandwidth of 3.1 MHz. The corresponding velocity range is 269–1511 km s^{-1}. The total bandwidth of the observations is 5.5 MHz and the central frequency of the final data is 1.41645 GHz. We used only those fields that contained a TDG candidate. Data sets for each of the pointings used were reduced following the standard spectral line data calibration procedure in the Astronomical Image Processing System (AIPS). The maps were Briggs weighted to detect faint, extended emission. The final angular resolution is 80″ × 80″. Assuming a distance to NGC 3628 of 12.15 Mpc (median distance calculated from the Tully–Fisher-determined values from the NASA Extragalactic Database), this yields a linear resolution of our maps of some 4.7 kpc. The velocity resolution is 20.7 km s^{-1} and the rms noise level (σ) of the final maps is approximately 0.63 mJy. This corresponds to a brightness temperature of 0.10 K and a H I column density threshold of 6.9×10^{19} cm^{-2} (per spectral channel).

2.2. Optical Observations

Searching for an optical counterpart requires sensitive optical and/or near-infrared data. We checked the Sloan Digital Sky Survey (SDSS) DR7 data (Abazajian et al. 2009) in all filters (u', g', r', i', and z') individually. A very low surface brightness structure is present in the g' image. To improve on this tentative detection, we applied our stacking/filtering procedure, which increases the detectability of very low surface brightness structures (see Miskolczi et al. 2011, for details).

The resulting processed stack of images in the three most sensitive SDSS filter bands g', r', and i' is presented in Figure 1.

[3] NRAO is a facility of the National Science Foundation operated under cooperative agreement by Associated Universities, Inc.

3. RESULTS

3.1. Optical Emission Distribution

The processed SDSS image stack (Figure 1) shows a faint extended region at the position of the H I plume (diffuse, low surface brightness patch at R.A.$_{2000}$ = 11^{h}23^{m}15^{s}, Decl.$_{2000}$ = 13°43′15″) and a (fainter) structure elongated along the east–west direction. This structure is also visible in a wide-field image showing the tail of NGC 3628, provided by S. Mandel (reproduced in Figure 4 in Miskolczi et al. 2011).

The detected patch shows an exponential brightness profile with a central surface brightness of 25.2 mag sqarcsec^{-1} (g' filter) and a scale length of 120″ × 60″ (7 × 3.5 kpc). The total brightness of the structure is 17.1^{m} (16.65^{m} in the r' filter). This means that $g'-r'$ is 0.45^{m}. Using the conversion factors by Jester et al. (2005), these translate to an apparent B-band brightness $m_{\rm B}$ of 17.45^{m}, $B-V$ of 0.615^{m}, and central surface brightness $\mu_{\rm B}$ of 25.55^{m} ($\mu_{\rm V}$ = 24.93^{m}). The distance modulus is 30.42, yielding an absolute B-band magnitude $M_{\rm B}$ of −12.97^{m}.

We also check the color of the tidal tail at two separate positions, one closer (≈2′ to the southwest from the TDG), one more distant (≈13′ to the southwest from the TDG). The surface brightness of the more distant position in the tidal arm is comparable to that of the TDG, while the position closer to the TDG is fainter, which unfortunately limits the accuracy of the measurement. Measuring the TDG and both regions in the stream with different methods of background determination implied that the uncertainty of the color measurements of each of these structures is at least 0.1 mag. With that in mind, the colors of both the distant stream clump (g'–r' = 0.3) and the fainter, closer one (g'–r' = 0.4) are the same as the color of the TDG itself. With the data at hand, any difference in color between the stellar population mix in the TDG and the two analyzed regions in the stream remains within the uncertainties. A detailed analysis of the stellar populations of the TDG and of the tidal stream must await much better data.

3.2. Neutral Hydrogen Distribution

Figure 2 presents the H I total intensity (zeroth moment) map of the TDG candidate. It shows a luminous, well-resolved source

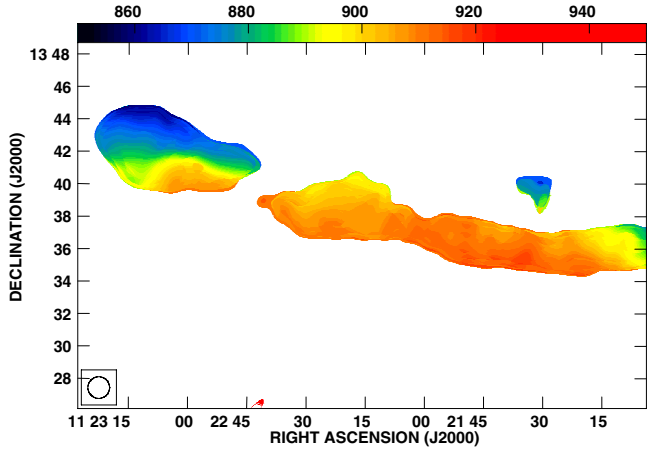

Figure 3. H I velocity distribution map made from the VLA observations. The colors represent gas species of velocities ranging from 850 (dark navy) to 950 km s^{-1} (red). The angular resolution is 80 arcsec, and the spectral resolution is 20.7 km s^{-1}.

(A color version of this figure is available in the online journal.)

of approximately ellipsoidal shape of a major axis of 300″ and a minor axis of 275″ with a position angle of 35°. This corresponds to a linear size of 17.5 × 16 kpc. The total intensity is ≈9.0 ± 0.5 Jy km s^{-1}. The neutral hydrogen data have clear counterparts in the optical regime. Both optical and H I emitting media are connected to the tidal tail.

The first moment (velocity) map is shown in Figure 3. The velocity gradient runs from the northern (approaching) to the southern (receding) side, where it sinks into the tidal plume. The measured values of the radial velocity range from 860 to 900 km s^{-1}. The tail's velocity is somewhat higher, with a mean of 910 ± 5 km s^{-1}. There is no observable trend along the east–west direction. As the velocities of the dwarf system and the tail are different, it appears likely that the dwarf is not bound to the tail. This identifies the dwarf as a separate object, which is self-gravitating—*thus, a galaxy*. This claim is also supported by the morphology of the tidal tail, which bends strongly in the direction of the TDG candidate in its close vicinity. Such behavior suggests that the TDG's gravitational influence on the tail is higher than expected for the internal gravity of the tail. This makes the existence of a self-gravitating object in the tip of the tidal tail even more likely.

To illustrate the separation of the two components, we made a contour plot of six channels in which the tail and/or the dwarf system is visible. This map, included as Figure 4, shows that the tidal tail and the dwarf galaxy are separated and there is at least one channel in which only one of them is visible.

4. DISCUSSION

4.1. Stellar Mass and Age

Due to the very low surface brightness, the SDSS data do not allow us to make a detailed fit to the spectral emission distribution (SED) that could be used to derive the star formation history and mass of the Leo TDG. Still, it is possible to estimate some information from the photometry. Using the scaling relation from Bell et al. (2003), we can use g' and r' magnitudes and the resulting color to get an estimate of the stellar mass. With $g' = 17.1^m$, $r' = 16.65^m$, $g'–r' = 0.45^m$, and the values in Table 7 of Bell et al. (2003), we calculate the M/L ratio = 3.12. With the measured $L_{r'}$ of 2.39 × 10^7 $L_\odot$, this results in a stellar mass of 7.4 × 10^7 $M_\odot$.

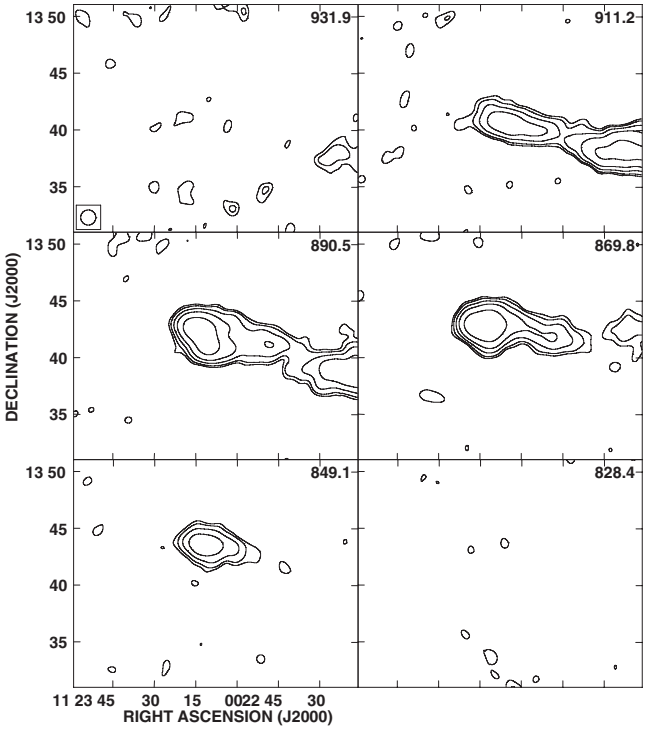

Figure 4. Six-channel map of the Leo TDG. Central velocities (in km s^{-1}) of each of the channels are written in the upper right corner of each of the planes. The angular resolution is 80 arcsec; the spectral resolution is 20.7 km s^{-1}.

A rough limit for the age of the dominant stellar population can be derived from comparison with the model integrated spectra. Assuming that the dwarf has at least some more or less recent star formation (given its large H I mass), we decided to use the STARBURST99 code (Leitherer et al. 1999, 2010; Vazquez et al. 2005) to model basic properties of the stellar population of the Leo TDG. Independent of the assumed metallicity (two times solar to 1/20 solar) and star formation law (continuous or instantaneous), for the measured $B-V = 0.62$ we get a lower age limit of 1 Gyr (which is the limit of the published models). If we assume a moderate internal reddening of 0.3 mag, the age limits are from 3 × 10^8 yr for a star formation burst and solar metallicity to ≈10^9 yr for 20% of the solar metallicity. Obviously, while being relatively blue, the majority of the stars formed significantly more than 10^8 yr ago. For a more detailed analysis much better photometry is required.

As estimated by Rots (1978), the closest encounter between NGC 3627 and NGC 3628 may have happened ≈8 × 10^8 yr ago. Thus, most of the stars in the Leo TDG (and probably the tidal dwarf itself) had to be formed shortly after the aforementioned collision of these galaxies. It is not likely that these stars formed in NGC 3628 and have been later dragged away, as the distance from the parent object is very large.

4.2. Gas Content

The gas mass of the Leo TDG was estimated assuming $M_{\rm H\,I}$ $[M_\odot] = 2.36 \times 10^5 D^2_{\rm Mpc} \int S_\nu {\rm d}\nu$, where $S_\nu {\rm d}\nu$ is in Jy× km s^{-1} (van Gorkom et al. 1986). Using a distance of 12.15 Mpc and total flux of 9.0 ± 0.5 Jy km s^{-1} (see Section 3.2), we obtained the total mass of the neutral hydrogen $M_{\rm H\,I}$ = 3.0–3.3 × 10^8 $M_\odot$. It is somewhat lower than the results from Stierwalt et al. (2009), but still of the same order of magnitude. The differences are most likely caused by the larger beam size of the Arecibo telescope

Table 1
Parameters of the Leo TDG Compared to TDGs and LSBs

Name	Leo TDG	F563–1	VCC 2062	NGC 3741
Type	TDG	LSB galaxy	TDG	LSB (very dark)
Opt. size (kpc)	7.5	3.4[a]	0.7[a]	1.7
H I size (kpc)	13	16[a]	4.2	14.6
μ_B (mag arcsec^{-1})	25.55	23.79	24.85	24.91
$B-V$	0.615	0.58	0.35	0.36[b]
Total mass ($M_\odot$)	7.9–14.1 $\times 10^8$	3.9×10^{10}	3–4 $\times 10^8$	4×10^9
Gas content ($M_\odot$)	3.3–4.3 $\times 10^8$	1.5×10^9	0.8×10^8	1.6×10^8
Stellar content ($M_\odot$)	7.4×10^7	2.3×10^8 [c]	0.2–0.7 $\times 10^8$	1.4×10^7
$M_{\rm H\,I}/L_B$	12–14	2.06	3	6.26
$M_{\rm B}$	−12.97	−16.7	−13	−13.13
$M_{\rm DYN}/M_{\rm BAR}$	1.6–3.5	≈17[c]	2–4	24
$M_{\rm DYN}/L_{\rm B}$	33–59	50.1	≈10	149

Notes.
[a] Derived from its angular size.
[b] From Taylor and Webster (2005).
[c] Derived from the M/L ratio calculated based on Bell (2003).

used by the authors of the former study, which causes confusion of the emission from the dwarf candidate with that from the tail.

4.3. Mass-to-Light Ratio and the Total Mass

The dynamical mass $M_{\rm DYN}$ of the Leo TDG can be derived from the rotational velocity at a given radius. For the Leo TDG, the radial velocity (not corrected for the inclination) gradient is about 35–40 km s^{-1} over some 13 kpc (with the tail contribution subtracted). The neutral hydrogen data do not allow us to reliably estimate the turbulent component. Therefore, we decided to use a conservative assumption of 10 km s^{-1} for a one-dimensional turbulent contribution. If this is used to calculate the dynamical mass, one can obtain a total mass of some $7.9 \times 10^8\ M_\odot$. With the inclination unknown, this value can be treated as a lower limit of the dynamical mass. For a reasonable inclination of about 60° (based on the elongation of the optical and H I shape of the dwarf), the total dynamical mass would rise to $M_{\rm DYN} = 1.41 \times 10^9\ M_\odot$. It should be strongly indicated here that the dynamical mass estimate comes with a large uncertainty. As the dependence of the dynamical mass on the (unknown) inclination is given by $M_{\rm DYN} \propto 1/\sin(i)^2$, the dynamical mass would largely increase if the Leo TDG was a more face-on-orientated system. In general, estimation of the masses of dwarf galaxies and their distributions is a complicated issue, as even if the inclination estimate is proper to some extent, the question of the finite disk thickness persists (Rhee et al. 2004). The total baryonic content of the Leo TDG can be calculated as a sum of the stellar mass ($7.4 \times 10^7\ M_\odot$) and gaseous component. Assuming a modest estimate of the molecular gas mass of 10%–30% of the H I mass (as $M_{\rm H_2}/M_{\rm H\,I}$ for NGC 3628 is equal to ≈20%; Obreschkow & Rawlings 2009), the total gas mass would be around 3.3–4.3 $\times 10^8\ M_\odot$, so the total baryonic content $M_{\rm BAR}$ is 4.0–5.0 $\times 10^8\ M_\odot$.

An estimate of $M_{\rm DYN}/L_{\rm B}$ can also be derived. $L_{\rm B}$ [$L_\odot$] is equal to $10^{-0.4\times(M-M_\odot)}$. The B-band magnitude of the Sun is equal to 5.47 (Cox 1998). This yields a total B-band luminosity of 2.4 $\times 10^7\ L_\odot$. The $M_{\rm DYN}/L_{\rm B}$ is then 33–59, and $M_{\rm H\,I}/L_{\rm B}$ is 12–14.

4.4. Magnetic Field

The resolutions used in our previous study (Nikiel–Wroczyński et al. 2013), 4.′3 in the radio continuum and 3.′5 in the H I data of Stierwalt et al. (2009), gave no grounds to reject the coincidence of the H I and radio continuum emitting regions. There were also no reliable optical images available. All of this was suggestive of the existence of a magnetic field in the Leo TDG.

With an almost four times smaller beam of H I data analyzed in this work and using our optical image we could state that the radio peak is shifted by approximately 1′ west from the neutral gas peak and seems to be located outside the optical emission. A large fraction of the radio continuum emission may be thus due to a background source. In light of the new data, we need to revise the estimate of the magnetic field strength. Setting an upper limit to the radio emission of 3.0 mJy beam^{-1} at the position of the gaseous and optical feature implies the total magnetic field in the TDG to be $B_{\rm TOT} \leqslant 2.8\ \mu$G. The magnetic and cosmic-ray energy density amounts therefore to $E_{\rm B+CR} \leqslant 6.8 \times 10^{-13}$ erg cm^{-3}.

4.5. TDG, or a Non-Tidal LSB Galaxy?

The Leo TDG shares many of its characteristics with other TDGs (Kaviraj et al. 2012). It is rather bluer than its supposed progenitor (0.65 compared to 0.8 for NGC 3628; Paturel et al. 2003), it is located exactly at the tip of the tidal tail, and has a mass of some $10^8\ M_\odot$, typical for such objects. On the other hand, if identified as a TDG, the discussed object would be the tidal dwarf most distant from its parent object, with a calculated separation of some 140–150 kpc, while 95% of the TDG candidates do not lie more than 20 kpc from their progenitors (Kaviraj et al. 2012). Compared to the statistical sample, the Leo TDG is dim, as it contains less stars than typical TDG candidates. Among the most distinct features of this galaxy are its low surface brightness ($\mu_{\rm B} = 25.55$) and very high abundance of neutral gas. Because of that, we compare its properties not only with the TDGs, but also Low Surface Brightness (LSB) galaxies. We decided to take a galaxy (F563–1) from the samples collected by de Blok et al. (1995, 1996) and the "dark" LSB NGC 3741 (Begum et al. 2005, 2008). As a comparison TDG, we have chosen the "old TDG" VCC 2062 (Duc et al. 2007). The data for the selected objects (TDGs and LSBs) are shown in Table 1.

The table clearly shows that the detected galaxy shares parameters of both TDGs and LSBs. In fact, it is not the

only dwarf system that is considered to be either a TDG or an LSB—likewise is the VCC 2062 in the Virgo Cluster (Duc et al. 2007). Both galaxies share similar characteristics: they are dim, low-mass systems with low surface brightness. They have a significant neutral hydrogen halo, showing signs of rotation independent from the tidal arc movement. The velocity gradients are—to the limits of inclination—similar. However, the sizes of the H I halos are different, as the one of VCC 2062 is just 4.2 kpc—approximately three times smaller than that of the Leo TDG. The main difference between the Leo TDG and nontidal LSBs is the dominance of the gas content in the former. In most of the LSBs, gas is not a dominant component: $M_{\rm H\,I}/L_{\rm B}$ is close to 1, and $M_{\rm H\,I}/M_{\rm DYN}$ is less than 10% (de Blok 1995). In case of the Leo TDG, H I dominates over other fractions, manifesting as a very high $M_{\rm H\,I}/L_{\rm B}$ (12–14) and $M_{\rm H\,I}/M_{\rm DYN}$ of 25–55%. Such high neutral gas content causes $M_{\rm DYN}/L_{\rm B}$ to be higher than in VCC 2062, while $M_{\rm DYN}/M_{\rm BAR}$ is very similar. As shown by de Blok (1996), nontidal LSBs have rather high $M_{\rm DYN}/M_{\rm H\,I}$ ratios, which is different from the case of the gas-dominated Leo TDG. $M_{\rm DYN}/M_{\rm BAR}$ of the non-tidal galaxies are also much higher than 1.6–3.5 estimated for the Leo TDG (Bournaud et al. 2010). All of these features strongly favor the scenario of a tidal origin of the Leo TDG.

5. SUMMARY

We used the archive VLA H I spectral data and the SDSS optical observations of the TDG candidate in the Leo Triplet of galaxies. We obtained maps of the zeroth and first kinematic moments of the H I content as well as the distribution of the visible light in the SDSS g', r', i' bands, yielding the following results.

1. There is a massive, star-forming H I clump at the tip of the tidal tail of the Leo Triplet.
2. The velocity field shows a nonnegligible gradient (approximately 35–40 km s^{-1} over 13 kpc) along the north–south (declination) axis, strongly supporting that the detected clump is a self-gravitating TDG.
3. The dwarf galaxy is unusually distant from its host galaxy (approximately 140–150 kpc), which is more than seven times farther than the typical values.
4. The optical counterpart has been detected in the SDSS g' and r' bands. The apparent B magnitude $m_{\rm B}$ is 17.45^m, $B-V$ is 0.615^m, and the central surface brightness $\mu_{\rm B}$ reaches 25.55^m. The absolute B-band magnitude is -12.97^m.
5. The total H I mass of the clump $M_{\rm H\,I}$ is 3.0–3.3 $\times 10^8\ M_\odot$. The stellar content is about $7.4 \times 10^7\ M_\odot$.
6. The stellar population age is 3×10^8–10^9 yr. This means that, despite a rather blue color, most of the stars are relatively old.
7. The estimated dynamical mass is just 1.6–3.5 times the baryonic mass. This means that the dark matter content plays a much less sound role than in the nontidal dwarf galaxies. The estimated $M_{\rm DYN}/L_{\rm B}$ is 33–59, but this value is mostly due to high $M_{\rm H\,I}/L_{\rm B}$ (12–14).
8. Compared to similar objects, the Leo TDG is relatively dim, and has a very high fraction of neutral gas, implying a short evolution time and/or low star formation rate since its formation.

We thank the anonymous referee for valuable comments and suggestions that helped us to improve our article. We acknowledge the use of the NASA/IPAC Extragalactic Database (NED), which is operated by the Jet Propulsion Laboratory, California Institute of Technology, under contract with the National Aeronautics and Space Administration. This research has made use of NASA's Astrophysics Data System. This research has been supported by a scientific grant from the National Science Centre (NCN), decision No. DEC-2011/03/B/ST9/01859. Funding for the SDSS and SDSS-II has been provided by the Alfred P. Sloan Foundation, the Participating Institutions, the National Science Foundation, the U.S. Department of Energy, the National Aeronautics and Space Administration, the Japanese Monbukagakusho, the Max Planck Society, and the Higher Education Funding Council for England. The SDSS Web site is http://www.sdss.org/.

REFERENCES

Abazajian, K. N., Adelman-McCarthy, J. K., Agüeros, M. A., et al. 2009, ApJS, 182, 543
Bell, E. F., McIntosh, D. H., Katz, N., et al. 2003, ApJS, 149, 289
Begum, A., Chengalur, J. N., & Karachentsev, I. D. 2005, A&A, 433, 1
Begum, A., Chengalur, J. N., & Karachentsev, I. D. 2008, MNRAS, 386, 1667
Brinks, E., Duc, P.-A., & Walter, F. 2004, in IAU Symp. 217, Recycling Intergalactic and Interstellar Matter, ed. P.-A. Duc, J. Braine, & E. Brinks (San Francisco, CA: ASP), 532
Bournaud, F. 2010, AdAst, 2010, 735284
Bournaud, F., & Duc, P.-A. 2008, ApJ, 672, 787
Cox, A. N. 2000, Allen's Astrophysical Quantities (4th ed.; New York: AIP Press)
de Blok, W. J. G., McGaugh, S. S., & van der Hulst, J. M. 1996, MNRAS, 283, 218
de Blok, W. J. G., van der Hulst, J. M., & Bothun, G. D. 1995, MNRAS, 274, 235
Duc, P.-A., Braine, J., Lisenfeld, U., et al. 2007, A&A, 475, 187
Duc, P.-A., Bournaud, F., & Brinks, E. 2008, in IAU Symp. 244, Dark Galaxies & Lost Baryons, ed. J. I. Davies & M. J. Disney (Cambridge: Cambridge Univ. Press), 216
Haynes, M. P., Giovanelli, R., & Roberts, M. S. 1979, ApJ, 229, 83
Hunter, D. A., Hunsberger, S. D., & Roye, E. W. 2000, ApJ, 542, 137
Jester, S., Schneider, D. P., & Richards, G. T. 2005, AJ, 130, 873
Karachentsev, I. D., Makarov, D. I., Karachentseva, V. E., & Melnik, O. V. 2008, AstL, 34, 832
Kaviraj, S., Darg, D., Lintott, C., et al. 2012, MNRAS, 419, 70
Kormendy, J., & Bahcall, J. N. 1974, AJ, 79, 671
Leitherer, C, Ortiz Otálvaro, P. A., & Bresolin, F. 2010, ApJS, 189, 309
Leitherer, C., Schaerer, D., & Goldader, J. D. 1999, ApJS, 123, 3
Makarova, L. N., Grebel, E. K., Karachentsev, I. D., et al. 2002, A&A, 396, 473
Mirabel, I. F., Dottori, H., & Lutz, D. 1992, A&A, 256, 19
Miskolczi, A., Bomans, D. J., & Dettmar, R.-J. 2011, A&A, 536, A66
Nikiel-Wroczyński, B., Soida, M., Urbanik, M., et al. 2013, A&A, 553, A4
Obreschkow, D., & Rawlings, S. 2009, MNRAS, 394, 1857
Paturel, G., Petit, C., Prugniel, Ph., et al. 2003, A&A, 412, 45
Rhee, G., Valenzuela, O., Klypin, A., et al. 2004, ApJ, 617, 1059
Rots, A. H. 1978, AJ, 83, 219
Schweizer, F. 1978, in Structure and Properties of Nearby Galaxies, ed. E. M. Berkhuijsen & R. Wielebinski (Dordrecht: Reidel), p. 279
Soida, M., Urbanik, M., Beck, R., et al. 2001, A&A, 378, 40
Stierwalt, S., Haynes, M. P., Giovanelli, R., et al. 2009, AJ, 138, 338
Taylor, E. N., & Webster, R. L. 2005, ApJ, 634, 1067
van Gorkom, J. H., Knapp, G. R., Raimond, E., et al. 1986, AJ, 91, 791
Vázquez, G. A., & Leitherer, C. 2005, ApJ, 621, 695
We żgowiec, M., Soida, M., & Bomans, D. J. 2012, A&A, 544, 113
Zwicky, F. 1956, ErNW, 29, 344

Monthly Notices of the ROYAL ASTRONOMICAL SOCIETY
MNRAS **444,** 1729–1737 (2014) doi:10.1093/mnras/stu1475

Multiwavelength study of the radio emission from a tight galaxy pair Arp 143

B. Nikiel-Wroczyński,* M. Jamrozy, M. Soida and M. Urbanik
Astronomical Observatory, Jagiellonian University, ul. Orla 171, PL-30-244 Kraków, Poland

Accepted 2014 July 22. Received 2014 July 18; in original form 2014 April 20

ABSTRACT

We present results of the recent low-frequency radio observations of a tight galaxy pair Arp 143 at 234 and 612 MHz. These data are analysed together with the archive data at 1490, 4860, 8440, and 14940 MHz. From the analysis of the radio emission we derive constraints on the age of the radio emitting structures as well as on the properties of their magnetic field. We show that the collisional ring of NGC 2445 hosts strong magnetic fields (reaching 12 μG in its northwestern part) manifesting as a steep-spectrum, non-thermal radiation at radio frequencies. The spectral age of this structure is higher than estimates derived for the star-forming regions from the Hα distribution, suggesting that the radio emission might have a different origin. The galactic core is of a very young spectral age, suggesting an ongoing starburst activity. Additionally, we identify a possible ridge of emission between the ring galaxy and its elliptical companion NGC 2444.

Key words: magnetic fields – galaxies: groups: individual: Arp 143 – galaxies: individual: NGC 2445 – galaxies: interactions – intergalactic medium – radio continuum: galaxies.

1 INTRODUCTION

Collisional ring galaxies are scarce, yet very interesting objects. Their most prominent feature is the lack of a typical spiral structure, replaced by a narrow, ring-shaped accumulation of gas and stars. Such a peculiar distribution of matter is believed to form during collision of a spiral, gas-rich galaxy with a small, early-type one (Lynds & Toomre 1976; Theys & Spiegel 1977). Galaxy pair consisting of NGC 2444 and 2445 is one of the few systems of ring galaxies that have been included in the Arp's Catalogue, denoted as Arp 143 (Arp 1966). However, it differs significantly from the usual image of a ring system, as the ring structure in NGC 2445 is distorted, similar in appearance to a trapezoid with rounded vertices. The whole visible structure is dominated by local maxima of optical emission that are regions of intensive star formation (Burbridge & Burbridge 1959; Appleton et al. 1987; Appleton, Schombert & Robson 1992). All of them are relatively young, and the central region is suspected to be undergoing starburst activity (Appleton et al. 1992). Moreover, the pair is known to be 'trailing smoke', as the H I morphology (Appleton et al. 1987) reveals a 150 kpc long tail of the neutral gas emission extending towards north. All this is suggestive of a collision of NGC 2445 with a compact galaxy – possibly its companion, NGC 2444 (Appleton et al. 1992; Beirão et al. 2009). This collision disrupted the spiral disc and resulted in morphological distortions as well as in intensification of the star formation in particular regions of the collisional ring.

Not much is known about the radio emission from Arp 143. In fact, the only work that aimed at revealing the morphology of the radio-emitting medium of this object was that of Burke & Miller (1973), who used the Westerbork Synthesis Radio Telescope to study several interacting galaxies. These authors identified a source of radio emission within NGC 2445, associating it with one of the H II regions. However, they excluded the possibility of a purely thermal origin of the emission, as the luminosity was far too high to be caused by thermal processes only. Apart from that paper, the only available radio data were that from large surveys (e.g. Sulentic 1976 or Davis & Seaquist 1983). Appleton & Struck-Marcell (1996) mention a study of Arp 143 (as well as of 10 other ring systems) made with the Very Large Array (VLA) at the frequency of 8440 MHz, but no detailed information is provided. Using Arp 10 as an example, these authors suggest that the spectral index of the emission from ring galaxies might steepen inwards from the ring. Such phenomenon could be a result of a change from thermal to non-thermal emission and/or of ageing of the highest energy electrons, which leads to their absence in the inner region of the ring. However, almost nothing is known about the magnetic field and its properties. Also, cross-identifications between radio-emitting structures and their counterparts in other domains of the electromagnetic spectrum have not yet been made.

In this paper we present results from our recent observing project at the Giant Metrewave Radio Telescope (GMRT), in which Arp 143 has been studied at 234 and 612 MHz. The new observations are analysed together with the previously unpublished, archive VLA data at 1490, 4860, 8440, and 14940 MHz to produce

* E-mail: iwan@oa.uj.edu.pl

Table 1. Basic information on the observational data sets used in this study

Freq. (MHz)	Telescope	Proj. code	Date	TOS (h)	Org. beam (arcsec)	Fin. beam (arcsec)	Noise (mJy/beam)
234	GMRT	23_025	10.02.2013	8.0	14×11	16	0.4
612	GMRT	23_025	10.02.2013	8.0	7.5×5	10	0.1
1490	VLA B	AD 182	05.09.1986	1.5	4×4	10	0.08
4860	VLA C	AD 182	14.11.1986	2.7	4×4	10	0.02
8440	VLA D	AA 146	25.08.1992	0.5	9×7	10	0.06
14 940	VLA C	AJ 105	29.05.1984	2.8	1.3×1.1	1.3×1.1	0.08

high-resolution maps of the radio emission and to study the magnetic field of this galaxy pair.

2 OBSERVATIONS AND DATA REDUCTION

2.1 GMRT data

The GMRT near Pune, India, was used to observe Arp 143 at 234 and 612 MHz. The observations were carried out in a dual frequency mode as a part of our project 'Magnetic field and galaxy interactions – from loose groups to mergers' (project code 23_025), in 2013 February. The total observing time was 8 h and the bandwidths were 16 and 32 MHz at 234 and 612 MHz, respectively. The (u,v) data were reduced using the Astronomical Image Processing System (AIPS), including calibration and RFI-flagging. After obtaining initial images at both frequencies, they were processed by a self-calibration pipeline in order to correct the phase information. The final images have been (u,v)-tapered to obtain circular beams and then corrected for the primary beam shape. Two images have been made: one with resolution of 16 arcsec at 234 MHz, and another at 612 MHz, with resolution of 10 arcsec. Original beam sizes and noise levels of these maps can be found in Table 1.

2.2 Archive VLA data

In order to construct the radio continuum spectrum, and to derive the spectral age as well as to provide the magnetic field strength estimates for Arp 143, we searched through the archive of the VLA of the National Radio Astronomy Observatory (NRAO).[1] We have obtained archived data at 1490, 4860, 8440, and 14940 MHz. Details on these observations can be found in Table 1. All these sets were calibrated, flagged and imaged using the AIPS. The 4860 MHz data allowed us to run self-calibration. Except for the highest frequency, all the data sets were (u,v)-tapered to obtain a circular beam of 10 arcsec. The 14940 MHz image has not been tapered, as it was intended to be used only to derive the size of the galactic core of NGC 2445 and its flux. Additionally, the size of the primary beam at this frequency is nearly the same as the size of NGC 2445, resulting in non-reliable flux values besides the very centre of this galaxy.

To include the calibration uncertainties, we have assumed a 5 per cent error for each integrated flux value for all the radio maps except the 234 MHz map, for which we adopt 8 per cent error.

3 RESULTS

Fig. 1 shows a composite RGB image built from *u, g, r* bands of the Sloan Digital Sky Survey (SDSS) data. An additional, Hα component (map from Romano, Mayya & Vorobyov 2008, taken from the NASA Extragalactic Database) was added to the red channel. Before merging, the Hα map was rescaled to have signal values significantly higher than the median value of the *r*-band emission in order to make the regions of molecular emission easily distinguishable. The colour image was then overlaid with the contours of radio emission at 612 MHz. Designations of different structures described in this paper – namely southern (S), northwestern (NW) and eastern (E) star-forming regions, intergalactic ridge and both galaxies – have also been marked. Measured fluxes of these structures are presented in Table 2.

The lowest frequency used in our study is 234 MHz and the map at this frequency is presented in Fig. 2(a). It has the lowest resolution (circular beam of 16 arcsec in diameter). The emission concentrates in the central–northern region of NGC 2445 and extends north-west, vanishing in the outer regions of NGC 2444 (which is otherwise a non-radio-emitting galaxy). The central part consists of the core and the NW region. Because of the beam size, the emission coming from these two entities is not separated. The radio emission coincides almost perfectly with the optically emitting material in the northern part of the ring, but diminishes abruptly about 10 arcsec south from the core of NGC 2445. Only an isolated patch of emission coincident with the southern star-forming region was detected. This is caused by the lower sensitivity to faint, extended structures at 234 MHz compared to 612 MHz.

The map at 612 MHz (Fig. 2b) has a modest resolution of 10 arcsec and a long integration time, resulting in a deep and detailed radio map. Despite higher resolution and frequency, this map shows more extended emission than that at 234 MHz. Apart from the core and the NW region, two other star-forming areas can be easily identified. Both in the eastern and the southern part of the ring, local maxima of the visible light distribution are coincident with peaks of the radio emission; the eastern structure is the weakest one. The northern extension that forms a ridge-like structure between NGC 2444 and NGC 2445 is also visible; it extends even further than that at 234 MHz, reaching NGC 2444.

The map at 1490 MHz (made from archive data) is presented in Fig. 2(c). Short integration time and lack of the shortest baselines (due to the wide B-configuration of the VLA) resulted in the absence of most of the extended emission as well as in higher noise level. Only the core and the NW region are visible. There is no trace of emission from other parts of the collisional ring, nor from the aforementioned intergalactic ridge. It should be noted that the archive VLA data used in this study are of worse (u,v) coverage than the GMRT ones, resulting in lower detectability of the weak, extended emission. This mostly applies to the 1490 and 8440 MHz data, for which the (u,v) plane sampling is poor due to the integration times lower than 2 h.

Considerably better (u,v) coverage and lack of strong RFI allowed us to obtain a detailed map of the extended emission at 4860 MHz (Fig. 2d). Similarly to the 612 MHz map, not only the

[1] NRAO is a facility of National Science Foundation operated under cooperative agreement by Associated Universities, Inc.

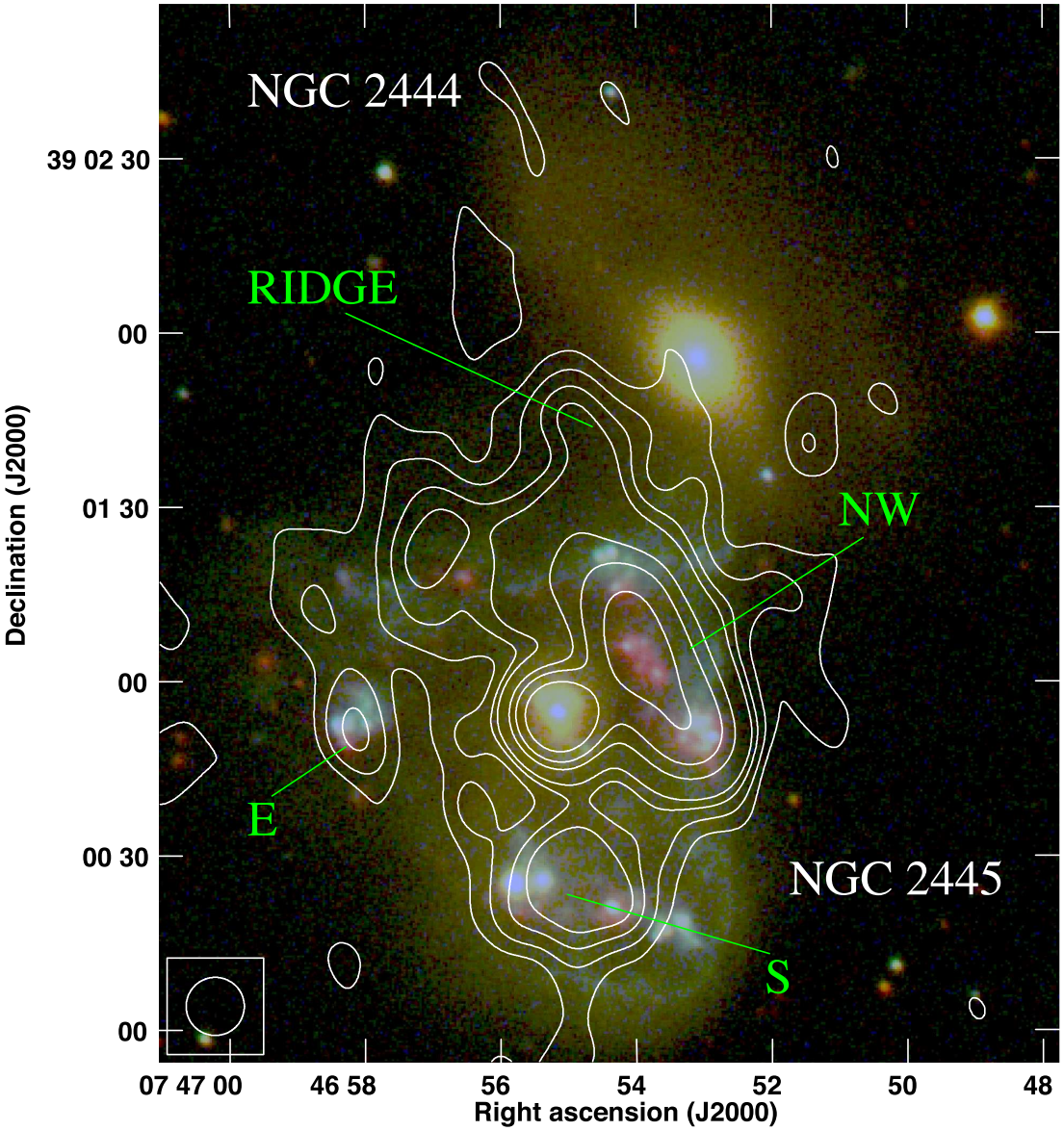

Figure 1. GMRT map of the total power (TP) emission from Arp 143 at 612 MHz overlaid upon an RGB image, with locations of the star-forming regions and intergalactic ridge indicated. The contour levels are 3, 5, 10, 20, 30, 50, 100 × 0.1 mJy beam^{-1} (r.m.s. noise level). The angular resolution is 10 arcsec. The beam is represented by a circle in the lower left corner of the image. Details of the maps used to produce this RGB composite can be found in the text (Section 3).

Table 2. Flux densities (with errors) obtained for the selected regions of radio emission. All values given in mJy. ND means no detection.

Region	234 MHz	612 MHz	1490 MHz	4860 MHz	8440 MHz	14960 MHz
Core	15.58 ± 1.40	11.14 ± 0.57	6.92 ± 0.36	3.59 ± 0.26	1.86 ± 0.11	0.81 ± 0.09
NW	30.97 ± 2.61	20.07 ± 1.01	9.33 ± 0.49	3.24 ± 0.16	1.39 ± 0.12	ND
S	ND	3.57 ± 0.25	ND	0.57 ± 0.04	ND	ND
E	ND	0.66 ± 0.11	ND	0.08 ± 0.02	ND	ND
Ridge	3.30 ± 0.69	1.28 ± 0.10	ND	0.16 ± 0.03	ND	ND

emission from the NW star formation region and the core can be seen, but also the whole collisional ring is emitting at this frequency. From its structure one can distinguish local maximum corresponding to the southern star-forming region. Surprisingly, the eastern star-forming region is indistinguishable from the extended emission. A patch of emission north from the ring, spatially coincident with the ridge detected both at 234 at 612 MHz, is easily visible. It should be noted here that, unlike at 612 MHz, the inner part of the galaxy – an area between the ring and the core – is not visible in emission at 4860 MHz; this effect is more pronounced in

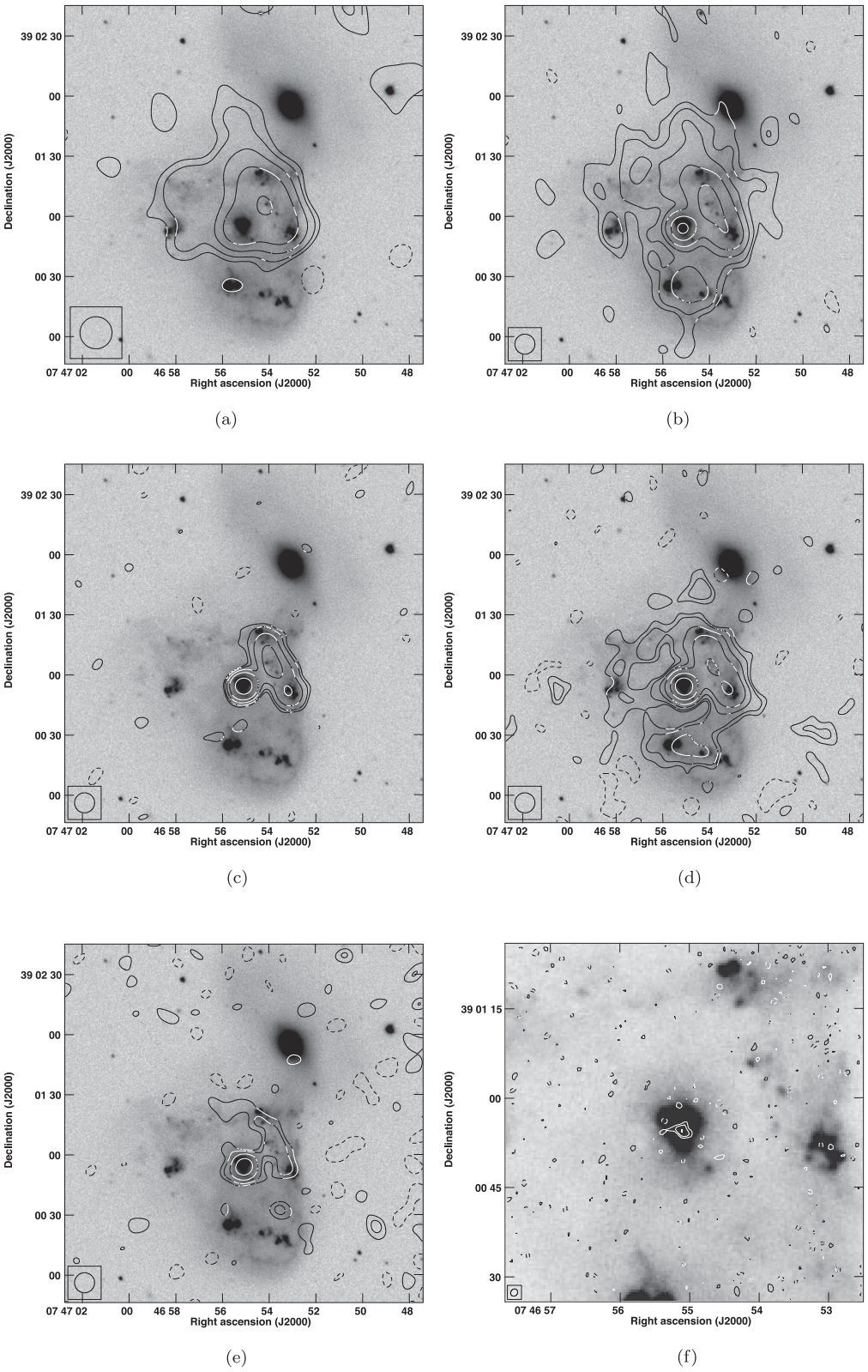

Figure 2. Maps of the TP emission from Arp 143 at various frequencies overlaid upon an SDSS *g*-band image. The contour levels are −3 (dashed), 3, 5, 10, 20, 50, 100 × r.m.s. noise level. The beam is represented by an ellipse in the lower left corner of the image. (a) GMRT map at 234 MHz. The r.m.s. noise level is 0.4 mJy beam^{-1}. The angular resolution is 16 arcsec. (b) GMRT map at 612 MHz. The r.m.s. noise level is 0.1 mJy beam^{-1}. The angular resolution is 10 arcsec. (c) VLA map at 1490 MHz. The r.m.s. noise level is 0.08 mJy beam^{-1}. The angular resolution is 10 arcsec. (d) VLA map at 4860 MHz. The r.m.s. noise level is 0.02 mJy beam^{-1}. The angular resolution is 10 arcsec. (e) VLA map at 8440 MHz. The r.m.s. noise level is 0.06 mJy beam^{-1}. The angular resolution is 10 arcsec. (f) VLA map of the core at 14940 MHz. The r.m.s. noise level is 0.08 mJy beam^{-1}. The angular resolution is 1.28x1.13 arcsec.

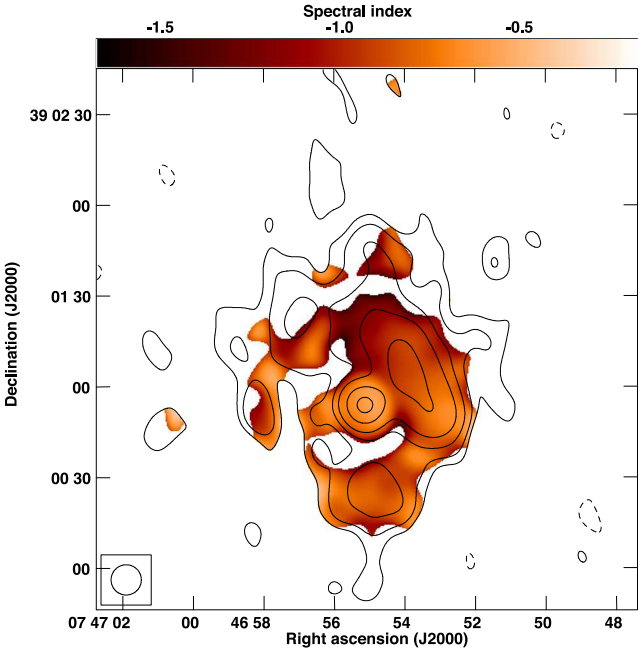

Figure 3. Map of the spectral index calculated between 612 and 4860 MHz with contours of the radio emission at 612 MHz overlaid. The contour levels are -3 (dashed), 3, 5, 10, 20, 30, 50 $\times$ 0.02 mJy beam^{-1} (r.m.s. noise level). The angular resolution is 10 arcsec.

the spectral index map (Fig. 3), indicating a significantly steeper spectrum there.

At 8440 MHz the NW region is still visible, albeit significantly less prominent than at lower frequencies. Most of the extended emission has not been detected, because of the very short integration time of these archival data. Despite that, there is some minor extension of the NW region into the northern part of the collisional ring, but it barely exceeds the 3σ level (Fig. 2e). Throughout the external parts of the image several isolated patches of noise-level radio emission, boosted by the primary beam correction, are visible.

The primary beam of the observations at the highest frequency (14940 MHz) is very small; therefore only the very central part of NGC 2445 is visible. Only the core emerges from the noise (Fig. 2f). With the high resolution of this map, we can estimate the angular size of the radio-emitting region, which is approximately 3×2 arcsec (at the 3σ level). This (assuming the distance estimate of 54.9 ± 3.8 Mpc from de Vaucoleurs et al. 1991) yields the linear size of approximately 0.8 by 0.5 kpc. Similarly to the 8440 MHz image (Fig. 2e), loose patches of emission resulting from the primary beam correction are visible in the outer parts of the image.

Large primary beams in our low-frequency observations allowed us to search for the continuum counterpart of the giant H I tail extending north from the ring galaxy (Appleton et al. 1987). However, nothing was detected above the noise level in all the maps. Some remarks on the upper limit of the magnetic field strength in this area can be found in Section 4.2.

4 DISCUSSION

4.1 Spectral index

The spectral index map has been calculated between 612 and 4860 MHz and has a resolution of 10 arcsec. The input maps have been clipped at the 5σ level to ensure that the noise fluctuations would not be taken into account. The choice of these two maps – instead of the ones at the lowest and highest frequencies – was dictated by their resolution and quality. The 234 MHz map (Fig. 2a) has a rather low resolution of 16 arcsec, which does not allow us to clearly distinguish different emitting regions. Moreover, despite large beamsize, it does not show larger extent of emission than the 612 MHz map. The 8440 MHz map (Fig. 2e) has a modest resolution of 10 arcsec, but it suffers from the short integration time, resulting in significant losses of the extended flux. This is not the case of the 4860 MHz map (Fig. 2d), which clearly shows the ring structure as well as a patch spatially connected to the intergalactic ridge. Therefore, the spectral index map – as well as all spectral index values used and presented in this study – has been calculated between the best-quality 612 and 4860 MHz maps. Throughout the paper we are using the $S_\nu \propto \nu^{-\alpha}$ definition of the spectral index α.

The emission from the core of NGC 2445 has a steeper spectrum (a mean spectral index of $\approx$0.64 $\pm$ 0.08) than expected if it were a purely thermal source. This indicates that it has a synchrotron origin, as we would expect the thermal emission to manifest with a significantly flatter spectrum, which is not the case here (see Pacholczyk 1973 for details).

The spectrum of the star-forming regions is steeper, with the mean spectral indices typical for an ageing population of relativistic electrons. The values for the particular regions are $\alpha \approx 0.81 \pm 0.07$ for the northwestern, $\alpha \approx 1.03 \pm 0.19$ for the eastern and $\alpha \approx 0.89 \pm 0.06$ for the southern region. This means that the synchrotron emission dominates everywhere over the thermal component, even at the higher of these frequencies. This is not unusual; Niklas, Klein & wielebinski (1997) have shown that the median thermal fraction at 1 GHz is 0.08 ± 0.01. The median non-thermal spectral index given by these authors is 0.83 ± 0.02, very close to the values derived for the star-forming regions in NGC 2445. This means domination of the high-energy, relativistic electrons supplied by the supernovae. Appleton & Struck-Marcell (1996) suggest that this process of electron supply would start some 10^6 yr after the collision. The estimated age of the density wave that gave birth to the NW region is $\approx$85 Myr (Beirão et al. 2009), indicating that such scenario is possible. The inner part of the ring has not been detected at 4860 MHz, indicating a very steep spectrum there. Assuming the 3 r.m.s. level as a constraint on the emission at 4860 MHz, we have estimated the spectral index to be >1.8 between 612 and 4860 MHz. Steepening of the spectral index inwards from the ring was mentioned by Appleton & Struck-Marcell (1996), who provided two possible explanations for such phenomenon: change from the mostly thermal to non-thermal radiation and/or ageing of the synchrotron electrons. Our findings suggest that in case of Arp 143 the second scenario is more probable.

The intergalactic ridge has a steep spectrum – characteristic for an ageing population of electrons – with a mean spectral index $\alpha \approx 1.01 \pm 0.12$. This is consistent with its identification as an intergalactic structure presented in Section 3. Also, it is steeper than that of the star-forming regions NW and S, suggesting a higher spectral age, as it is far away from the star-forming areas.

4.2 Magnetic field

Both the strength of the magnetic field $B_{\rm TOT}$ and its energy density $E_{\rm B}$ in the selected areas were calculated assuming the energy equipartition between the cosmic rays and the magnetic field, following the formulae presented in Beck & Krause (2005). We applied the BFELD code, which uses following parameters: total pathlength through the source D, proton-to-electron energy density ratio K_0,

Table 3. Parameters used for the estimation of the magnetic field properties and resulting values.

Region	D (kpc)	α	$S_{4.86}$ (mJy)	$B_{\rm TOT}$ (μG)	$E_{\rm B}$ (erg cm^{-3})
Core	0.65 ± 0.15	0.64 ± 0.08	3.59 ± 0.13	38.8 ± 1.7	$60 \pm 5 \times 10^{-12}$
NW	5.5 ± 0.5	0.81 ± 0.07	3.24 ± 0.16	12.0 ± 0.4	$5.8 \pm 0.5 \times 10^{-12}$
S	5.5 ± 0.5	0.89 ± 0.06	0.57 ± 0.04	9.9 ± 0.3	$3.9 \pm 0.3 \times 10^{-12}$
E	5.5 ± 0.5	1.03 ± 0.19	0.08 ± 0.02	8.7 ± 0.6	$3.0 \pm 0.4 \times 10^{-12}$
Ridge	5.5 ± 0.5	1.01 ± 0.12	0.16 ± 0.03	9.2 ± 0.6	$3.3 \pm 0.3 \times 10^{-12}$

spectral index α, and the mean synchrotron surface brightness of the chosen region to estimate its total field strength as well as the magnetic energy density. The mean brightness has been obtained from the region's integrated flux density S by dividing it by the square root of the number of the beams in the integration area. K_0 was fixed as 100; such a value is suggested also for starburst galaxies (Lacki & Beck 2013). Values of all parameters used, together with the results of the estimation, are presented in Table 3. The spectral index was calculated between the maps at 612 and 4860 MHz, which have the best quality. According to Niklas et al. (1997), thermal fraction at 1490 MHz for majority of galaxies does not exceed 10 per cent; even at 10000 MHz its mean value is about 25 per cent. This consistently yields thermal fraction at 4860 MHz significantly less than some 15–20 per cent. Except for the nucleus, a low thermal fraction is implied by steep radio spectra of discussed regions. Even in case of maximum value of 20 per cent, its neglecting leads to an overestimate of magnetic field strength by no more than 5–7 per cent. Therefore, we decided not to take thermal emission into account.

For the NW part of the ring, we have used a pathlength of 5500 pc – derived from the angular size of the emitting region under an assumption of a cylindrical symmetry. The same size has been also adopted for all the other regions within the disc of NGC 2445 as well as for the ridge between it and NGC 2444. The estimated strength of the magnetic field in the NW region is therefore 12.0 ± 0.4 μG, and the energy density is $5.8 \pm 0.5 \times 10^{-12}$erg cm^{-3}. This means that the magnetic field in this region is somewhat stronger than the average found in normal, spiral galaxies (9 ± 1.3 μG – Niklas 1995). It is also comparable to that found in the shock region between the galaxies forming Stephan's Quintet (11.0 ± 2.2 μG – Nikiel-Wroczyński et al. 2013). Values derived for the other star-forming regions are very similar (see Table 3).

Estimates for the intergalactic ridge do not differ much from that for the star-forming regions. As its spectrum is steeper than that of the star-forming regions (except for the eastern region, which has a comparable α), the strength of the magnetic field is nearly the same despite lower surface brightness. For an intergalactic structure, value of ≈9 μG is a rather high strength. There is no clear counterpart to this entity in any other spectral domain. Most possibly, the magnetic field – enhanced in the star-forming NW region – is dragged with the intergalactic gas during the tidal interaction with the companion galaxy. Such a structure can result from a partially ordered B-field, dragged and stretched during the interaction. The total magnetic field is, in terms of its strength and energy density, similar to that of the iconic colliding pair of galaxies, the Taffies (Condon et al. 1993). Unfortunately, the setup of the low-frequency observations (simultaneous dual-frequency mode 234/612 MHz) did not allow us to perform full Stokes observations, and we have not detected polarization in any of the VLA data sets. Polarization data are necessary to confirm or reject this scenario.

As the core of the collisional ring galaxy exhibits a spectrum that suggests a non-thermal origin of the emission ($\alpha \approx 0.64 \pm 0.08$), we derived estimates for the magnetic field of the core, too. We used a pathlength of 650 pc – a mean of its linear dimensions (see Section 3). The resulting field is strong, as it reaches 38.8 ± 1.7 μG. Its energy density is equal to $6.0 \pm 0.5 \times 10^{-11}$erg cm^{-3}. The core is supposed to undergo starburst activity (Appleton et al. 1992), and for a compact region of efficient electron supply such a number is not surprising.

The radio continuum counterpart for the tidal tail has not been detected, but we could obtain the upper limit for the magnetic field strength and energy in its area. We have assumed that the tail has a cylindrical symmetry with a diameter of 20 kpc (Appleton et al. 1987) and a steep spectral index of 1.0. Once again, we used the BFELD code, calculating the magnetic field strength using information at 234, 612 and 4860 MHz. The upper limit for the strength was estimated as <4.6 μG. The corresponding limit for the magnetic field energy is $<1.1 \times 10^{-12}$erg cm^{-3}. However, these values are of high uncertainty, as the estimates of the tail parameters are rather rough. Assuming the radio-emitting medium to be more shallow (which is possible, as there are hints of narrowing in certain regions of the tail), the limit for the magnetic field strength would rise up – to approximately 8.5–12 μG (in case of the depth of 5 and 1 kpc, respectively) and its energy density would reach $2.8–6.3 \times 10^{-12}$erg cm^{-3}. This indicates that a relatively strong magnetic field could remain undetected.

4.3 Age of the structures

Good frequency coverage allows us to estimate the spectral age of the core and the NW region. The amount of time elapsed since the last acceleration of the particles in a given structure can be calculated under assumption that the observed steepening of the radio spectrum is caused by the synchrotron and/or inverse-Compton processes. We decided to use the SYNAGE package (Murgia 1996), which has an implementation of the Jaffe–Perola (Jaffe & Perola 1973, JP), Kardashev–Pacholczyk (Kardashev 1963; Pacholczyk 1973, KP), and continuous injection (CI; Pacholczyk 1973; Myers & Spangler 1985; Carilli et al. 1991) models of electron energy losses. The JP model assumes that the particles get isotropized in the pitch angle with the time-scale of isotropization much smaller than the radiative lifetime. The KP model assumes that each electron maintains its original pitch angle. The CI model includes the continuous injection of power-law distributions of relativistic electrons. The observed spectrum in this case is the sum of the emission from the various electron populations at different synchrotron ages, ranging from zero to the age of the source. The flux density at frequencies below the synchrotron break rises with time, since new particles are being added. All these models assume a constant magnetic field. SYNAGE uses the flux values at different wavelengths (spectral energy distribution, SED) to determine the spectral index of the injected electron population $\alpha_{\rm inj}$, and the spectral break frequency $\nu_{\rm break}$ (frequency above which the observed spectrum

Table 4. Parameter of the spectral fits.

Region	Model	χ^2	$\alpha_{\rm inj}$	$\nu_{\rm break}$(GHz)	Spectral age (Myr)
Core	JP	0.25	$0.38^{+0.04}_{-0.01}$	$12.1^{+2.7}_{-1.0}$	1.6–2.1
Core	KP	0.48	$0.38^{+0.03}_{-0.01}$	$6.2^{+1.3}_{-0.5}$	2.2–2.9
Core	CI	12.18	0.46 ± 0.05	$2.8^{+1.6}_{-1.0}$	2.9–5.2
NW	JP	5.77	0.49 ± 0.07	$9.3^{+4.8}_{-2.5}$	9.0–14.1
NW	KP	6.34	$0.49^{+0.08}_{-0.07}$	$5.0^{+3.2}_{-1.4}$	11.8–19.5
NW	CI	10.81	$0.54^{+0.09}_{-0.10}$	$2.3^{+2.7}_{-1.4}$	15.1–39.1
NW-SIM	CI	2.77	$0.52^{+0.11}_{-0.14}$	$2.8^{+5.0}_{-2.4}$	12.1–58.6

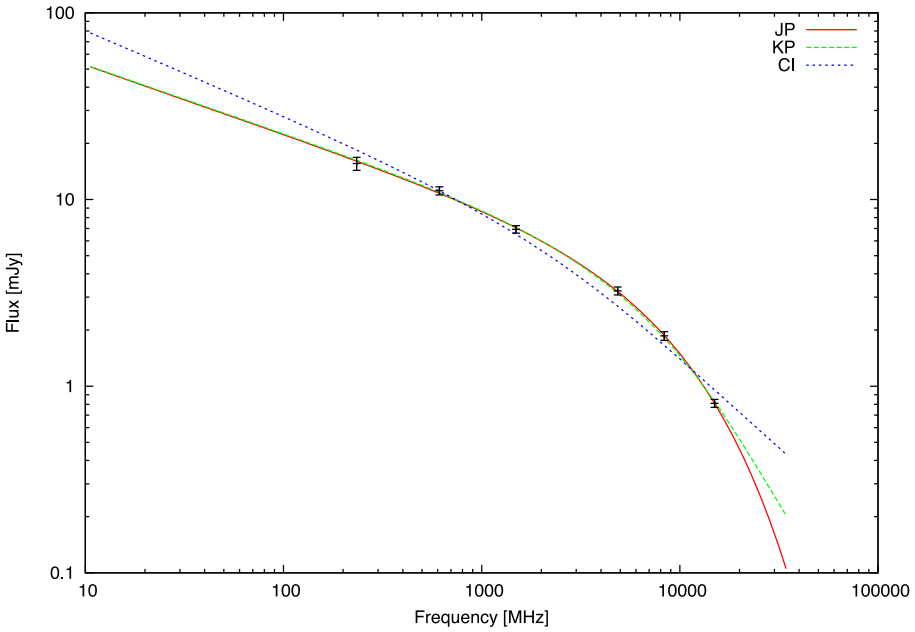

Figure 4. Three different models of the electron energy loss models fitted to the SED of the core of NGC 2445: JP (red), KP (green) and CI (blue). Details of the fitting scheme and characteristic fit parameters are provided in Section 4.3.

steepens from the initial one, in GHz). Using the magnetic field strength determined in Section 4.2, now expressed in nT, the spectral age can be calculated as:

$$\tau = 50.3 \frac{B^{1/2}}{B^2 + B_{\rm IC}^2} \times (\nu_{\rm break}(1+z))^{-1/2} \ [\rm Myr] \qquad (1)$$

where $B_{\rm IC} = 0.338(1+z)^2$ is the CMB magnetic field equivalent (Alexander & Leahy 1987). Estimated values of the injection spectral index $\alpha_{\rm inj}$, break frequency $\nu_{\rm break}$, and the spectral age are summarized in Table 4.

Both standard JP and KP models give a good representation of the data, but the fit derived using the JP model is slightly better (judging on the χ^2 value; see Fig. 4). The fit given by the CI model is worse, as the goodness-of-fit parameter χ^2 is of an order of magnitude higher than for JP and KP. No matter the chosen model, it is clearly visible that the spectral age of the core is very low, ranging from 1.6 to 5.2 Myr. Bearing in mind the possible starburst occurrence (Appleton et al. 1992) this is a reasonable value; starburst activity would result in an efficient supply of young electrons, producing a flat spectrum. The derived spectral index of the injected electron population (significantly below 0.5 for JP and KP, and 0.46 ± 0.05 for CI) indeed suggests a very flat, albeit still reliable spectrum; Weiler & Sramek (1988) give $\alpha = 0.3$ as the flattest spectrum available for the supernova remnants (SNR), and supernovae are the main sources of the non-thermal emitting electrons in the star-forming galaxies. Moreover, Hummel (1991) lists several galaxies for which the injection spectra have α in the range of 0.3–0.5, similar to our estimates, both for the core and for the NW region.

The spectral fits for the NW region can be seen in Fig. 5. Similarly to the case of the core, the JP and KP fits give better representation than the CI model. The age estimates range from 9.0 to 39.1 Myr. Even in case of the lowest value, the result is higher than the estimates of the age of the star-forming knots given by Beirão et al. (2009), who identifies two very young (2.5 and 3.5 Myrs) structures in the area coincident with our NW region. This means that the high energy electrons associated with the magnetic field are older than those involved in the recent star-forming processes. This is consistent with the steep, non-thermal spectrum of this area (Section 4.1). Most likely the magnetic field has been enhanced during the propagation of the density wave that formed the collisional ring (see Appleton & Struck-Marcell 1996), and the recent star-forming activity has weaker effect on its properties (e.g. flattens the spectrum, but as for it is a non-dominant component, the overall spectrum is still relatively steep). The injection spectral index of around 0.5 is reasonable for an extended region of synchrotron radio emission.

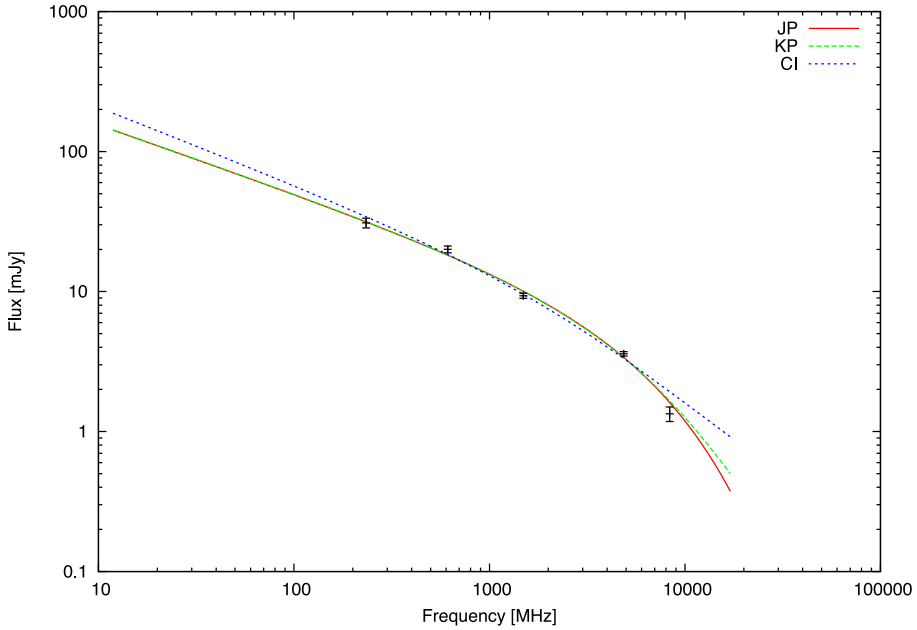

Figure 5. Three different models of the electron energy loss models fitted to the SED of the NW region of NGC 2445: JP (red), KP (green) and CI (blue). Details of the fitting scheme and characteristic fit parameter are provided in Section 4.3.

Finally, we note that the definite rejection of the CI model on the basis of available data may be premature. While for the core the mentioned fitted spectrum (Fig. 4) has generally an overmuch small curvature, for the NW region the CI model differs from the data and other fits only at the high and low ends of the analysed spectrum (Fig. 5). We keep in mind that the flux measurements at low frequencies may be affected by free–free absorption caused by ionized gas. This would decrease the flux at 234 MHz. At the high-frequency end of the radio spectrum, a small λ/D ratio and a short integration time (hence a poor (u,v) plane coverage) of interferometric observations may cause a substantial flux loss of faint extended emission. With the currently available data both effects cannot be evaluated quantitatively. We estimated possible effects of hypothetical free–free absorption and of loss of extended structures at lowest and highest frequencies, respectively, upon the results of CI model fits. We performed an experiment by increasing arbitrarily the measured flux densities of the NW region at extreme frequencies by values needed to improve the χ^2 for the CI model. It turns out that achieving similar goodness-of-fit as for the JP and KP models for the NW region requires approximately 10 per cent higher flux at 234 MHz and 30 per cent higher flux at 8440 MHz. We found that the break frequency, and thus the age estimate (noted as NW-SIM in Table 4), appeared to be similar to those obtained from the original CI fit. In the light of these estimates and of the current data status we cannot simply reject the CI model. Though it implies (regardless of possible flux losses) substantially higher limits to the spectral age than JP and KP spectral fits, it should be still kept in mind as an acceptable solution for the NW region.

4.4 Morphology of the radio emission distribution

As mentioned in Section 1, the collisional ring of NGC 2445 is far from being circular/elliptical. So is the radio emission distribution in this galaxy: its SE side is less prominent than the NW one (not only in the radio regime). The emission is weaker – not only at 234 MHz (Fig. 2a), but also in better quality maps at 612 (Fig. 2b) and 4860 MHz (Fig. 2d). Star-forming regions in the SE part have also somewhat weaker magnetic fields and are less extended. Additionally, the angular distance from the core to the ring is lower in the NW part than in the SE part. The asymmetry may result from an ongoing interaction with NGC 2444, resulting in the compression of the NW part of the ring, which leads to the amplification of the magnetic field. Such interaction has been suggested multiple times (e.g. Appleton et al. 1992, Beirão et al. 2009). The distribution of the radio-emitting medium is very similar to that of the molecular emission (Beirão et al. 2009), including lack of the PAH radio emission in the southernmost knot (labelled *D* in Beirão et al. 2009) and weak emission in the northernmost knot (*G* in Beirão et al. 2009). Both these knots have the lowest far-UV star-forming rates. This suggests that the radio emission deficiency might be the result of faster CR diffusion when compared to the synchrotron losses. Weaker magnetic field – especially in the southern part – allows CR electrons to diffuse regardless of their energy.

In general, the overall radio distribution seems to confirm the scenario of an off-axis collision and later, on-going interaction with NGC 2444. The radio ring follows the distribution of the neutral and ionized gas (Higdon, Rand & Hummel 1997; Beirão et al. 2009), which is suspected to have formed as a result of such collision. The asymmetry of the emission together with the intergalactic ridge provides evidence of an interaction with the companion galaxy. However, further details of the interaction history would need examination of the regular magnetic field properties, i.e. analysis of the polarization data (like that done for NGC 3627 by Soida et al. 2001, or the Virgo cluster spirals, by Weżgowiec et al. 2012),

5 CONCLUSIONS

We observed the tight galaxy pair Arp 143 with the GMRT at 234 and 612 MHz. Radio emission maps were analysed together with the archive VLA data at 1490, 4860, 8440, and 14940 MHz to study the spectral age of the features seen in the system, morphology

of the radio emitting medium and the magnetic field strength and energy within the pair. The results obtained are summarized below.

(i) The radio emission from NGC 2445 concentrates in the northwestern part of the optical ring, extending to the outer parts of NGC 2444. Several distinct radio emitting regions can be identified: the core, three star-forming regions, and an intergalactic ridge.

(ii) The galactic core is not very compact (0.8 on 0.5 kpc), synchrotron-emitting source. It possesses a strong magnetic field of 38.8 ± 1.7 μG. It has a relatively flat spectrum ($\alpha = 0.64 \pm 0.08$) and the age estimate yields 1.6–5.2 Myr (depending on the model fitted). This is consistent with its identification as a starburst region.

(iii) The northwestern region of radio emission, coincident with the star-forming knots, possesses magnetic field with strength of 12.0 ± 0.4 μG – somewhat stronger than the typical galactic fields. Its spectrum is typical for an ageing, yet not very old electron population, with a mean spectral index of 0.81 ± 0.07. The spectral age estimate of 9.0–39.1 Myr is higher than that of the star-forming knots given by Beirão et al. (2009), indicating that most of the radio emission is associated with an older electron population, that was injected while a density wave was propagating through the intergalactic medium.

(iv) Two other – southern and eastern – regions of star formation have been detected. Their magnetic fields (9.9 ± 0.3 and 8.7 ± 0.6 μG, respectively) are somewhat weaker than that of the northwestern one.

(v) Distribution of the radio emission from NGC 2445 shows significant asymmetry, with the northwestern part being more luminous than the southeastern one. This supports the scenario of an ongoing interaction with NGC 2444.

(vi) NGC 2444 is in general a non-radio-emitting galaxy, apart from the intergalactic radio ridge connecting it with NGC 2445. The magnetic field in the ridge is comparable to those found in the star-forming regions. It is also similar to that found in the intergalactic bridge of the Taffy galaxies (Condon et al. 1993).

(vii) There are no signs of radio emission from the H I tail reported by Appleton et al. (1987). Depending on the – yet unknown – depth of the radio emitting medium, the upper limit for the magnetic field in the tidal tail is <4.5-12 μG, yielding <1.1–6.3×10^{-12} erg cm^{-3} for its energy density.

ACKNOWLEDGEMENTS

We wish to thank the anonymous referee, whose comments and suggestions allowed us to significantly improve this article. We thank the staff of the GMRT that made these observations possible. GMRT is run by the National Centre for Radio Astrophysics of the Tata Institute of Fundamental Research. BNW is indebted to Eric Greisen, NRAO, for his help in preparing the RGB composite maps using the AIPS. This research has been supported by the scientific grant from the National Science Centre (NCN), dec. No. 2011/03/B/ST9/01859. This research has made use of the NASA/IPAC Extragalactic Database (NED) which is operated by the Jet Propulsion Laboratory, California Institute of Technology, under contract with the National Aeronautics and Space Administration. This research has made use of NASA's Astrophysics Data System. Funding for the SDSS and SDSS-II has been provided by the Alfred P. Sloan Foundation, the Participating Institutions, the National Science Foundation, the U.S. Department of Energy, the National Aeronautics and Space Administration, the Japanese Monbukagakusho, the Max Planck Society, and the Higher Education Funding Council for England. The SDSS Web Site is http://www.sdss.org/.

REFERENCES

Alexander P., Leahy J. P., 1987, MNRAS, 225, 1
Appleton P. N., Struck-Marcell C., 1996, Fund. Cosm. Phys., 16, 111
Appleton P. N., Ghigo F. D., van Gorkom J. H., Schombert J. M., Struck-Marcell C., 1987, Nature, 330, 140
Appleton P. N., Schombert J. M., Robson E. I., 1992, ApJ, 385, 491
Arp H., 1966, ApJS, 14, 1
Beck R., Krause M., 2005, Astron. Nachr., 326, 414
Beirão P., Appleton P. N., Brandl B. R., Seibert M., Jarrett T., Houck J. R., 2009, ApJ, 693, 1650
Burbridge E. M., Burbridge G. R., 1959, ApJ, 130, 12
Burke B. F., Miley G. K., 1973, A&A, 28, 379
Carilli C. L., Perley R. A., Dreher J. W., Leahy J. P., 1991, ApJ, 383, 554
Condon J. J., Helou G., Sanders D. B., Soifer B. T., 1993, ApJ, 105, 1730
Davis L. E., Seaquist E. R., 1983, ApJS, 53, 269
de Vaucouleurs G., de Vaucouleurs A., Corwin H. G., Buta R. J., Paturel G., Fouque P. 1991, Third Reference Catalogue of Bright Galaxies (RC3). Springer-Verlag, New York
Higdon J. L., Rand R. J., Lord S. D., 1997, ApJ, 489, L133
Hummel E., 1991, A&A, 251, 442
Jaffe W. J., Perola G. C., 1973, A&A, 26, 423
Kardashev N. S., 1962, SvA, 6, 317
Lacki B., Beck R., 2013, MNRAS 430, 3171
Lynds R., Toomre A., 1976, ApJ, 209, 382
Murgia M., 1996, Laurea thesis, University of Bologna
Myers S. T., Spangler S. R., 1985, ApJ, 291, 52
Nikiel-Wroczyński B., Soida M., Urbanik M., Beck R., Bomans D. J., 2013, MNRAS, 435, 149
Niklas S., 1995, PhD thesis, University of Bonn
Niklas S., Klein U., Wielebinski R., 1997, A&A, 322, 19
Pacholczyk A. G., 1973, Radio Astrophysics. Freeman, San Francisco (1970, Mir, Moscow)
Romano R., Mayya Y. D., Vorobyov E. I., 2008, AJ, 136, 1259
Soida M., Urbanik M., Beck R., Wielebinski R., Balkowski C., 2001, A&A, 378, 40
Sulentic J. W., 1976, ApJS, 32, 171
Theys J. C., Spiegel E. A., 1977, AJ, 212, 616
Weiler K. W., Sramek R. A., 1988, ARA&A, 26, 295
Weżgowiec M., Urbanik M., Beck R., Chyży K. T., Soida M., 2012, A&A, 545, 69

This paper has been typeset from a TEX/LATEX file prepared by the author.

MONTHLY NOTICES of the Royal Astronomical Society

Probing the magnetic field of the nearby galaxy pair Arp 269

Journal:	*Monthly Notices of the Royal Astronomical Society*
Manuscript ID:	MN-15-1764-MJ
Manuscript type:	Main Journal
Date Submitted by the Author:	10-Jun-2015
Complete List of Authors:	Nikiel-Wroczyński, Błażej; Astronomical Observatory, Jagiellonian University, Radio Astronomy and Space Physics Jamrozy, Marek; Astronomical Observatory, Jagiellonian University, Stellar and Extragalactic Astronomy Soida, Marian; Astronomical Observatory, Jagiellonian University, Radio Astronomy and Space Physics Urbanik, Marek; Astronomical Observatory, Jagiellonian University, Radio Astronomy and Space Physics Knapik, Jacek; Astronomical Observatory, Jagiellonian University, Radio Astronomy and Space Physics
Keywords:	galaxies: individual:... < Galaxies, galaxies: interactions < Galaxies, galaxies: magnetic fields < Galaxies, galaxies: ISM < Galaxies, radio continuum: galaxies < Resolved and unresolved sources as a function of wavelength

MNRAS 000, 1–13 (xxxx) Preprint 10 June 2015 Compiled using MNRAS LATEX style file v3.0

Probing the magnetic field of the nearby galaxy pair Arp 269

B. Nikiel-Wroczyński*, M. Jamrozy, M. Soida, M. Urbanik, and J. Knapik
Astronomical Observatory, Jagiellonian University, ul. Orla 171, Kraków PL 30-244, Poland

Accepted xxxx. Received xxxx; in original form xxxx

ABSTRACT

We present a multiwavelength radio study of the nearby galaxy pair NGC 4490/85. High sensitivity to extended structures gained thanks to the merged interferometric and single dash maps allowed us to reveal a previously undiscovered extension of the continuum emission. Its direction is significantly different from the one of the neutral gas tail, suggesting that there it might be associated with another outflow. The population of radio electrons is in general young, suggesting an ongoing vigorous star formation – this claim is supported by strong magnetic fields, similar to that found in much larger spiral galaxies. From the study of the spectrum we conclude that the electron population in the intergalactic bridge between member galaxies originates from the disk areas and therefore its age (app. 4–17 Myrs, depending on the model used) reflects the timescale of the interaction. We have also discovered an angularly near Compact Steep Source at a redshift of approximately 0.125.

Key words: galaxies: magnetic fields – galaxies: individual: NGC 4490, NGC 4485 – galaxies: pairs: individual: VV 030, Arp 269 – galaxies: interactions – intergalactic medium – radio continuum: galaxies

1 INTRODUCTION

Among the diversity of forms that intergalactic structures can take, giant gaseous tails or streams accompanying galaxy interactions constitute the most impressive phenomena. Widespread, dense and wide, they are able to transport matter tens of kiloparsecs away from the parent galaxies. These tails are sometimes accompanied by streams of stars, either formed in the tail, or inherited from the galaxy. Galaxy systems that contain such tails are usually referred to as the "gas streamers". Notable examples include the Leo Triplet, where the tail extends by more than 140 kpc from NGC 3628 (Haynes et al. 1979; Stierwalt et al. 2009), or Arp 143, where close encounter of the pair members results in mass loss experienced by one of the galaxies, while the tail traces its trajectory around the companion (Appleton et al. 1987). The gaseous tails are often the site of formation of the so–called tidal dwarf galaxies (TDG)

An open question concerning these intergalactic giants is the existence and importance of magnetic fields inside them. Ability to transport gas far away from the intra-system medium gives a possibility that the magnetic field – frozen into the gas – can be supplied to the large volumes of intergalactic space. This raises an interesting question, whether the outflows and tidal tails can play a crucial role in the magnetisation of cosmic space. Also, the dynamical importance of the magnetic field in the evolution of such structures is yet unknown. Magnetic fields are known to be one of the major part-takers in dynamics and evolution of galaxies (Beck & Wielebinski 2013). Outside the galaxies their importance should rise because the density of thermal gas and gravitational energy is lower than in galactic disks. Study of the intergalactic structures yields a possibility to learn more about the magnetic field itself. Unfortunately, though some neutral gas structures with magnetic field were found between the galaxies, there is no definite observational evidence for magnetisation of large–scale outflows and tails.

Nearby galaxy pair NGC 4490/85, the so-called "Cocoon Galaxy" is one of the bright, nearby galaxies from the Shapley-Ames Catalogue (Sandage & Tammann 1981). The intergalactic space between these two objects is filled with numerous areas of star formation. This is a clear sign of the interaction between the pair members. NGC 4490 is a very special case of an interacting system. Despite the small distance between member galaxies of the pair and

* E-mail:iwan@oa.uj.edu.pl

the "cocoon" outlook, tidal forces have not yet disrupted its disk, as the interaction is just starting. There is just one hint for this process (apart from the mutual proximity of galaxies): a large stream of star-forming regions between the galaxies, accompanied by the bridge of radio emission . However, two other phenomena that are usually explained on the basis of tidal interactions – giant neutral gas tails, and generally rapid star formation – are not triggered by the merging process. Clemens et al. (1998) suggests, that NGC 4490 is a very young galaxy, that rapidly forms stars at a constant rate and the giant tails result from the wind caused by frequent supernovae explosions.

Given a high efficiency of the star formation in this system one can conclude that strong magnetic fields can be found inside galaxies, and, hopefully, also outside of them. Studying magnetic fields in Arp 269 is also interesting as it provides a unique possibility to study the gas magnetisation in the eve of the interaction process. As this galaxy is also a dwarfish system, the merging process might be similar to that which gave rise to the present time large galaxies by the agglutination of small objects. Particularly interesting is the chance to survey the HI envelope for the traces of radio continuum emission.

A detailed study of the radio emission from this galaxy pair has been made by Clemens et al. (1999). These authors have presented interferometric maps of the emission at various radio frequencies. High resolution of these images – 12 arcseconds – provided a detailed insight into the morphology of the radio emission. However, achieving such a small beam requires a loose configuration of the interferometer. This leads to an incomplete sampling of the innermost part of the (u,v) plane, hence, the loss of extended emission. This effect turns out to be important in studies of NGC 4490/85 made by Clemens et al. (1999) who state substantial flux loss of 40% at 8.46 GHz. This precluded any search for diffuse intergalactic structures.

An useful solution that allows to regain the missing flux information whilst retaining high resolution can be obtained by merging the interferometric and single dish data. The resultant image has both high resolution and sensitivity to the extended structures. In a propitious situation, nearly all the missing flux and structures can be successfully restored.

High frequency interferometric observations of intergalactic, diffuse emission also suffer of limited primary beam size. Moreover, without the continuous supply of relativistic particles the radio spectrum of intergalactic structures quickly steepens making the intergalactic emission undetectable at high frequencies. For this reason we performed sensitive, low-frequency observations using the Giant Metrewave Radio Telescope (GMRT) at 0.61 GHz. This enabled us to search for the radio emission produced by the low energy electrons that have longer lifetimes thus, their emission can be traced at larger distances from their sources in galactic disks. As there were no previous, detailed studies of this galaxy that made use of the under-gigahertz frequencies, our observations enable more accurate estimations of the spectral parameters, like the break frequency, or synchrotron age. Additionally, the large primary beam of GMRT permits to study structures of larger angular scales than at several GHz.

In our paper we present the merged maps of the radio emission at the previously studied frequencies, and also we include new map at 0.61 GHz from our own GMRT observations. This data are used to probe the magnetic field in various regions within and outside the member galaxies, allowing a study the radio emission of a very young galaxy in the beginning of the galaxy merging process with unprecedented fidelity and in a broad frequency range.

2 OBSERVATIONS AND DATA REDUCTION

2.1 GMRT data

The lowest frequency used in our study is 0.61 GHz. These data have been recorded using the GMRT interferometer. The observations were carried out in February, 2013. The total bandwidth was 32 MHz (divided into 256 channels) and the total time-on-source (TOS) was 5.5 h (integration time of 16 s). Calibration, flagging and further reduction of these data was carried out using the Astronomical Image Processing System (AIPS). We used 3C 286 to calibrate amplitudes (and bandpass) and the angularly source 1227+365 to calibrate phases. A set of 49 sub-images, (u,v)-tapered to obtain a circular beam, has been made, and all of them have been processed by a self-calibration pipeline to correct the phase information. The final map has been made by the means of tessellation of the sub-images. Primary beam correction has also been applied.

2.2 Archive VLA data

The over-gigahertz interferometric data have been taken from the NRAO JVLA Data Archive. We used data at 1.49, 4.86, 8.46, 14.9 and 22.5 GHz, recorded in different configurations and time windows. An overview of the datasets used can be found in Table 1. All these data have been calibrated following the standard procedure outlined in the AIPS Cookbook.

2.3 Effelsberg data

The single-dish total power data at 4.86 and 8.35 GHz have been obtained in 2005, using the Effelsberg radio telescope [1]. The lower frequency observations consisted of 32 coverages scanned in azimuth-elevation frame, whereas the higher frequency ones were made from 35 coverages recorded in R.A. and Dec. Both datasets were calibrated with 3C 286 as the flux calibrator (flux values as given by Baars et al. 1977) and reduced using the NOD2 package (Haslam 1974). Further details on how these maps have been processed will be

[1] Based on observations with the 100m telescope of the MPIfR (Max-Planck-Institut für Radioastronomie) at Effelsberg

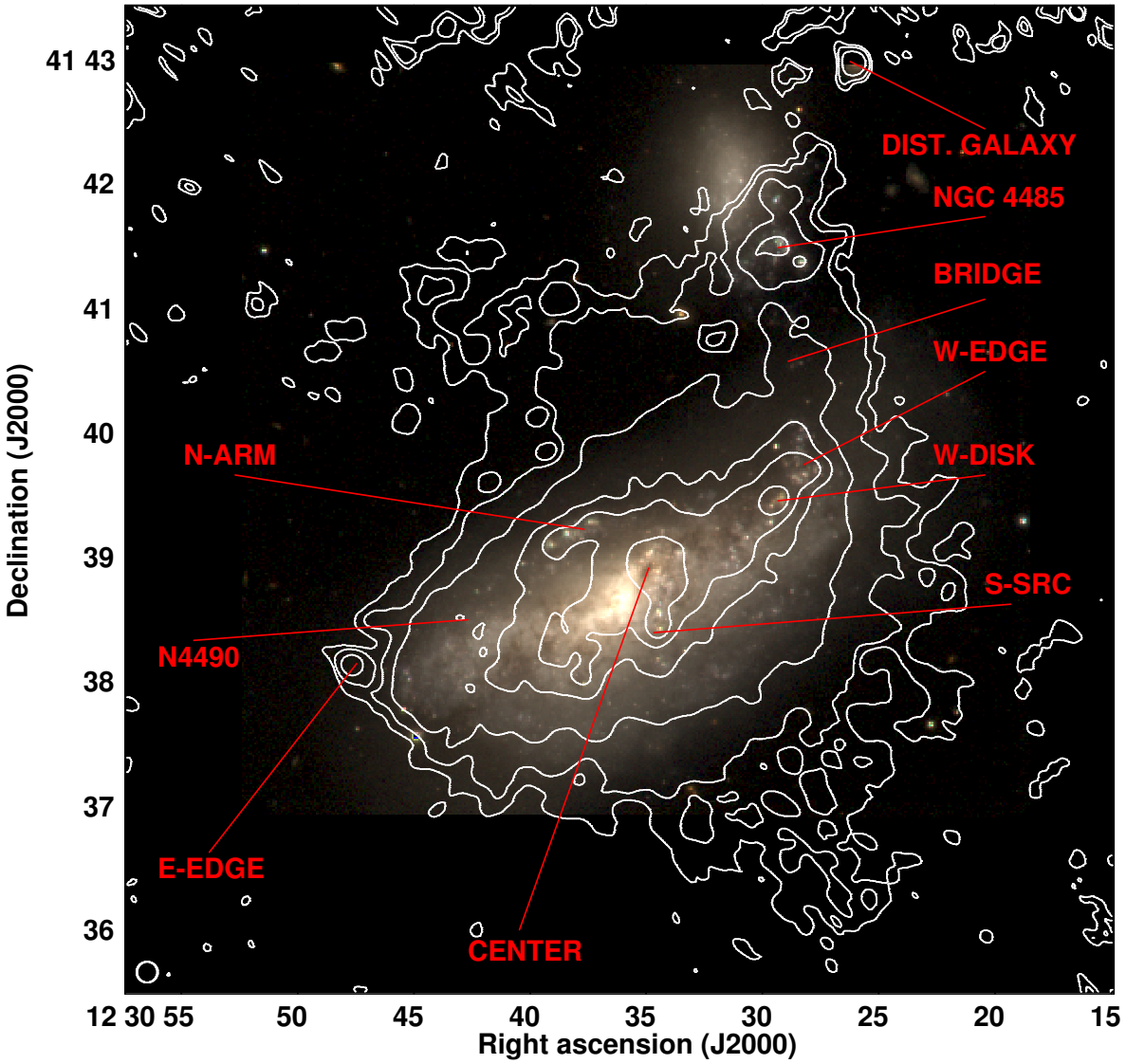

Figure 1. Merged VLA + Effelsberg map of the TP emission at 4.86 GHz overlaid upon an RGB image, with locations of the regions discussed in this paper indicated. The contour levels are $3, 5, 10, 20, 30, 50, 100\times$ 40 μJy/beam (r.m.s. noise level). The angular resolution is 10 arcsec. The beam is represented by a circle in the lower left corner of the image. Details of the maps used to produce this RGB composite can be found in the text (Sect. 3).

presented in a forthcoming paper on the polarised emission from this galaxy pair (Knapik et al. 2015, in preparation).

2.4 Merging procedure

As mentioned in Sect. 1, one of the goals of our study was to achieve a modest resolution while having most of the flux retained. In order to do so, merging procedure has been performed. We used AIPS task IMERG and followed an approach previously used eg. by Soida et al. (2001). To fulfill the procedure requirements, the single dish maps were multiplied by the VLA primary beam at a given frequency and their size was transformed into a power of 2 (FFT requirement). The interferometric data have been transformed using the task HGEOM to make the geometry of the high- and low-resolution images consistent. The (u,v)-range of overlapment was chosen basing on the task's internal calculation of the normalisation factor (which should be equal to the ratio of the beam areas of the images merged). The resulting maps have been corrected for the primary beam. As a sanity check, we

Table 1. Basic information on the interferometric datasets used in this study. In case of multiple configuration datasets, the time-on-source (TOS) and noise values are given for the final ones. The angular resolution is 10 arcseconds.

Freq. GHz	Telescope	Proj. code	Date	TOS [min]	r.m.s. [μJy/10"]
0.61	GMRT	23_025	10.02.2013	335	60
1.49	VLA B	AA 116	21.08.1990	109	55
	VLA C	AA 181	18.10.1994		
	VLA D		15.03.1995		
4.86	VLA C	AA 181	18.10.1994	86	40
	VLA D		15.03.1995		
8.44	VLA B	AA 181	26.12.1995	147	55
	VLA C		21.08.1990		
	VLA D		16.03.1995		
14.94	VLA B	AJ 115	16.04.1985	132	100
22.46	VLA C	AJ 291	15.11.2002	215	50

measured the total flux in the maps before and after merging. The values for the final maps agree within the 5 per cent error with the single-dish data; as fluxes of the point sources before and after merging are also consistent, we consider that the merging procedure went out with a success. For the sake of strictness we note here, that the central frequencies of the used X-band (8 GHz) data differ insensibly; however, the flux difference does not exceed 1 per cent for the radio sources with spectral indices not steeper than 1 (using the $S_\nu \propto \nu^{-\alpha}$ definition of the spectral index α) – far lower than the assumed calibration errors. A detailed description of the merging process with the theoretical basis explained can be find in Stanimirovic (2002).

3 RESULTS

To familiarise the reader with the different structures described and analysed in this paper, we include a demonstration image of the radio emission with designations of individual sources marked (Fig. 1). Contours from our merged (VLA+Effelsberg) radio data at 4.86 GHz have been overlaid upon a composite RGB image made from the Johnson's RVB maps produced by the Vatican Advanced Technology Telescope (Taylor et al. 2005). Details on the characteristics of the emission of these entities can be found in Sect. 4.6.

The GMRT map at 0.61 GHz (Fig. 2a) constitutes the lowest frequency image in our study. The radio emission from the galaxy pair is fairly strong, emerging not only from the disk of NGC 4490, but also from several sources associated to NGC 4485, and from an intergalactic bridge that connects members of this galaxy pair. The northwestern side of NGC 4490 is more pronounced than the opposite one. North from the pair, a point-like source can be seen. This source is a distant galaxy, not related to two main galaxies.
It is clearly visible that the emission in the GMRT map is less extended in the southern direction than in the high-frequency map at 4.86 GHz. At the same time, the northern part reaches its maximum extension at 0.61 GHz. This is because the GMRT lacks short spacing information; the (u,v)-plane coverage is moreover comparable to the VLA B/C configuration at L-band (1.49 GHz). This results in lower sensitivity to extended structures and hence only the northwestern extension, which is bright enough, is visible. Sharp edges of the emission – manifesting as an overdensity of the 3 and 5 σ contours – confirm this statement.

The 1.49 GHz data (Fig. 2b) also come from the interferometer only. Merged B, C, and D configurations of the VLA provide (u,v)-coverage dense enough in the innermost part of the plane to recover more extended emission than at 0.61 GHz. Not only does the disk extend in the NW direction, but also a weaker, albeit still easily detectable extension can be found on the SE side. Intergalactic bridge and distant galaxy can also be seen.

The merged 4.86 GHz (Fig. 2c) map combines high resolution of the VLA with an excellent sensitivity to extended emission provided by the single dish data. Also, the primary beam is reasonably large, so that regions relevant to our study do not fall into its outskirts, where flux uncertainties are higher. Worth noticing is the extent of the intergalactic emission, which at 4.86 GHZ spans wide in both NE and SW directions. A detailed comparison of this structure to the giant HI tails is presented in Sect. 4.5. The intergalactic bridge between NGC 4490 and 4485 is still visible, but less prominent than at lower frequencies. The distant radio galaxy lies close to the edge of the primary beam area, but still is easily detectable.

At 8.44 GHz (Fig. 2d), losses of relativistic electrons become much more pronounced. Large extensions of the radio emitting area vanish. Only a small remnant of the northern structure can be seen. There is no hint for emission from the intergalactic bridge. The galactic disk is visibly shrunk in all directions, and its boundaries lie within the outermost areas of the lowest contour. There are several "holes" in this contour and it barely reaches the easternmost source. The primary beam at this frequency is rather small (the cutoff lies directly beyond the optical contour of the companion galaxy), hence the distant galaxy is not detected.
It should be noted here that the quality of the 8.44 GHz

map is considerably lower than the one at 4.86 GHz. The main problem of this map is that due to the worse (u,v)-coverage at this frequency the galaxy is surrounded by a negative 'bowl'. Nevertheless, lower extent of the radio emission seems to be connected with the spectrum steepness, not data quality; there is no clear evidence for large extensions found at 4.86 GHz even in the original, low-resolution Effelsberg map.

At two highest frequencies, 14.93 and 22.46 GHz, the primary beam is so small that it does not contain the whole galaxy. Also, the sampling of the (u,v)-plane becomes more sparse and thus the sensitivity to extended structures drops significantly. In both of these maps, only the brightest, compact sources are visible. One of them is the point-like source south from the galactic centre; because of the low quality of the 14.93 GHz map, more emission surrounding it is detected at 22.46 GHz – there is a short ridge of extended emission elongated in the N–S direction. The second source that is visible on both of these maps is the western disk region of star formation (W–DISK).

4 ANALYSIS AND DISCUSSION

In this section we describe the procedure used for the separation of thermal and non-thermal emission contents (Sect. 4.1) and results of estimation of parameters for which it is required: non-thermal spectral index (Sect. 4.2), total magnetic field (Sect. 4.3), and spectral age of the electron population (Sect. 4.4). Particular sources are described in Sect. 4.6. Coincidence between the continuum structures that extend north and south from NGC 4490 and the neutral hydrogen distribution is also discussed (Sect. 4.5). Remarks on the (non-detected) remnant of SN2008ax and the detected distant galaxy can be found in Sect. 4.7 and 4.8, respectively. Values measured and derived can be found in two tables: Table 2 lists the total and non-thermal fluxes of the selected structures, while Table 3 contains information regarding the magnetic field, injection spectral index, break frequency and spectral age of these entities. Location of the specific sources have been marked in Fig. 1.

4.1 Thermal flux separation

A crucial issue when describing the radio emission is proper separation of the thermal and non-thermal components. There are several possible ways to deal with this issue. The spectrum can be described by a following function (Niklas et al. 1997):

$$\frac{S_\nu}{S_{\nu_0}} = f_{\rm th}^{\nu_0} \left(\frac{\nu}{\nu_0}\right)^{-0.1} + (1 - f_{\rm th}^{\nu_0}) \left(\frac{\nu}{\nu_0}\right)^{\alpha_{\rm nth}} \qquad (1)$$

This function is a sum of two power-law components: thermal (scaling with the power of –0.1) and synchrotron (scaling with the parameter $\alpha_{\rm nth}$) ones. Unlike the aforementioned authors, who fitted only the total spectra of the selected galaxies, we attempted to do a pixel-by-pixel fit of the values from the radio maps. As the 14.93 GHz map has a very small primary beam, its quality is insufficient to be used in the spectral study. Therefore, to broaden the frequency coverage at the higher end of the SED, we used also the Ryle Telescope 15.2 GHz map from Clemens et al. (1999), courtesy of M. Clemens. However, it turns out that even broader range of frequencies is necessary, as the fitted values have shown strong dependence on the initial ones, yielding the results unreliable. Hence, we decided to attempt to perform a direct subtraction of the thermal flux. This can be done basing on the knowledge of the H_α flux, which is closely related to the radio emission.

We made an attempt to re-create the procedure described by Heesen et al. (2015): we took the map of the H_α emission from Spitzer Local Volume Legacy (LVL) database (Dale et al. 2009). The map was calibrated using the standard procedure described in the LVL cookbook. It was then re-scaled to more useful units to be used for the thermal flux estimation using the conversion equation presented by Deeg et al. (1997), where the correction for galactic extinction was conducted using $E(B-V) = 0.019$, as basing on Schlegel et al. (1998); Schlafly & Finkbeiner (2011). The H_α flux is a subject to the dust absorption in the host galaxy; this effect can be corrected with the usage of the dust emission flux multiplied by a specific coefficient (Calzetti et al. 2007; Kennicutt & Evans 2012). We decided to use the Spitzer MIPS 24 μm data, also available from the LVL archive. It should be explicitly noted here, that despite very low (several per cents) foreground extinction, the unknown internal one (inside the dense regions of radio emission) can still be significant (see Sect. 4.6). Therefore, derived values for the thermal flux should be assumed to be the lower boundaries for its real value; this, in turn, implies that the non-thermal flux values can be considered as its upper limit (however, one should bear in mind that the purely interferometric maps might be a subject to the zero spacing problem).

AIPS was used to subtract the thermal content in order to produce maps of the non-thermal emission. These maps (which can be found in Table 2) were then used for the magnetic field and spectral parameters estimation.

4.2 Spectral index

The sole non-thermal emission yields a possibility to calculate the non-thermal spectral index. We decided to use the GMRT 0.61 GHz map and the VLA+Effelsberg 4.86 GHz data. These maps have the highest fidelity among our set, and the extent of the intergalactic structure is the largest. The map of the spectral index can be seen in Fig. 3. The disk emission is characterised by indices of 0.6–0.75, typical for a non-thermal, not yet aged electron population. Several spots of flatter spectrum can be seen. The most notable one is S-SRC, for which the separation of the thermal and non-thermal content was not entirely successful (see Sect. 4.6 for details). The other areas correspond to the star-forming regions dispersed through the disk. From the spectral index map, no significant steepening of the spectrum in the intergalactic areas can be found, suggesting that the electron population is still young. A noticeable feature of the spectral index map is the flat spectrum of both of the outflows mentioned in Sect. 3. This effect shows how much of the 4.86 GHz diffuse flux has been recovered compared to the low frequency maps.

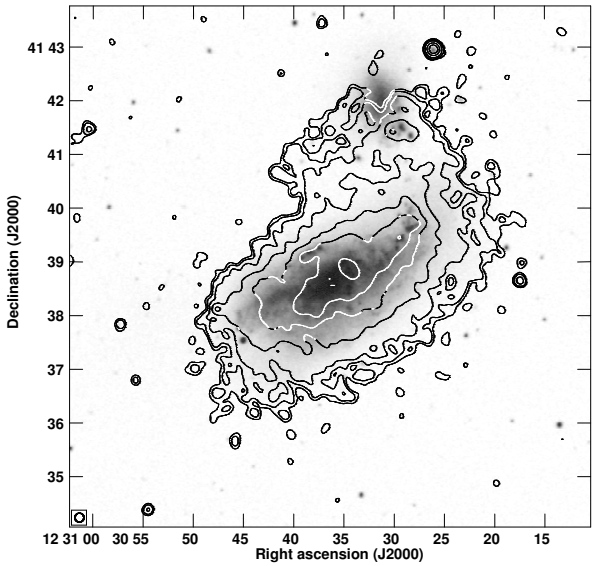

(a) GMRT map at 0.61 GHz. The r.m.s. noise level is 60 μJy/beam

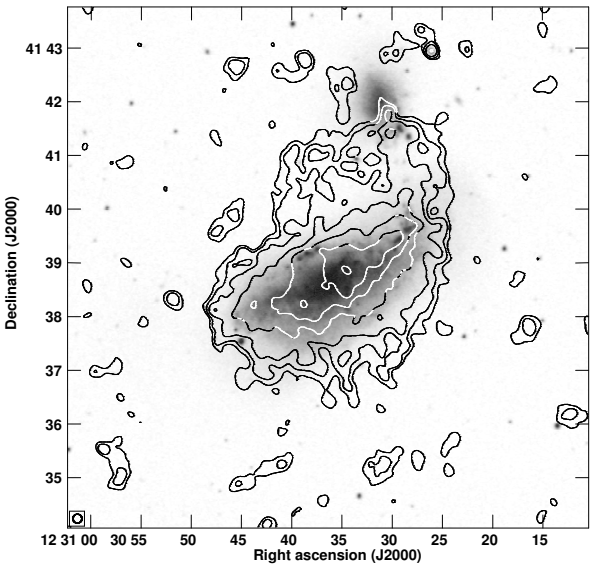

(b) VLA map at 1.49 GHz. The r.m.s. noise level is 55 μJy/beam.

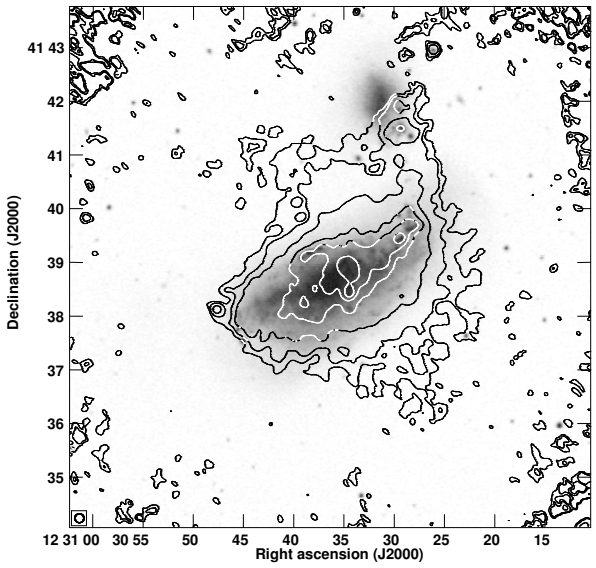

(c) Effelsberg+VLA map at 4.86 GHz. The r.m.s. noise level is 40μJy/beam.

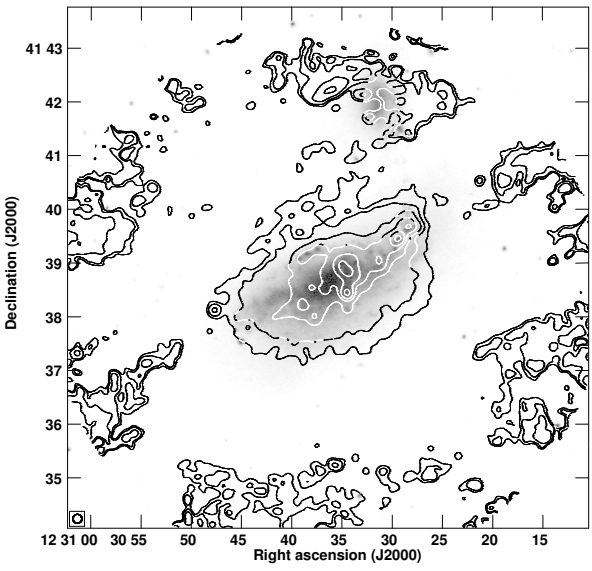

(d) Effelsberg+VLA map at 8.35 GHz. The r.m.s. noise level is 55μJy/beam.

Figure 2. Maps of the TP emission of NGC 4490 overlaid upon an POSS-II R-band image. The contour levels are 3, 5, 10, 20, 50, 100, 250× r.m.s. noise level. The 10-arcsec beam is represented by a circle in the lower left corner of the image.

4.3 Magnetic field

Estimates for the strength and energy density of the magnetic field can be derived from the non-thermal intensity and non-thermal spectral index under the assumption of energy equipartition between the cosmic rays and the magnetic field. A set of necessary formulae was presented by Beck & Krause (2005). These Authors have also released the code BFELD, that computes the magnetic field strength as well as its energy density. BFELD uses following parameters: total pathlength through the source D, proton–to–electron energy density ratio K_0, non-thermal spectral index α, and the mean synchrotron surface brightness of the chosen region. For K_0 we used the typical value of 100, which is right even for the starburst galaxies (Lacki & Beck 2013).

Table 2. Flux densities (with errors) obtained for the selected regions of radio emission.

Region	Component	Flux in mJy at a given frequency, expressed in GHz					
		0.61	1.49	4.86	8.35	15.21	22.46
Total	TOT	1426 ± 114	800 ± 40	357 ± 18	151 ± 7	95 ± 5	*
	NTH	1386 ± 111	761 ± 38	322 ± 16	121 ± 5	69 ± 4	*
Smooth Disk	TOT	1360 ± 114	763 ± 40	328 ± 18	131 ± 7	74 ± 5	*
	NTH	1336 ± 111	733 ± 38	302 ± 16	100 ± 5	56 ± 4	*
NGC 4485	TOT	2.80 ± 0.17	1.85 ± 0.11	0.90 ± 0.07	*	0.94 ± 0.09	*
	NTH	2.45 ± 0.17	1.36 ± 0.10	0.46 ± 0.07	*	0.42 ± 0.09	*
Bridge	TOT	27.82 ± 1.42	15.43 ± 0.80	6.54 ± 0.37	*	1.34 ± 0.19	*
	NTH	27.39 ± 1.40	15.04 ± 0.78	6.19 ± 0.36	*	1.03 ± 0.19	*
N-Arm	TOT	7.80 ± 0.44	4.50 ± 0.23	3.31 ± 0.16	2.50 ± 0.17	1.41 ± 0.13	*
	NTH	5.43 ± 0.35	3.20 ± 0.20	1.69 ± 0.14	0.99 ± 0.15	0.46 ± 0.12	*
Center	TOT	28.85 ± 2.32	16.37 ± 0.85	12.03 ± 0.62	7.99 ± 0.46	9.98 ± 0.53	1.24 ± 0.16
	NTH	23.99 ± 1.93	11.66 ± 0.62	8.24 ± 0.44	4.18 ± 0.31	6.61 ± 0.37	0.04 ± 0.01
E-Edge	TOT	2.25 ± 0.19	1.09 ± 0.09	0.46 ± 0.05	0.42 ± 0.06	0.27 ± 0.05	*
	NTH	2.25 ± 0.19	1.16 ± 0.09	0.46 ± 0.05	0.43 ± 0.06	0.27 ± 0.05	*
W-Disk	TOT	9.69 ± 0.78	6.07 ± 0.32	4.65 ± 0.24	4.02 ± 0.22	2.70 ± 0.15	1.41 ± 0.11
	NTH	7.97 ± 0.65	4.59 ± 0.25	3.93 ± 0.21	2.87 ± 0.17	1.90 ± 0.12	0.86 ± 0.09
W-Edge	TOT	10.34 ± 0.84	4.12 ± 0.24	3.43 ± 0.19	1.68 ± 0.15	1.77 ± 0.13	*
	NTH	6.01 ± 0.50	2.83 ± 0.19	2.70 ± 0.16	1.28 ± 0.14	1.10 ± 0.11	*
Dist. Galaxy	TOT	5.06 ± 0.26	1.47 ± 0.09	0.49 ± 0.05	*	*	*
	NTH	**	**	**	**	**	**

* Area not included into the primary beam
** Area not covered by the H_α map

Table 3. Parameters used and derived in magnetic field and spectral properties estimations. Explanation is provided in the text.

Region	α_{NTH}	B_{TOT} [μG]	U_B [erg cm^{-3}]	$\alpha_{inj,JP}$	$\alpha_{inj,CI}$	$\nu_{break,JP}$ [GHz]	$\nu_{break,CI}$ [GHz]	Age (JP) [Myr]	Age (CI) [Myr]
Total	0.70	21.9 ± 2.9	1.91 ± 0.50	0.73	0.63	21.83 – 92.62	1.32 – 5.76	1.39 – 3.76	5.57 – 15.30
Sm. Disk	0.71	21.5 ± 2.8	1.85 ± 0.48	0.68	0.69	13.84 – 37.49	1.59 – 6.96	2.25 – 4.83	4.61 – 14.25
NGC 4485	0.80	15.5 ± 2.0	0.96 ± 0.24	0.71	0.71	> 48.98	> 6.95	< 4.12	< 10.94
Bridge	0.72	18.3 ± 2.0	1.39 ± 0.28	0.45	0.59	7.86 – 16.03	1.82 – 8.91	4.15 – 8.08	5.56 – 16.80
N-Arm	0.56	25.5 ± 3.5	2.61 ± 0.71	0.43	0.44	11.81 – 77.96	1.87 – 38.48	1.20 – 4.08	1.72 – 10.34
Center	0.51	39.3 ± 5.4	6.19 ± 1.71	0.44	0.44	> 513.37	> 172.82	< 0.27	< 0.54
E-Edge	0.76	21.7 ± 2.8	1.89 ± 0.49	0.69	0.69	> 97.02	> 22.20	< 1.80	< 3.76
W-Disk	0.61	26.0 ± 3.5	2.72 ± 0.73	0.38	0.38	> 92.30	> 28.95	< 0.73	< 2.72
W-Edge	0.84	18.2 ± 2.3	1.33 ± 0.33	0.38	0.38	40.88 – 8989	11.03 – 2836	0.20 – 1.85	0.33 – 6.89

4.4 Age of the structures

Successful separation of the thermal and non-thermal emission opens also a possibility to calculate the so-called spectral age. This parameter is defined as the amount of time elapsed since the last acceleration of the electrons that are responsible for the observed radiation. However, as various physical processes are characterised by different time-scales of the electron spectrum decay, one can choose from several models of the electron losses. We decided to follow the procedure utilised by us in a previous paper (Nikiel-Wroczyński et al. 2014). Hence, estimations of the break frequency were done using the SYNAGE package (Murgia 1996), which allows to test Jaffe–Perola (Jaffe & Perola 1973, JP), Kardashev–Pacholczyk (Kardashev 1963; Pacholczyk 1973, KP), or continuous injection (Pacholczyk 1973; Myers & Spangler 1985; Carilli et al. 1991, CI) models of electron energy losses. SYNAGE uses the spectral energy distribution (SED) to determine following parameters: spectral index of the injected electron population α_{inj} and the frequency above which the observed spectrum steepens from the initial one – the spectral break frequency ν_{break} (expressed in GHz). The common assumption for all these three models is that the magnetic field stays constant. The first two models present a similar approach to the problem, differing in the matter of the evolution of the pitch angles of charges gyrating in the magnetic field. JP assumes its isotropisation (time-scale of this process is significantly lower than the radiative lifetime), whereas KP postulates its conservation. The third one (CI) is significantly different, as it includes the continuous injection of a power-law distributions of relativistic electrons. The resulting electron spectrum is then an outcome of emission from various synchrotron populations. Final calculation of the spectral age implies knowledge of the magnetic field strength. In the previous studies, constant value of the magnetic field throughout the pair area was assumed. To improve the age estimates, we used the values calculated in Sect. 4.3 (expressed in nT) and substituted them to the following equations:

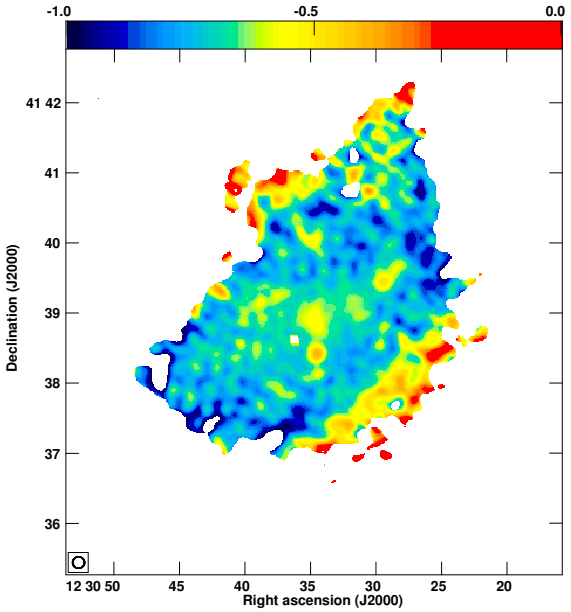

Figure 3. Map of the non-thermal spectral index calculated between 0.61 and 4.86 GHz. The angular resolution is 10 arcsec.

$$\tau = 50.3 \frac{B^{1/2}}{B^2 + B_{\rm IC}^2} \times (\nu_{\rm break}(1+z))^{-1/2} [\rm Myr] \qquad (2)$$

where $B_{\rm IC} = 0.338(1+z)^2$ is the CMB magnetic field equivalent (Alexander & Leahy 1987). Obtained values of $\alpha_{\rm inj}$, $\nu_{\rm break}$, and of the spectral age are summarised in Table 3.

4.5 Coincidence between the radio and neutral hydrogen emission

One of the most distinctive features of the NGC 4490/85 system are the giant neutral hydrogen tails that extend in the north and south direction from NGC 4490. The unusual HI morphology of this pair was first reported by Dean & Davies (1975), who used the Jodrell Bank Mark II telescope to create square grids of pointings for a selected list of nearby galaxies. For NGC 4490, they noticed that the gaseous halo is much larger in diameter than the optical counterpart. The first maps, made by Viallefond et al. (1980), revealed the morphology of the emission. Arp 269 is a "gas streamer", a system in which the neutral gas is not confined between member galaxies (like it happens for eg. HCG 95, Verdes-Monenegro et al. 2000, or NGC 691, van Moorsel 1988), but extends beyond them, a good example being Leo Triplet, Haynes et al. 1979, or Arp 143 – Appleton et al. 1987). An issue if such structures can also transport magnetic field outside the galaxy systems is still open, as the radio data on galaxy groups are still scarce. If common, this mechanism can lead to the magnetisation of large volumes of intergalactic space – which happens in the case of Arp 244 (the Antennae galaxies, Chyży & Beck 2004f).
In both of the aforementioned streamers, not even single spot of radio emission does coincide with the neutral hydrogen filaments (Nikiel-Wroczyński et al. 2014, 2013). Compared to them, NGC 4490 looks like it lights the candle of solace, as – so it can be seen in Fig. 5 – both northern and southern extensions of the radio continuum envelope follow the hydrogen distribution. However, the angle between the galactic disk and the magnetised outflow is different than this between the disk and neutral gas tails; whereas the tails are oriented in the NW–SE direction, the outflows are oriented the other way round: NE–SW. As the continuum extensions do not exceed the innermost part of the HI halo, it is impossible to judge if the magnetic field is being pulled through the tails, or in another direction. Despite the question of the coincidence being left open, the morphology still suggests that a bubble of dense, magnetised matter does extend from the disk and might eventually be transported further as the matter propagates. As for the neutral component, this might be driven by the wind caused by supernovae having their progenitors in the still-active star forming regions of the galactic disk (Clemens et al. 1998), but not necessarily do this two outflows constitute of the same intergalactic gas phase.
Attempts to connect the continuum extension with the Hα outflow detected by Clemens et al. (2000) were also unsuccessful, as the radio extension reaches much further into the intergalactic medium.

Such a doubt does not apply to the bridge that connects the pair members; in this case the intergalactic radio emission is accompanied by a stream of stars, and a maximum in the neutral gas emission. This clearly suggests the interaction-based origin of this structure.

4.6 Details on the galaxy pair and individual regions

4.6.1 Galaxy pair as a whole

The whole envelope of the radio emission is fitted well by both JP and CI models. Only small deviations from the model curve can be seen (Fig. 4). The biggest outlier is the one that represents the 4.86 GHz flux. This is because of the aforementioned extent of the radio envelope at this frequency. The injection spectral index $\alpha_{\rm inj}$ 0.73 and 0.63 for JP and CI models, respectively) is somewhat flatter than the non-thermal spectral index value calculated by Niklas et al. (1997), 0.76±0.03; however, this is not unusual, as the injection index refers to the value calculated at the lowermost edge of the SED, while the value given by Niklas et al. (1997) refers to higher frequencies. As the non-thermal spectrum steepens with the increasing frequency due to the electron losses, these values can be considered to be in an agreement. Age estimates for the disk follow the general tendency of CI model returning higher values. The JP model estimates the spectral age to be between 1.4 and 3.8 Myrs, while CI returns 5.6 and 15.3 Myrs, respectively. This suggests a rather young population of the electrons, which was still supplied in the nearest past of this galaxy.
As a supplement, we also performed fitting for the "smooth disk" – the flux from the galaxy pair with all the individual regions of enhanced radio emission (hence, star formation) subtracted. These estimates are in general very similar to the

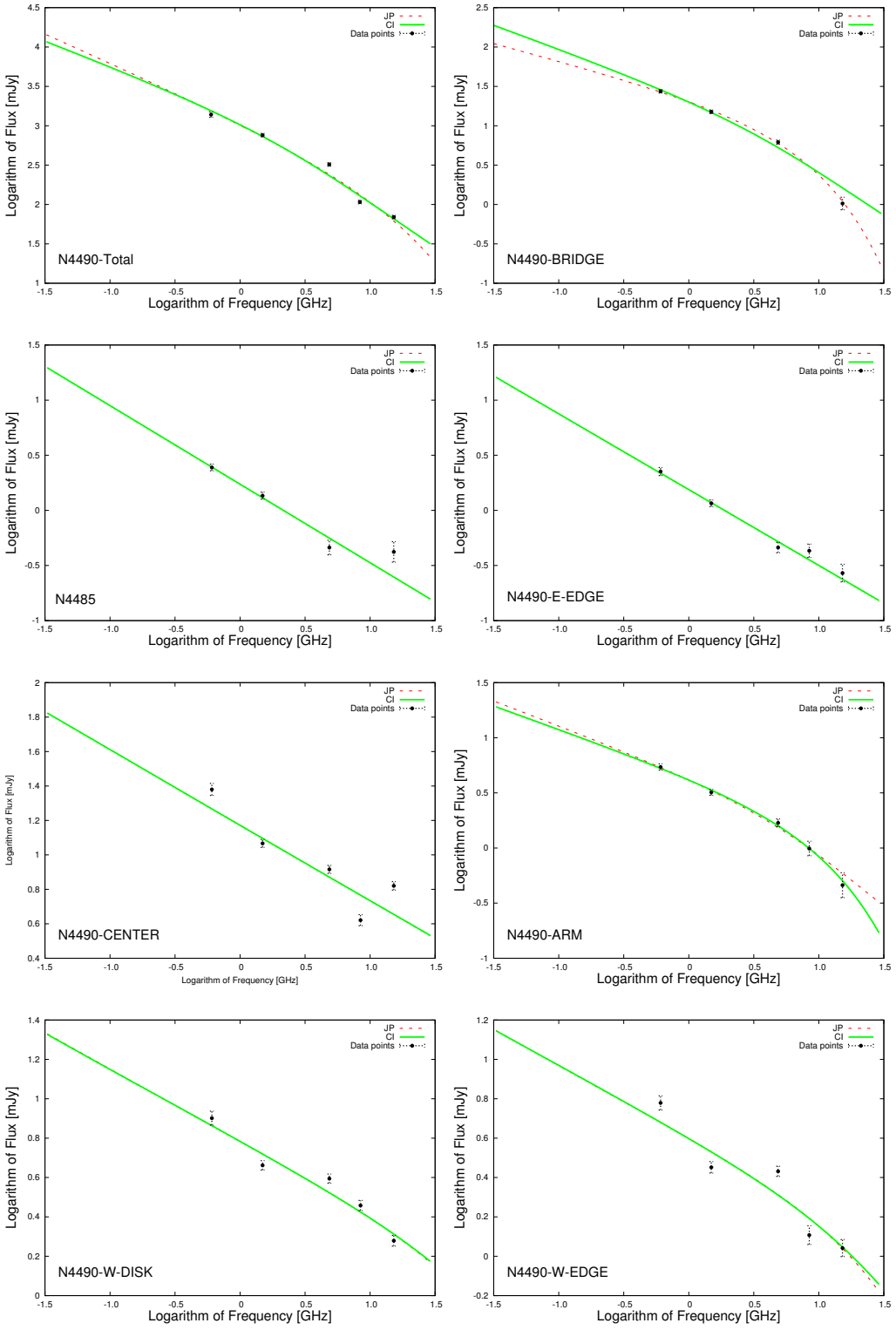

Figure 4. Fitted Jaffe-Perola (dashed line) and Continuous Injection (solid line) model curves for the various regions of NGC 4490/85 galaxy pair. Explanation is provided in the text.

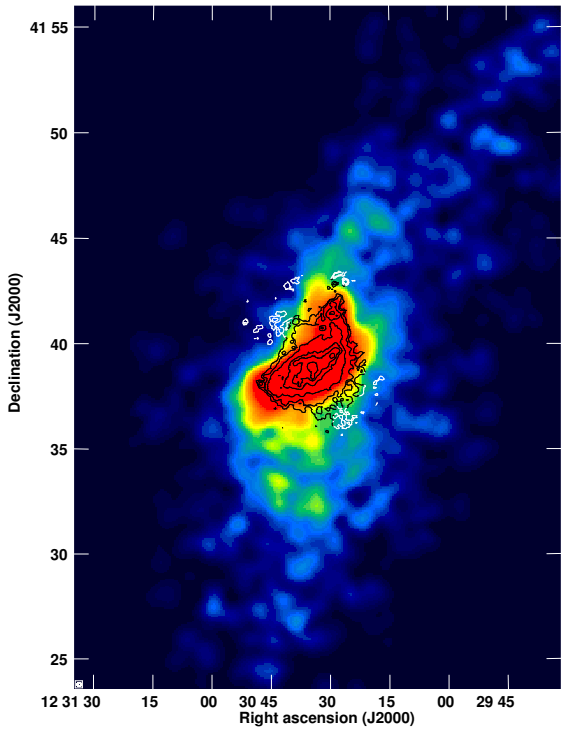

Figure 5. Contours of the 4.86 GHz radio emission superimposed on the neutral hydrogen distribution map from Swaters et al. (2002), taken from the NED database. The contour levels are $3, 5, 10, 20, 30, 50\times$ 0.02 mJy/beam (r.m.s. noise level). The angular resolution of the continuum data is 10 arcsec.

ones derived for the galaxies as whole. From the flux densities one can easily see that the diffuse emission is dominating. Surprisingly, the CI model yields lower age estimates for the smooth disk than for the whole galaxy; however, these deviations are very small compared to the uncertainty of the fit so they can be regarded as insignificant.

The total magnetic field strength is $21.9 \pm 2.9\,\mu$G. This suggests strong magnetic field in the whole system (similar values have been obtained for the smooth disk case), higher than the typical one found in spiral galaxies ($9\pm 1.3\,\mu$G, Niklas et al. 1997), and similar to that found in M51 (Fletcher et al. 2011). It is remarkable, as NGC 4490 ia a rather small galaxy, compared to the latter one, and smaller systems are usually less efficient in magnetic field amplification (Beck & Wielebinski 2013). The star formation rate (SFR), which is closely related to the magnetic field strengths, is very similar in NGC 4490 and M 51: Clemens et al. (1999) estimates the SFR of NGC 4490 to be around $4.7\,M_\odot\,yr^{-1}$ (basing on the radio data), whereas Calzetti et al. (2005) suggests $4.3\,M_\odot\,yr^{-1}$ for M 51 (basing on the ultraviolet data, 50–100 Myr old stellar populations). As NGC 4490 is much smaller than the latter galaxy, the surface star formation rate is higher, providing a sensible explanation for the estimated magnetic field strength.

4.6.2 Intergalactic bridge

NGC 4490 and 4485 are connected by a narrow radio bridge, that coincides with a stream of stars. Surprisingly, there is not much thermal flux there, suggesting deficiency of star forming regions. This hypothesis is supported by the shape of the spectrum: it falls rather quickly and weakens abruptly already at 4.86 MHz (where flux decrement can not be administered to the zero spacing problem). The injection spectral indices reveal flat initial spectrum, suggesting that the observed radio emission originated in regions of effective supply of charged particles. The CI spectral age estimate for the intergalactic bridge (5.56 – 16.8 Myrs) is almost the same as for the galactic disk, whereas the JP estimates (4.15 – 8.08 Myrs) are the highest (among the other ones derived with the JP model) for the structures in this system. For this structure, the JP model provides a better fit to the data. The magnetic field of the bridge is strong, only slightly weaker than that found inside the galaxy. The density of energy contained within is approximately 1.39 ± 0.28 erg cm^{-3}, of the same order as that between the Taffy galaxies (Condon et al. 1993). Given the above information, a possible conclusion is that the radio emission in the bridge is a product of magnetic field amplification inside one of the galaxies, and the emitting matter has been torn from them during the interaction process (or due to the wind of star formation). As there are no effective sources of accelerated particles (judging on the steepening of the spectrum, and low thermal flux), the spectral age refers to the last acceleration event in the galactic disk, and thus it can be considered the starting point of the merging process. As the extent of the bridge is equal to few kiloparsecs, it would imply that the charged particles travel with velocities of several kilometres per second, which is not an exotic value.

4.6.3 Optical center of the galaxy

The data points for the galaxy center show some scatter (Fig. 4), but the models fit well. Estimated injection spectral index is flat (0.45 for both models), close to the theoretical minimum for the young supernovae remnants (0.3 – Weiler & Sramek 1988). The fitted models show nearly straight lines (they follow each other so exactly that distinguishing between them is almost impossible) and therefore determination of the break frequency is complicated, if not impossible. The derived frequency is not well localised, and the upper boundary (which corresponds to the lower age limit of 0.2 Myrs for JP and 0.6 Myrs for CI models) suggests extremely young electron population. This indicates ongoing star formation and electron supply. The magnetic field is strong ($39.3 \pm 5.44\,\mu$G), but not unusual for central region of a nearby galaxy. Beck & Wielebinski (2013) states that centers of barred spirals are regions of intense star formation and strong magnetic fields can be found there; notable examples include NGC 1097 with app. $55\,\mu$G, or NGC 1365 with maximum of $63\,\mu$G (Beck et al. 2005).

4.6.4 Northern spiral arm

The northern spiral arm can be easily distinguished from the galactic disk because of three local emission maxima. They

show high fraction of thermal emission, which becomes dominant at the frequencies higher than 4.86 GHz. The remaining non-thermal electron population is older than that of the central region. For this case, both lower and upper limits for the spectral age can be derived. The several Myr wide range of possible values suggests moderately aged population of electrons. The magnetic field is strong (25.5±3.5 μG), higher than in typical spiral galaxies, yet still comparable to the arm regions of M51.

4.6.5 W-DISK

This region lies in the western part of the disk of NGC 4490. Compared to the arm regions, it hosts very similar magnetic field with B_{TOT} = 26.0±3.5 μG, but as the model curve (Fig. 4) is very weakly bent, break frequency is poorly determined and again, only the upper age limit can be derived. Values of 1.4 Myrs (JP) and 2.6 Myrs (CI) are reasonable for an area of intensive, ongoing star formation.

4.6.6 W-EDGE

The westernmost star forming region of the disk does not differ much from the other areas of enhanced star formation. It hosts strong magnetic field (18.3±2.3 μG), albeit somewhat lower than in the neighbouring W-DISK region. The SED (Fig. 4) shows more pronounced curvature and the break frequency is quite well localised, allowing estimation of both lower and upper limits for the spectral age. Both models yield spectral ages of several Myrs, again reasonable for this kind of source.

4.6.7 E-EDGE

This unresolved source lies on the easternmost edge of the galactic disk of NGC 4490. It shows barely any thermal emission, suggesting that it is a background radio galaxy, not related to the foreground galactic system. Constant slope of the SED (Fig. 4) causes low localisation of the break frequency, but it is clearly visible that this source is a subject to a continuous electron supply, resulting in low spectral age.

4.6.8 S-SRC

This source exhibits an extremely flat spectrum, with an average band-to-band (total) spectral index value of 0.13. Such a value clearly indicates an almost purely thermal character of the emission, as it agrees with the theoretical value of 0.1 (Pacholczyk 1973). This conclusion is not astounding in the light of its identification as an HII region (Clemens & Alexander 2002). Radio emission from such a structure should be dominated by the thermal radiation with the synchrotron component almost negligible. However, the thermal fraction derived from our LVL maps is much lower than expected, as it does not exceed 40 per cent at any frequency; a value closer to 100 per cent would be expected. This is most likely due to the high internal extinction in this dense area. High extinction of the thermal flux has also been noticed by Clemens & Alexander (2002), who suggested a possibility that the obscuring dust is related not to the region itself, but to the surrounding atomic gas.

4.6.9 Star forming regions of NGC 4485

The companion galaxy NGC 4485 is a rather radio quiet one, compared to its neighbour. Most of its emission is due to the small group of three sources, compact in character. This group lies in the outskirts of the galactic disk, and Clemens et al. (2000) identifies it with a bow-shock in the IGM. Emission from these sources has a significant thermal component (reaching 50% at 15.2 GHz). The values for the remaining, non-thermal flux lie on a moreover straight line, suggesting low spectral age. As in some of the previous cases, only upper limit for the spectral age can be derived: 4.1 Myrs for the JP model and 10.9 Myrs for the CI. These limits are higher than those obtained for the disk regions; this might indicate the age of the structure formed by the shock. The magnetic field is somewhat weaker than that found in the intergalactic bridge. Lack of amplification suggests that the shock is rather weak and does not compress the magnetised IGM sufficiently to enhance the magnetic field bound to it.

4.7 Tracing the remnant of SN2008ax

On 3rd March 2008, a supernova was discovered in the eastern part of NGC 4490 disk, at R.A.$_{2000}$ = $12^h30^m40.8^s$, Dec$_{2000}$ = +41°38′14.5″ (Mostardi et al. 2008). Denoted SN2008ax, it belongs to the rarest type of the SNe, namely Type IIb (Mostardi et al. 2008): their progenitors are similar to those of the SNIb, but unlike the latter ones, they have small hydrogen envelopes (Woosley et al. 1987; Pastorello et al. 2008). There is no evidence for an increased radio flux density at that position in our GMRT observations (Fig. 2a); in the high-res maps used for spectral fitting, there is no sign of emission at all. This means that the SNR flux on the 1805th day since explosion does not exceed 4.07 ± 0.06 mJy (a mean value from a small area surrounding the position of SNR).s

4.8 The origin of the unusually steep spectrum of the distant galaxy

A distant galaxy at R.A.$_{2000}$ = $12^h30^m26.1^s$, Dec$_{2000}$ = +41°42′158″ (z = 0.124880, basing on the SDSS data), not related to the VV 030 pair can be seen north from NGC 4485 in our 0.61, 1.49 and 4.86 GHz maps (as a point source). This object is also part of a galaxy system, as there is another galaxy at virtually the same redshift (z=0.124696), located app. 140 kpc away. Unfortunately, neither emission from the second component, nor from any intergalactic structure was detected.

Our analysis shows that the distant galaxy has a steep spectral index of 1.13 ± 0.07 between 0.61 and 4.86 GHz, suggesting domination of the non-thermal emission originating from a moderately aged population of relativistic electrons. As this object is identified as an AGN, much flatter spectrum might be expected. This distant galaxy may be host a Gigahertz-Peaked Source (GPS) or Compact Steep Source (CSS, O'Dea 1998). These sources are steep-spectrum, compact objects with the emission peak around 100 MHz (CSS) or 1 GHz (GPS). Among possible explanations for their origin, two are being generally accepted as the most probable ones: either these are old,

frustrated objects (Wilkinson et al. 1984; van Breugel et al. 1998), obscured by the dust in the host galaxy, or young objects, that did not evolve sufficiently yet (Shklovsky 1965). Due to the significant distance (z = 0.125) the source is unresolvable at any of the frequencies used in this study. However, there is no evidence of radio structures that might extend beyond the contour of the optical emission. A quick look at the MIPS map shows that the dust emission locally peaks at the position of this distant galaxy. This might be a hint that the frustrated source hypothesis is indeed correct here.

5 CONCLUSIONS

We studied the nearby galaxy pair NGC 4490/85 at 0.61, 1.49, 4.86, 8.35, 15.21 and 22.46 GHz. The radio emission was separated into the thermal and non-thermal components. Magnetic field properties, spectral age and coincidence with the neutral gas distribution were examined. We came to the following conclusions:

(i) There is an intergalactic extension of the continuum emission envelope visible at several frequencies. This extension is double–sided, and is visible even at the higher frequency maps.

(ii) The aforementioned extension is orientated nearly perpendicular to the neutral hydrogen tail (which does not coincide with any radio emission exceeding the intra-pair area). The reasons for such a layout are yet unknown; it might suggest that there are indeed two different outflows, formed eg. by different gas phases, and the magnetic field is present only in the second one.

(iii) The magnetic field strength – the mean value for the galaxy ($21.9 \pm 2.9\,\mu$G), as well as values estimated for particular disk regions (18–40 μG) – is strong and comparable to the grand-design, or barred spiral galaxies, like M 51, NGC 1097, or NGC 1365 – despite NGC 4490 being much smaller object. This can be explained on the basis of high surface star formation rate, providing effective source of relativistic particles.

(iv) The age of electron population of the disk has been studied using Jaffe-Perola and Continuous Injection models. No matter the model used, the resulting spectral ages are very low and suggest an ongoing star formation throughout both galaxies that form the pair – supporting the hypothesis that ongoing rapid star formation is responsible for the magnetic field strength.

(v) There is a magnetised bridge between member galaxies. It hosts strong magnetic field, and its age estimate – which, for the JP model, is the highest obtained in the whole system – suggests that the spectral age signifies the moment in which merging process started (4.15–8.08 Myrs and 5.5 – 16.8 Myrs for the JP and CI models, respectively).

(vi) There is no evidence of a supernovae remnant in the position of SN2008ax; the upper limit for this SN on the day 1805th from explosion is therefore 4.07 ± 0.06 mJy (mean flux value in the closest vicinity of the suspected SNR's position).

(vii) In the angular vicinity of NGC 4490, a distant (z=0.125) galaxy with a very steep spectrum lies. This object might be a compact steep source (CSS): an unevolved, or frustrated active galactic nuclei. This object forms a pair with another one, although its companion is a radio-quiet one and there are no signs of intergalactic emission between them.

ACKNOWLEDGEMENTS

We wish to thank Dr Marcel Clemens for his 15.2 GHz Ryle Telescope map that allowed us to improve our estimates basing on the spectral properties of this galaxy system. We thank the staff of the GMRT that made these observations possible. GMRT is run by the National Centre for Radio Astrophysics of the Tata Institute of Fundamental Research.

This research has been supported by the scientific grant from the National Science Centre (NCN), dec. No. 2011/03/B/ST9/01859.

This research has made use of the NASA/IPAC Extragalactic Database (NED) which is operated by the Jet Propulsion Laboratory, California Institute of Technology, under contract with the National Aeronautics and Space Administration. This research has made use of NASA's Astrophysics Data System. Funding for the SDSS and SDSS-II has been provided by the Alfred P. Sloan Foundation, the Participating Institutions, the National Science Foundation, the U.S. Department of Energy, the National Aeronautics and Space Administration, the Japanese Monbukagakusho, the Max Planck Society, and the Higher Education Funding Council for England. The SDSS Web Site is http://www.sdss.org/.

REFERENCES

Alexander P., Leahy J. P., 1987, MNRAS, 225, 1
Appleton P. N., Ghigo F. D., van Gorkom J. H., Schombert J. M., Struck-Marcell C., 1987, Nature, 330, 140
Arp H., 1966, ApJS, 14, 1
Baars J. W. M., Genzel R., Pauliny–Toth I. I. K., Witzel A., 1977, A&A, 61, 99
Beck R., Fletcher A., Shukurov A., Snodin A., Sokoloff D. D., Ehle M., Moss D., Shoutenkov V., 2005, A&A, 444, 739
Beck R., Krause M., 2005, AN, 326, 414
Beck R., Wielebinski R., 2013, in: Planets, Stars and Stellar Systems. Volume 5: Galactic Structure and Stellar Populations, ed. T. D. Oswalt & G. Gilmore (New York: Springer), 64
Beirão P., Appleton P. N., Brandl B. R., Seibert M., Jarrett T., Houck J. R., 2009, ApJ, 693, 1650
Calzetti D., et al., 2005, ApJ, 633, 871
Calzetti D., et al., 2007, ApJ, 666, 870
Carilli C. L., Perley R. A., Dreher J. W., Leahy J. P., 1991, ApJ, 383, 554
Chyży K. T., Beck R., 2004, A&A, 417, 541
Clemens M. S., Alexander P., Green D. A., 1998, MNRAS, 297, 1015
Clemens M. S., Alexander P., Green D. A., 1999, MNRAS, 307, 481
Clemens M. S., Alexander P., Green D. A., 2000, MNRAS, 312, 236
Clemens M. S., Alexander P., 2002, MNRAS, 333, 39
Condon J. J., Helou G., Sanders D. B., Soifer B. T., 1993, ApJ, 105, 1730
Dale D. A. et al., 2009, ApJ 703, 517
Davis L. E., Seaquist E. R., 1983, ApJS, 53, 269
Dean J. F., Davies R. D., 1975, MNRAS, 170, 503

Deeg H. J., Duric N., Brinks E., 1997, A&A, 323, 323
de Vaucouleurs G., de Vaucouleurs A., Corwin H. G., Buta R. J., Paturel G., Fouque P. Third Reference Catalogue of Bright Galaxies (RC3). Springer-Verlag, New York, 1991
Jaffe W. J., Perola G. C., 1973, A&A, 26, 423
Fletcher A., Beck R., Shukurov A., Berkhuijsen E. M, Horellou C., 2011, MNRAS, 412, 2396
Haslam C. G. T., 1974, A&AS, 15, 333
Haynes M. P., Giovanelli R., Roberts M. S., 1979, ApJ, 229, 83
Heesen V. et al., 2015, MNRAS 447, L1
Higdon J. L., Rand, R. J., Lord, S. D., 1997, ApJ, 489, L133
Hummel E., 1991, A&A, 251, 442
Kardashev N. S., 1962, SvA, 6, 317
Kennicutt R. C., Evans N. J., 2012 ARA&A, 50, 531
Lacki B., Beck R., 2013, MNRAS 430, 3171
Lynds R., Toomre A., 1976, ApJ, 209, 382
Murgia M., 1996, Laurea Thesis, University of Bologna
Mostardi R., Li W., Filippenko A. V., 2008, Central Bureau Electronic Telegrams, 1280, 1
Myers S. T., Spangler S. R., 1985, ApJ, 291, 52
Nikiel-Wroczyński, B., Soida, M., Urbanik, M., Weżgowiec, M., Beck, R., Bomans, D. J., Adebahr, B., 2013, A&A, 553, 4
Nikiel-Wroczyński B., Soida M., Urbanik M., Beck R., Bomans D. J., 2013, MNRAS, 435, 149
Nikiel-Wroczyński B., Jamrozy M., Soida M., Urbanik M., 2014, MNRAS, 444, 1729
Nikiel-Wroczynski, B., Soida, M., Bomans, D. J., Urbanik, M., 2014, ApJ, 786, 144
Niklas S., 1995, PhD thesis, University of Bonn
Niklas S., Klein U., Wielebinski R., 1997, A&A, 322, 19
O'Dea C. P., 1998, PASP, 110, 493
Pacholczyk A. G., Radio Astrophysics. Freeman, San Francisco, 1970, Mir, Moscow, 1973
Pastorello A., et al., 2008, MNRAS, 389, 955
Romano R., Mayya Y. D., Vorobyov E. I., 2008, AJ, 136, 1259
Sandage A., Tammann G. A., 1981, A Revised Shapley-Ames Catalog of Bright Galaxies. Carnegie Institution, Washington
Schlafly E. F., Finkbeiner D. P., 2011, ApJ, 737, 103
Schlegel D. J., Finkbeiner D. P., Davis, M., 1998, ApJ, 500, 525
Shklovsky, I. S., 1965, Nature, 206, 176
Soida M., Urbanik M., Beck R., Wielebinski R., Balkowski C., 2001, A&A, 378, 40
Stanimirovic, S., 2002, ASPC, 278, 375
Stierwalt, S., Haynes, M. P., Giovanelli, R., Kent, B. R., Martin, A. M., Saintonge, A., Karachentsev, I. D., Karachentseva, V. E., 2009, ApJ, 138, 338
Sulentic J. W., 1976, ApJS, 32, 171
Swaters R. A., van Albada T. S., van der Hulst J. M., Sancisi R., 2002, 390, 829
Taylor V. A., Jansen R. A., Windhorst R. A., Odewahn S. C., Hibbard J. E., 2005, 630, 784
Theys J. C., Spiegel E. A., 1977, AJ, 212, 616
van Breugel W., Miley G., Heckman T., 1984, AJ, 89, 5
van Moorsel, G. A., 1988, A&A, 202, 59
Verdes-Montenegro L., Yun M. S., Williams B. A., Huchtmeier W. K., Del Olmo A., Perea, J., 2000, IAU Colloq. 174, Small Galaxy Groups, ed. M. Valtonen & C. Flynn (San Francisco: ASP), 167
Viallefond F., Allen R. J., de Boer J. A., 1980, A&A, 82, 207
Vorontsov-Velyaminov B. A., 1959, VV, 0
Wilkinson P. N., Booth R. S., Cornwell T. J., Clark R. R., 1984, Nature, 308, 619
Weiler K. W., Sramek R. A., 1988, Ann. Rev. AfcA, 26, 295
Weżgowiec M., Urbanik M., Beck R., Chyży K. T., Soida M., 2012, A&A, 545, 69
Woosley S. E., Pinto P. A., Martin P. G., Weaver T. A., 1987, ApJ, 318, 664

BIBLIOGRAPHY

Adebahr, B., Krause, M., Klein, U., Weżgowiec, M., Bomans, D. J., Dettmar, R.-J., 2013, A&A, 555, 23

Appleton P. N., Ghigo F. D., van Gorkom J. H., Schombert J. M., Struck-Marcell C., 1987, Nature, 330, 140

Appleton P. N., Struck-Marcell C., 1996, Fund. of Cosm. Phys., 16, 111

Arp H., 1972, ApJ, 174, L111

Arp H., Kormendy, J., 1972, ApJ, 178, L111

Beck R., Krause M., 2005, AN, 326, 414

Beck R., Fletcher A., Shukurov A., Snodin A., Sokoloff D. D., Ehle M., Moss D., Shoutenkov V., 2005, A&A, 444, 739

Beirão P., Appleton P. N., Brandl B. R., Seibert M., Jarrett T., Houck J. R., 2009, ApJ, 693, 1650

Beck, R., 2007, A&A 470, 539

Beck, R., Wielebinski, R., in: Stars and Stellar Systems, Vol. 5: Galactic Structure and Stellar Populations, ed. G. Gilmore, Springer, Berlin 2013

Biermann, L., 1950, Zeitschrift Naturforschung Teil A, 5, 65

Brentjens M. A., de Bruyn A. G., 2005, A&A, 441, 1217

Calzetti D., et al., 2007, ApJ, 666, 870

Clemens M. S., Alexander P., Green D. A., 1998, MNRAS, 297, 1015

Clemens M. S., Alexander P., Green D. A., 1999, ApJ, 307, 481

Clemens M. S., Alexander P., Green D. A., 2000, MNRAS, 312, 236

Clemens M. S., Alexander P., 2002, MNRAS, 333, 39

Condon J. J., Helou G., Sanders D. B., Soifer B. T., 1993, ApJ, 105, 1730

Condon J. J., Cotton W. D., Greisen E. W., Yin Q. F., Perley R. A., Taylor G. B., Broderick J. J, 1998, ApJ, 115, 1693

Condon J. J., Helou G., Jarrett T. H., 2002, ApJ, 123, 1881

Chyży K. T., Beck R., Kohle S., Klein U., Urbanik M., 2000, A&A, 355, 128

Chyży, K. T., Beck, R., 2004, A&A 417, 541

Curtis, H. D. 1921, The Scale of the Universe, Bull. Nat. Res. Coun. 2, 171

Darwin, Ch., 1859, On the Origin of Species by Means of Natural Selection, or the Preservation of Favoured Races in the Struggle for Life, London, John Murray

Davis, L. J., Greenstein, J. L., 1951, ApJ, 114, 206

Dean J. F., Davies R. D., 1975, MNRAS, 170, 503

Deeg H. J., Duric N., Brinks E., 1997, A&A, 323, 323

Dumke, M., Krause, M., Lecture Notes in Physics, vol.506, The Local Bubble and Beyond. Lyman-Spitzer Colloquium, Proceedings of the IAU Colluquium No. 166 held in Garching, Germany, 21-25 April, 1997, XXVII, 603

Drzazga, R. T., Chyży, K. T., Jurusik, W., Wiórkiewicz, K., 2011, A&A, 533, 22

Elder, F. R., Gurewitsch, A. M., Langmuir, R. V., Pollock, H. C., 1947, Phys. Rev., 71, 11, 829

Fletcher, A., 2010, in: The Dynamic Interstellar Medium, eds. R. Kothes et al., ASP Conf. Ser. 438, p. 197

Fletcher, A., Beck, R., Shukurov, A., Berkhuijsen, E.M., Horellou, C., 2011, MNRAS 412, 2396

Gastaldello, F. et al., 2013, ApJ, 770, 56

Giacintucci S. et al., 2011, ApJ, 732, 95

Haynes M. P., Giovanelli R., Roberts M. S., 1979, ApJ, 229, 83

Hickson P., 1982, ApJ, 255, 382

Hickson P., 1997, Annual Review of Astronomy and Astrophysics, 35, 357

Hiltner, W.A., 1958, ApJ 128, 9

Hubble, E., 1926, ApJ, 64, 321

Holmberg, E., 1937, Annals of the Observatory of Lund, Lund Observatory, 1937

Kant, I., 1755, Allgemeine Naturgeschichte und Theorie des Himmels, Part I, J.F. Peterson, Königsberg und Leipzig.

Klein U., Haynes R. F., Wielebinski R., Meinert, D., 1993, A&A, 271, 402

Kuśper A., Promieniowanie radiowe zwartych grup galaktyk Hicksona, MSc Thesis, Jagiellonian University, 2006

Lazar, M., Schlickeiser, R., Wielebinski, R., Poedts, S., 2009, ApJ 693, 1133

Messier, C., 1781, Connaissance des temps ou des mouvements cèlestes, pp. 227

Moles M., Marquéz I., Sulentic J. W., 1997, ApJ, 485L, 69

Moles M., Sulentic J. W., Marquéz I., 1998, A&A, 334, 473

Niklas S., 1995, PhD thesis, University of Bonn

O'Sullivan E., Giacintucci S., Vrtilek J. M., Raychaudhury S., David L. P., 2009. ApJ, 701, 1560

Parker, E.N.: 1979, Cosmical Magnetic Fields, Clarendon Press, Oxford

Pacholczyk A. G., Radio Astrophysics. Freeman, San Francisco, 1970, Mir, Moscow, 1973

Scott, T. C., Cortese, L., Brinks, E., Bravo-Alfaro, H., Auld, R., Minchin, R., 2012, MNRAS, 419, 19

Schlickeiser, R., 2012, Phys. Rev. Lett. 109, 261101

Serra et al., 2013, MNRAS, 428, 370

Shapley, H. 1921, The Scale of the Universe, Bull. Nat. Res. Coun. 2, 194

Siejkowski H., Soida M., Otmianowska-Mazur K., Hanasz M., Bomans D. J., 2010, A&A, 510, 97

Siejkowski, H., Otmianowska-Mazur, K., Soida, M., Bomans, D. J., Hanasz, M., 2014, A&A, 562, 136

Soida, M., Urbanik, M., Beck, R., Wielebinski, R., Balkowski, C. 2001, A&A, 378, 40

Stephan, È. J.-M., 1877, MNRAS, 37, 334

Stocke, J. T., Tifft, W. G., Kaftan-Kassim, M. A., 1978, AJ, 83, 322

Subramanian, K., 2008, in: Proceedings of "From Planets to Dark Energy: the Modern Radio Universe", eds. R. Beswick et al., published by PoS, PoS MRU:071,2007

Tabatabaei, F. S., Krause, M., Fletcher, A., Beck, R., 2008, A&A 490, 1005

Toomre, A., and Toomre, J. 1972, Ap. J., 178, 623

Viallefond F., Allen R. J., de Boer J. A., 1980, A&A, 82, 207

Vorontsov-Velyaminov, B. A., Atlas and catalog of interacting galaxies. 1959, Sternberg Institute, Moscow State University.

Vollmer, B., Braine, J., Soida, M., 2012, A&A, 547, 39

Vrtilek, J. M., O'Sullivan, E., David, L. P., Kolokythas, K., Giacintucci, S., Raychaudhury, S., Ponman, T. J., 2013, AAS HEAD meeting 13, 116.06

Xu C. K., Lu N., Condon J. J., Dopita M., Tuffs R. J., 2003, ApJ, 595, 665

Zwicky, F., 1941, in: Theodore van Karman Anniversary volume Contribution to Applied Mechanics and Related Subjects,California Institute of Technology, 137

Zwicky, F., 1956, Ergebnisse der Exakten Naturwissenschaften 29, 344

COLOPHON

This document was typeset using the typographical look-and-feel `classicthesis` developed by André Miede. The style was inspired by Robert Bringhurst's seminal book on typography "*The Elements of Typographic Style*". `classicthesis` is available for both LaTeX and LyX:

http://code.google.com/p/classicthesis/

Happy users of `classicthesis` usually send a real postcard to the author, a collection of postcards received so far is featured here:

http://postcards.miede.de/

Final Version as of June 11, 2015 (`classicthesis` version 4.0).

DECLARATION

Wydział Fizyki, Astronomii i Informatyki Stosowanej
Uniwersytet Jagielloński

Oświadczenie

Ja niżej podpisany Błażej Nikiel-Wroczyński (nr indeksu: 1007086), doktorant Wydziału Fizyki, Astronomii i Informatyki Stosowanej Uniwersytetu Jagiellońskiego oświadczam, że przedłożona przeze mnie rozprawa doktorska pt. *Existence and importance of magnetic fields in tight pairs and groups of galaxies* jest oryginalna i przedstawia wyniki badań wykonanych przeze mnie osobiście, pod kierunkiem prof. dr. hab. Marka Urbanika i dr. Marka Jamrozego. Pracę napisałem samodzielnie. Oświadczam, że moja rozprawa doktorska została opracowana zgodnie z *Ustawą o prawie autorskim i prawach pokrewnych z dnia 4 lutego 1994 r. (Dziennik Ustaw 1994 nr 24 poz. 83 wraz z późniejszymi zmianami)*. Jestem świadom, że niezgodność niniejszego oświadczenia z prawdą ujawniona w dowolnym czasie, niezależnie od skutków prawnych wynikających z ww. ustawy, może spowodować unieważnienie stopnia nabytego na podstawie tej rozprawy.

Błażej Nikiel-Wroczyński
Kraków, 10.06.2015